NATIONAL AERONAUTICS AND SPACE ADMINISTRATION

Technical Report No. 32-849

Utilizing Large Planetary Perturbations for the Design of Deep-Space, Solar-Probe, and Out-of-Ecliptic Trajectories

M. Minovitch

JET PROPULSION LABORATORY
CALIFORNIA INSTITUTE OF TECHNOLOGY
PASADENA, CALIFORNIA

December 15, 1965

NATIONAL AERONAUTICS AND SPACE ADMINISTRATION

Technical Report No. 32-849

Utilizing Large Planetary Perturbations for the Design of Deep-Space, Solar-Probe, and Out-of-Ecliptic Trajectories

M. Minovitch

T. Hamilton

T. Hamilton, *Manager*
Systems Analysis Section

JET PROPULSION LABORATORY
CALIFORNIA INSTITUTE OF TECHNOLOGY
PASADENA, CALIFORNIA

December 15, 1965

Prepared Under Contract No. NAS 7-100
National Aeronautics & Space Administration

CONTENTS

TABLES

TABLES (Cont'd)

TABLES (Cont'd)

FIGURES

FIGURES (Cont'd)

FIGURES (Cont'd)

FIGURES (Cont'd)

ABSTRACT

15224

This Report (a sequel to JPL TR 32-464) is concerned with three types of free-fall missions that are primarily designed for unmanned vehicles, viz. deep space, solar probe, and out-of-ecliptic missions. The energies required to attain these trajectories are beyond present direct-transfer capability using available boosters. Solar-impact and 90-deg-inclination trajectories require launch energies so high that second-generation nuclear upper stages or ion engines would be absolutely necessary. By utilizing large planetary perturbations, it is possible that a rocket like *Titan* II-*Centaur* with an extra kick stage can, by sacrificing a few extra pounds for planetary approach guidance, obtain trajectories that a *nuclear Saturn* V cannot obtain.

Author

I. INTRODUCTION

In order that one may clearly understand what is involved in carrying out the high-energy missions considered in this report, we shall, as an introduction, give a brief description of the extreme penalties one encounters if conventional trajectory profiles are used.

We begin by considering two important equations called the energy and rocket equations. The energy equation expresses the relation between a vehicle's velocity V (i.e., the length of its velocity vector $\mathbf{V}$) and its distance R from the center of the body setting up the gravitational field. It takes the form

$$V^2 = \mu\left(\frac{2}{R} - \frac{1}{a}\right) \tag{1}$$

where μ is a constant equal to the product of the gravitational constant and the body's mass. The second constant a is equal to the trajectory's semimajor axis. This quantity is either positive or negative depending on whether the path is elliptical or hyperbolic.

Suppose that a fully fueled liquid rocket carrying a payload is orbiting the Earth in a circular "parking orbit," r kilometers high, waiting to be injected onto its prescribed interplanetary trajectory. The energy equation (Eq. 1) then shows that the orbital velocity V_0 will be

$$V_0 = \left(\frac{\mu}{R_0 + r}\right)^{1/2}$$

where R_0 is the Earth's radius. Now at that height the minimum velocity V_e needed to escape the Earth is

$$V_e = \lim_{a \to \infty} \left[\mu\left(\frac{2}{R_0 + r} - \frac{1}{a}\right)\right]^{1/2} = \left(\frac{2\mu}{R_0 + r}\right)^{1/2}$$

Thus since the vehicle is already moving V_0 km/sec, the required velocity increase ΔV that the orbiting rocket must supply is simply

$$\Delta V = V_e - V_0$$

If the mission requires the vehicle to proceed into interplanetary space, its departing trajectory after injection will be hyperbolic with respect to the Earth. The value of its semimajor axis will lie in the range $-\infty < a < 0$. The velocity V_h, assumed by the vehicle with respect to the Earth when its distance becomes very great, is called the trajectory's hyperbolic excess velocity. In the tables this important quantity will be abbreviated to HEV. It is defined as

$$V_h = \lim_{R \to \infty} \left[\mu\left(\frac{2}{R} - \frac{1}{a}\right)\right]^{1/2} = \left(\frac{-\mu}{a}\right)^{1/2}$$

Since actual parking orbits may vary in height, it is convenient to describe required launch energies for interplanetary trajectories by simply stating their required hyperbolic excess velocities.

Table 1. Some popular types of free-fall interplanetary trajectories and their required hyperbolic excess velocities

No.	Mission	HEV, km/sec
1.1	Escape from Earth	0
1.2	Earth–Venus and Earth–Mars (110- and 200-day flyby, respectively)	3.00
1.3	Earth–Venus–Earth (360-day reconnaissance flyby)	3.50
1.4	Earth–Venus–Mars–Earth (600-day 1970, 480-day 1972 reconnaissance flyby)	3.50
1.5	Earth–Mars–Earth (1000-day reconnaissance flyby)	4.50
1.6	Earth–Mercury (85-day flyby)	6.40
1.7	Earth–Mars–Earth (600–700 day reconnaissance flyby)	6.50
1.8	Earth—13-deg out-of-ecliptic (a = 1 AU, e = 0)	6.74
1.9	Earth–Jupiter (800–900-day minimum-energy flyby)	9.30
1.10	Earth–Saturn (6.05-yr minimum-energy flyby)	10.43
1.11	Earth–Jupiter (450–500-day flyby)	11.00
1.12	Solar probe (to within 0.25 AU of Sun)	11.00
1.13	Earth–Uranus (16.00-yr minimum-energy flyby)	11.23
1.14	Earth–Neptune (30.70-yr minimum-energy flyby)	11.62
1.15	Earth–Pluto (45.70-yr minimum-energy flyby)	11.63
1.16	Escape from solar system $(HEV)_{Sun} = 0$	12.43
1.17	Earth–Mars–Earth (480-day reconnaissance flyby)	13.50

Table 1 gives a list of some popular types of free-fall trajectories along with their associated hyperbolic excess velocities. By a free-fall, or ballistic, trajectory we mean one that is not changed by any on-board propulsive forces after injection, other than those used for attitude control and midcourse and approach guidance. The launch trajectory is assumed to be so accurate that only very small corrections are necessary. These velocities associated with transfers to other planets may change because of planetary eccentricities and inclinations. In these cases we give only an average value over several launch opportunities. Most of the trajectories given are within easy reach of *Saturn* SIB. Recent studies by Lockheed Aircraft Corp. show that the 450–500-day Earth–Jupiter trajectories are within the capability of a *Titan* II–*Centaur* equipped with an extra stage on top of the *Centaur*. The resulting payload is in the neighborhood of 500 lb. For the *Saturn* SIB the payload can of course be much higher.

Table 2 gives a list of the trajectories we shall be concerned with. The full meaning of this table can only be understood when one makes a few simple calculations with the rocket equation. This equation deals with the total mass of propellant a rocket consumes while changing its velocity by an amount ΔV. It can be expressed mathematically by

$$\frac{M_2}{M_1} = \exp\left(-\frac{\Delta V}{c}\right) \tag{2}$$

where M_1 denotes the rocket's initial mass before ΔV, and M_2 denotes the total mass after ΔV. The constant c is equal to the rocket engine's exhaust velocity. The left-hand side of the equation is usually called the mass ratio. For a fixed ΔV the mass ratio increases with c. Hence, it is related to the performance of the rocket engine.

Table 2. The high-energy missions: deep space solar probe, out-of-ecliptic

No.	Mission	HEV, km/sec
2.1	Deep space (escape from solar system $(HEV)_{Sun}$ = 20 km/sec)	17.00
2.2	Earth—45-deg out-of-ecliptic (a = 1 AU, e = 0)	22.80
2.3	Sun impact (minimum energy)	29.77
2.4	Earth—90-deg out-of-ecliptic (a = 1 AU, e = 0)	42.20
2.5	Earth—90-deg out-of-ecliptic (a = 2.9 AU, e = 0.74)	48.50

Now suppose that our rocket is circling the Earth in a circular parking orbit waiting to be injected onto its prescribed interplanetary trajectory. Let V_h be the hyperbolic excess velocity of the desired trajectory. Then the amount of velocity ΔV which the rocket must add to its orbital velocity is

$$\Delta V = \left(V_e^2 + V_h^2 \right)^{1/2} - \frac{V_e}{\sqrt{2}}$$

where V_e is the escape velocity at the parking orbit altitude. Consequently,

$$\frac{M_2}{M_1} = \exp\left[\frac{1}{c\sqrt{2}} V_e - \frac{1}{c} \left(V_e^2 + V_h^2 \right)^{1/2} \right]$$

Second-generation liquid oxygen-hydrogen engines will have exhaust velocities near 4.17 km/sec. This corresponds to a specific impulse of about 426 sec. Such engines are now being developed for *Apollo* and will soon be operational. Figure 1 is a graph of mass ratio vs V_h corresponding to an engine of this type in a parking orbit 200 km high. From this graph one can now easily understand the difficulties encountered when the high energy missions of Table 2 are attempted. This graph can be used to construct tables giving the total weight injected onto an interplanetary trajectory for specified initial weights. Tables 3 and 4 are such tables corresponding to initial weights of 40,000 and 220,000 lb, respectively. These are the approximate boost capabilities for *Saturn* SIB and *Saturn* V, respectively.

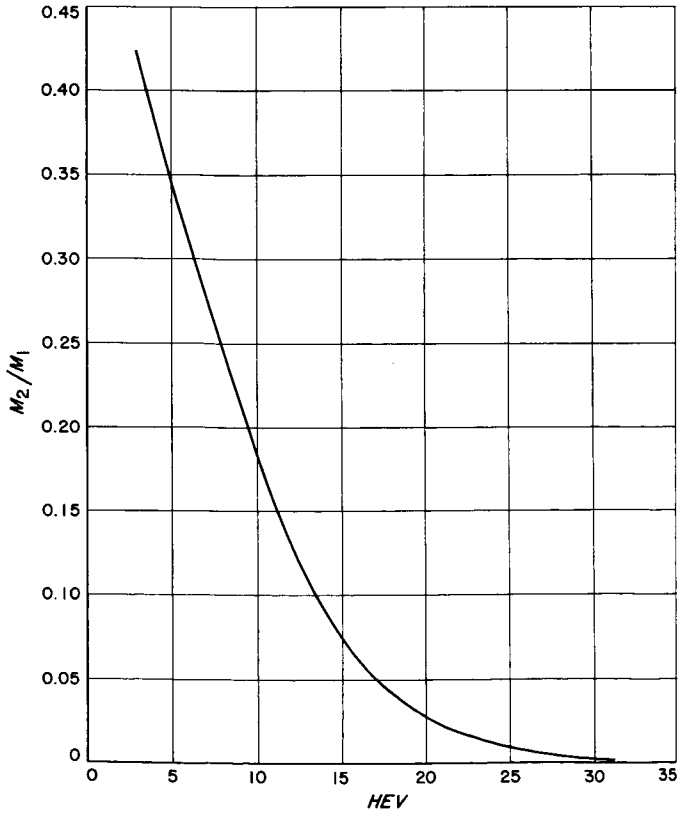

Fig. 1. Mass ratio vs V_h corresponding to a rocket engine in a circular parking orbit 200 km high

It is clear that to attempt the high-energy missions requires exhaust velocities much higher than 4.17 km/sec. This can only be done by going to nuclear or ion propulsion. It is possible that solid-core nuclear fission engines having a specific impulse of about 1000 sec will

Table 3. Approximate payload weights corresponding to 40,000 lb initial weight (I_{sp} = 426 sec)

Mission number	Injected weight, lb	Nonpayload weight, lb	Payload weight, lb
1.1	18440	4800	13440
1.2	16820	5000	11820
1.3	16200	5000	11200
1.4	16200	5000	11200
1.5	15450	5000	10450
1.6	12200	5100	7100
1.7	12060	5100	6960
1.8	11770	5200	6570
1.9	8170	5300	2870
1.10	6780	5400	1380
1.11	6200	5400	800
1.12	6200	5400	800
1.13	5930	5400	530
1.14	5560	5560	0

Table 4. Approximate payload weights corresponding to 220,000 lb initial weight (I_{sp} = 426 sec)

Mission number	Injected weight, lb	Nonpayload weight, lb	Payload weight, lb
1.14	30600	6000	24600
1.15	30600	6000	24600
1.16	26400	7000	19400
1.17	21600	9000	12600
2.1	11000	11000	0

be available within the next decade. These engines will have exhaust velocities near 9.8 km/sec. By a simple calculation one finds that the mass ratio for this injection engine will be 0.014 for the last of our high-energy missions. Since the dry weight of such a rocket may exceed 30,000 lb, the required initial weight will be nearly two million pounds, well beyond the boost capability of *Saturn* V. Figure 2 is a graph of mass ratio vs c for constant HEV = 50 km/sec.

With this rather lengthy introduction, we shall show how all the high-energy missions of Table 2 can be carried out, not by building enormous boosters with nuclear upper-stage injection engines (although these are vital in the overall picture) but by simply utilizing planetary gravitational fields.

References 1 through 3 were used as basic sources for this study.

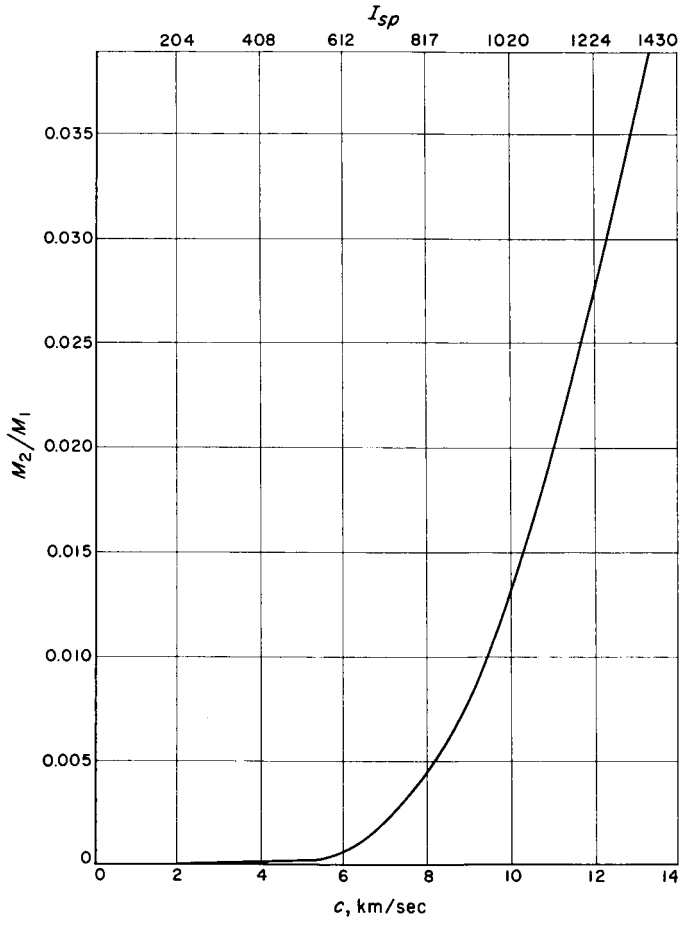

Fig. 2. Mass ratio vs c for constant HEV = 50 km/sec

II. MATHEMATICAL ANALYSIS

A. Preliminaries

We begin by stating the problem we wish to solve. Suppose a free-fall vehicle is launched from a planet P_1 at a given time T_1 and makes a closest approach with a second planet P_2 at the given time T_2. Consider the set of all possible interplanetary postencounter trajectories satisfying these given initial conditions (P_1, T_1; P_2, T_2). Out of this infinite set we single out those characterized by the following important properties:

1. Those trajectories having greatest energy.
2. Those trajectories taking a vehicle closest to the Sun.
3. Those trajectories having maximum inclination.

Our problem will be to determine these trajectories and the trajectories in the vicinity of P_2 which will generate them. We shall see that in many cases the resulting distances of closest approach to the surface of P_2 will be negative; that is to say, the trajectories pass closer to the center of P_2 than its own radius. In these cases we shall give this quantity a specified value and incorporate it as an additional initial condition.

An exact analytical solution to this problem is not known. Thus, as in the case of Ref. 1, we shall proceed by making a fundamental assumption. It shall be assumed that at any time during the flight, one and only one body influences the vehicle's motion. When the vehicle comes within a distance ρ^* of a planet, it will be assumed that only this planet influences the motion. Otherwise, the Sun will be the only body acting on the trajectory.

This region τ with radius ρ^* is called the planet's "activity sphere" or "sphere of influence." Its radius is given by

$$\rho^* = \left(\frac{m}{M}\right)^{\frac{2}{5}} R_p$$

where R_p is its distance from the Sun. The masses of the planet and the Sun are denoted by m and M, respectively. Since we shall not be concerned with the actual launch trajectory, we may forget about this portion and take m of P_1 equal to zero.

This fundamental assumption means that the trajectory will be a conic with respect to an inertial frame Σ_P centered at the center of the influencing body. When the Sun is the influencing body, we shall take Σ to be an ecliptic frame Σ_s. When P_2 is the influencing body, Σ_P will be a parallel translation of Σ_s. The $P_1 - P_2$ transfer trajectory will always be elliptical. Although this fundamental assumption greatly simplifies the solution, it produces trajectories which agree remarkably well with actual trajectories under the continuous influence of all the planets.

The mathematical tools which shall be used to solve this problem are those developed in Ref. 1. Thus to obtain a clearer understanding of the following analysis, the reader should refer to that source.

The classical methods of describing interplanetary motion by giving its orbital elements Ω, i, ω, a, e, T_p will be replaced by two orthogonal vectors denoted by **e** and **h**. The **e** vector points in the direction of perihelion passage and has magnitude equal to the trajectory's eccentricity. The **h** vector is the angular momentum vector when the mass of the vehicle is unity.

$$\mathbf{h} = \mathbf{R} \times \mathbf{V} \tag{3}$$

With the aid of these vectors the velocity at any point on the trajectory can be calculated by the formula

$$\mathbf{V} = \frac{1}{l}\, \mathbf{h} \times (\hat{\mathbf{R}} + \mathbf{e}) \tag{4}$$

where l is the trajectory's semilatus rectum given by

$$l = a(1 - e^2)$$

and $\hat{\mathbf{R}}$ is the unit position vector of the point.

The following notations will be used throughout this report:

W.R.T.S.	= with respect to the Sun
W.R.T.P_2	= with respect to P_2
$\mathbf{V}_1 = (v_1, v_2, v_3)$	= asymptotic approach velocity vector of vehicle as it enters τ W.R.T.S.

$\mathbf{V}_1' = (v_1, v_2, v_3)$ = asymptotic approach velocity vector of vehicle as it enters τ W.R.T.P_2

$\mathbf{V}_p = (u_1, u_2, u_3)$ = velocity vector of P_2 W.R.T.S. at time T_2

$\mathbf{V}_2 = (x, y, z)$ = asymptotic departing velocity vector of vehicle as it leaves τ W.R.T.S.

$\mathbf{V}_2' = (\eta_1, \eta_2, \eta_3)$ = asymptotic departing velocity vector of vehicle as it leaves τ W.R.T.P_2

$\mathbf{R}_p = (R_1, R_2, R_3)$ = position vector of P_2 at time T_2 W.R.T.S.

$\mu_s = GM$, where G is the universal gravitational constant

$\mu_p = Gm$

d = distance of closest approach to surface of P_2

r_p = radius of P_2

Trajectory parameters subscripts 1, 2, 3 refer to the $P_1 - P_2$ transfer, the hyperbolic passing trajectory in τ, and the postencounter trajectory, respectively.

B. Formulas Used in the Solution

Consider a free-fall vehicle moving on an elliptical path under the continuous influence of the Sun. Suppose it has known position vectors $\mathbf{R}_1$ and $\mathbf{R}_2$ at times T_1 and T_2, respectively. Assume that 0 deg $< \measuredangle \mathbf{R}_1, \mathbf{R}_2 <$ 180 deg. The linear distance between these two points shall be denoted by c and the semiperimeter of the resulting triangle by $s = \frac{1}{2}(R_1 + R_2 + c)$. An important theorem in celestial mechanics known as Lambert's theorem can now be applied to calculate the trajectory's semimajor axis a_1. For this particular case it can be expressed as

$$T_2 - T_1 = \left(\frac{a_1^3}{\mu_s}\right)^{1/2} \left[(1 - x_2^2)^{1/2} + \sin^{-1} x_2 - (1 - x_1^2)^{1/2} - \sin^{-1} x_1 \right] \tag{5}$$

where

$$x_1 = 1 - \frac{s}{a_1}$$

and

$$x_2 = 1 - \frac{(s - c)}{a_1}$$

After determining the value of a_1, the eccentricity can be calculated by

$$e_1 = \left\{ 1 - \frac{2}{c^2} (s - R_1)(s - R_2) \left[1 - x_1 x_2 + (1 - x_1^2)^{1/2} (1 - x_2^2)^{1/2} \right] \right\}^{1/2} \tag{6}$$

The semilatus rectum can be calculated by

$$l_1 = a_1 (1 - e_1^2) \tag{7}$$

On an interplanetary scale the position vector of our vehicle at T_2 is almost identical to the position vector of P_2. Consequently in determining the transfer trajectory $P_1 - P_2$ we may take $\mathbf{R}_2$ to be the position vector of P_2; that is, we may set $R_2 = R_p$. Since we assume the mass of P_1 is zero, we set R_1 equal to the position vector of P_1. Hence the above formulas enable us to calculate the semimajor axis, eccentricity, and semilatus rectum of the $P_1 - P_2$ transfer trajectory.

Since the $\mathbf{e}$ vector lies in the plane of motion, there exists two scalars α and β, such that

$$\mathbf{e}_1 = \alpha \mathbf{R}_1 + \beta \mathbf{R}_p \tag{8}$$

Omitting the algebra, it can be shown that this vector can be calculated by the following formulas:

$$\alpha = \frac{\begin{vmatrix} b_1 & a_{12} \\ b_2 & a_{22} \end{vmatrix}}{D} \quad ; \quad \beta = \frac{\begin{vmatrix} a_{11} & b_1 \\ a_{21} & b_2 \end{vmatrix}}{D}$$

where

$$b_i = \frac{l_1}{R_i} + e_1^2 - 1$$

$$a_{ii} = l_1$$

$$a_{ij} = \hat{\mathbf{R}}_i \cdot \mathbf{R}_j + l_1 - R_j \qquad (i \neq j)$$

$$D = \begin{vmatrix} a_{11} & a_{12} \\ a_{21} & a_{22} \end{vmatrix}$$

The perihelion distance q_1 is given by

$$q_1 = a_1 (1 - e_1)$$

Substituting this quantity into the energy equation (Eq. 1), we find that the velocity at perihelion V_q is

$$V_q = \left[\frac{\mu_s}{a_1}\left(\frac{1 + e_1}{1 - e_1}\right)\right]^{1/2}$$

Since the vehicle's velocity vector is perpendicular to its position vector at perihelion, the definition of the **h** vector in Eq. (3) enables us to calculate its magnitude as

$$h_1 = q_1 V_q = \left[\mu_s a_1 \left(1 - e_1^2\right)\right]^{1/2} \tag{9}$$

The h_1 vector, being perpendicular to the plane of motion, can now be easily calculated by

$$\mathbf{h}_1 = \frac{\mathbf{R}_1 \times \mathbf{R}_p}{|\mathbf{R}_1 \times \mathbf{R}_p|} h_1 \tag{10}$$

Suppose $\mathbf{V}'_1$ and $\mathbf{V}'_2$ are the vehicle's asymptotic vectors relative to P_2. These vectors are the velocity vectors when the vehicle enters τ at a time $T_1^* < T_2$ and when it leaves τ at a time $T_2^* > T_2$. The total time ΔT which the vehicle remains inside τ is simply

$$\Delta T = T_2^* - T_1^*$$

With respect to the Sun, these vectors are written as $\mathbf{V}_1$ and $\mathbf{V}_2$, respectively. Now at this stage in our calculations, T_1^* and T_2^* are not known. However $\frac{1}{2}\Delta T$ is very small compared with the periods of interplanetary motion; that is to say, the heliocentric angle swept out by a celestial body or vehicle during a time interval $\frac{1}{2}\Delta T$ is very small. This observation enables us to write the following equations:

$$\mathbf{V}_1 = \frac{1}{l_1} \mathbf{h}_1 \times (\hat{\mathbf{R}}_p + \mathbf{e}_1) \tag{11}$$

$$\mathbf{V}_1 = \mathbf{V}_p + \mathbf{V}'_1 \tag{12}$$

$$\mathbf{V}_2 = \mathbf{V}_p + \mathbf{V}'_2 \tag{13}$$

The first equation follows from Eq. (4) together with the fact that $\frac{1}{2}\Delta T$ is small compared with periods of interplanetary motion. Hence $\mathbf{V}'_1$ can be calculated by

$$\mathbf{V}'_1 = \frac{1}{l_1} \mathbf{h}_1 \times (\hat{\mathbf{R}}_p + \mathbf{e}_1) - \mathbf{V}_p \tag{14}$$

When the energy equation is applied to the trajectory inside τ, we find that energy is always conserved. The vehicle's velocity V'_1 with respect to P_2 as it enters τ is the same as V'_2 when it leaves τ. We shall denote this common velocity by V'. With respect to the Sun this is not true. The conservation of energy no longer holds. The amount of energy change depends upon how the vehicle enters the sphere of influence of P_2. This energy change can be easily expressed by employing conservation of energy with respect to P_2. We write

$$V'^2_1 = V'^2_2$$

Therefore

$$(\mathbf{V}_1 - \mathbf{V}_p)^2 = (\mathbf{V}_2 - \mathbf{V}_p)^2$$

which can be written as

$$V_2^2 - V_1^2 = 2\,\mathbf{V}_p \cdot (\mathbf{V}_2 - \mathbf{V}_1) \tag{15}$$

Consequently, the total energy change with respect to the Sun is simply $\mathbf{V}_p \cdot (\mathbf{V}_2 - \mathbf{V}_1)$. The asymptotic velocity $\mathbf{V}_1$ relative to the Sun as the vehicle enters τ has already been calculated. Thus, the energy change depends solely on $\mathbf{V}_2$. In terms of components this equation becomes

$$x^2 + y^2 + z^2 - 2(u_1 x + u_2 y + u_3 z) + 2\mathbf{V}_p \cdot \mathbf{V}_1 - V_1^2 = 0$$

We shall call the left-hand side of this equation G_1.

$$G_1 = x^2 + y^2 + z^2 - 2(u_1 x + u_2 y + u_3 z) + 2\mathbf{V}_p \cdot \mathbf{V}_1 - V_1^2 \tag{16}$$

It, therefore, follows that all postencounter trajectories associated with the given transfer must satisfy the equation

$$G_1 = 0 \tag{17}$$

The distance of closest approach to the surface of P_2 is very important. It must be great enough to avoid any harmful atmospheric drag. To calculate this, we first use the energy equation to calculate the trajectory's semi-major axis.

$$a_2 = \frac{\mu_p \rho^*}{2\mu_p - \rho^* V'^2} \tag{18}$$

Figure 3 describes a typical trajectory in τ with respect to P_2. It is easy to show that e_2 and ϕ are related by

$$\cos \phi = \frac{1}{e_2}$$

With the aid of this equation, we obtain

$$e_2 = \left[\frac{2V'^2}{V'^2 - \mathbf{V}'_1 \cdot \mathbf{V}'_2} \right]^{1/2} \tag{19}$$

If $\mathbf{V}_2$ is *any* velocity vector which satisfies Eq. (15), the vector $\mathbf{V}'_2$ can be determined. The eccentricity e_2 is then calculated by the above equation. The important distance of closest approach can now be calculated by

$$d = a_2 (1 - e_2) - r_p$$

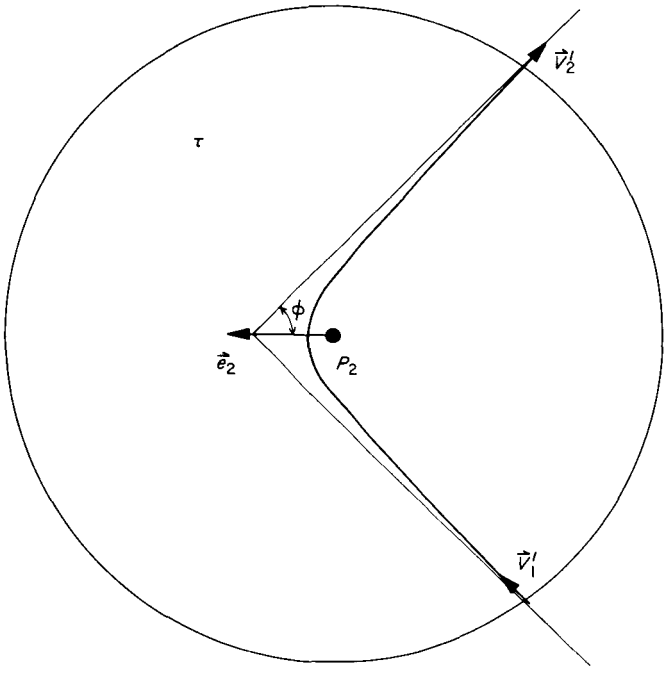

Fig. 3. Description of a typical trajectory in τ with respect to P_2

Now it may turn out that d is negative. This means that the total trajectory is physically unrealizable. It is always possible to make d positive by changing the initial conditions T_1 and T_2. However, in many cases these changes may be unacceptable. We can get around this situation by giving d a specified value beforehand. Thus, our initial conditions become (P_1, T_1; P_2, T_2; d). (In either case, $\mathbf{V}_1$, $\mathbf{V}'_1$, and a_2 are already determined.) Consequently, in this situation we must have

$$e_2 = 1 - \frac{d + r_p}{a_2}$$

Therefore, with the aid of Eq. (19) we find

$$\mathbf{V}'_1 \cdot \mathbf{V}'_2 = V'^2 \left(1 - \frac{2}{e_2^2} \right)$$

Using Eq. (12) and (13), this equation can be written as

$$\nu_1 x + \nu_2 y + \nu_3 z - K = 0$$

where

$$K = \mathbf{V}'_1 \cdot \mathbf{V}_p + V'^2 \left(1 - \frac{2}{e_2^2} \right)$$

We shall denote the left-hand side of this equation by G_2.

$$G_2 = \nu_1 x + \nu_2 y + \nu_3 z - K \tag{20}$$

Consequently, we conclude that when the initial conditions are (P_1; P_2, T_2; d), the departing asymptotic vector $\mathbf{V}_2$ must satisfy the two equations

$$G_1 = 0$$

$$G_2 = 0$$

Suppose that we have calculated a vector $\mathbf{V}_2$ compatible with the initial conditions. We now turn to the determination of T_1^* and T_2^*. If ν denotes the true anomaly of a vehicle moving on any arbitrary conic trajectory T, time unites after perihelion passage, and it can be shown that

$$T = \frac{1}{h} \int_0^{\nu} R^2 d\theta$$

where

$$R = \frac{l}{1 + \mathbf{e} \cdot \hat{\mathbf{R}}}$$

and

$$\mathbf{e} \cdot \hat{\mathbf{R}} = e \cos \theta$$

For elliptical trajectories, this becomes

$$T_E(a, e; \nu) = \gamma \left\{ \frac{2}{(1 - e^2)^{1/2}} \tan^{-1} \left[\left(\frac{1 - e}{1 + e} \right)^{1/2} \tan \frac{\nu}{2} \right] - \frac{e \sin \nu}{1 + e \cos \nu} \right\}$$

while for hyperbolic trajectories, it becomes

$$T_H(a, e; \nu) = \gamma \left\{ \frac{e \sin \nu}{1 + e \cos \nu} - \frac{1}{\sqrt{e^2 - 1}} \log \left| \frac{(e - 1) \tan \frac{\nu}{2} - (e^2 - 1)^{1/2}}{(e - 1) \tan \frac{\nu}{2} + (e^2 - 1)^{1/2}} \right| \right\}$$

where

$$\gamma = \left[\frac{a^3(1 - e^2)}{\mu} \right]^{1/2}$$

In terms of R these equations become

$$T_E(a, e; R) = \gamma \left\{ \frac{2}{(1 - e^2)^{1/2}} \tan^{-1} \left[\left(\frac{1 - e}{1 + e} \right)^{1/2} \frac{r}{R(e - 1) + l} \right] - \frac{r}{l} \right\}$$

$$T_H(a, e; R) = \gamma \left\{ \frac{r}{l} - \frac{1}{(e^2 - 1)^{1/2}} \log \left| \frac{(e - 1)r + [R(e - 1) + l] (e^2 - 1)^{1/2}}{(e - 1)r - [R(e - 1) + l] (e^2 - 1)^{1/2}} \right| \right\}$$

where

$$r = [R^2(e^2 - 1) + 2lR - l^2]^{1/2}$$

The total time ΔT spent in τ can now be calculated.

$$\Delta T = 2T_H(a_2, e_2; \rho^*)$$

Hence,

$$T_1^* = T_2 - \frac{1}{2}\Delta T \qquad (21)$$

$$T_2^* = T_2 + \frac{1}{2}\Delta T \qquad (22)$$

Let $\mathbf{R}(T_1^*)$ denote the position vector of the vehicle at time T_1^*. We can now go back to obtain a better approximation of the $P_1 - P_2$ transfer and better values for $\mathbf{V}_1$, $\mathbf{V}'_1$, $\mathbf{V}_2$, a_2, and e_2. This can be carried out by first using Lambert's theorem (Eq. 5) with $\mathbf{R}_2$ replaced by $\mathbf{R}(T_1^*)$. In our first approximation, we used $\mathbf{R}_p$. The new eccentricity e_1 and semilatus rectum l_1 are determined by Eq. (6) and (7). The new $\mathbf{e}$ vector is obtained by Eq. (8) and the new $\mathbf{h}$ vector is calculated by Eq. (9) and (10). The new approach asymptotic velocity vector $\mathbf{V}_1$ is now calculated by Eq. (11) where $\hat{\mathbf{R}}_p$ is replaced by $\hat{\mathbf{R}}(T_1^*)$. With respect to P_2 we calculate $\mathbf{V}'_1$ by

$$\mathbf{V}'_1 = \mathbf{V}_1 - \mathbf{V}_p(T_1^*)$$

These vectors determine a new function G_1 and a new equation which $\mathbf{V}_2$ must satisfy $G_1 = 0$, and a new semimajor axis a_2 by Eq. (18). If the initial conditions were given by the set (P_1, T_1; P_2, T_2; d), a new G_2 function is calculated and our $\mathbf{V}_2$ vector must satisfy the new equations $G_1 = 0$ and $G_2 = 0$. After determining the new asymptotic vector $\mathbf{V}_2$, we obtain new values for T_1^* and T_2^* by Eq. (21) and (22). It is now clear that this iteration process can be repeated, obtaining better and better approximations. However, it turns out that the first approximation is so good very little improvement occurs while seeking more iterations. Comparison with exact trajectories when all bodies influence the motion also shows that the first approximation is remarkably accurate. Thus, in practice we shall only determine the first approximation.

After calculating a suitable departing asymptotic velocity vector $\mathbf{V}_2$, the total trajectory can be easily calculated. By referring to Fig. 3 we notice that the $\mathbf{e}$ vector associated with the trajectory in τ can be calculated by

$$\mathbf{e}_2 = \frac{\mathbf{V}'_1 - \mathbf{V}'_2}{|\mathbf{V}'_1 - \mathbf{V}'_2|} e_2$$

The $\mathbf{h}$ vector is obtained by

$$\mathbf{h}_2 = \frac{\mathbf{V}'_1 \times \mathbf{V}'_2}{|\mathbf{V}'_1 \times \mathbf{V}'_2|} [\mu_p a_2 (1 - e_2^2)]^{1/2}$$

The time of perihelion passage is simply T_2. The postencounter trajectory is just as easy to calculate as the trajectory in τ. The $\mathbf{h}$ vector is determined by

$$\mathbf{h}_3 = \mathbf{R}_p \times \mathbf{V}_2$$

The $\mathbf{e}$ vector follows from Eq. (4) by cross multiplying on the right by $\mathbf{h}_3$.

$$\mathbf{e}_3 = \frac{1}{\mu_s} \mathbf{V}_2 \times \mathbf{h}_3 - \mathbf{R}_p$$

III. DEEP SPACE POSTENCOUNTER TRAJECTORIES

In this Section we shall consider postencounter trajectories designed for deep space probes, i.e., trajectories taking a vehicle as far as possible from the Sun. From the analysis laid down in Section II we have seen that when the initial conditions are (P_1, T_1; P_2, T_2), the dedeparting asymptotic velocity vector $\mathbf{V}_2$ must satisfy $G_1 = 0$. When the initial conditions are (P_1, T_1; P_2, T_2; d) this vector must satisfy two equations: $G_1 = 0$ and $G_2 = 0$. In either case the total trajectory is then determined. Now if all possible postencounter trajectories associated with particular initial conditions are elliptical, their aphelion distance q is defined as

$$q = a_3(1 + e_3)$$

This is the greatest distance the postencounter trajectory has from the Sun. In this case one can calculate the vector $\mathbf{V}_2$ which will yield the greatest possible value for q by maximizing the function $a_3(1 + e_3)$ such that the constraining equation or equations are satisfied. However, when hyperbolic postencounter trajectories are possible, there is no maximum distance q. In this case we shall seek that trajectory which has maximum hyperbolic excess velocity. This will be the trajectory having greatest energy. Thus when hyperbolic postencounter trajectories are possible, we shall seek to find that vector $\mathbf{V}_2$ which maximizes V_2^2. We shall see later that in the case of elliptical postencounter trajectories, the highest energy postencounter trajectory will

be very nearly the one with greatest aphelion q. Thus in either case deep space postencounter trajectories will be determined by simply maximizing V_2^2 such that the constraining equation or equations are satisfied. This will be done by the method of Lagrange multipliers.

A. The Determination of Deep Space Postencounter Trajectories Corresponding to the Initial Conditions ($P_1, T_1; P_2, T_2$)

To maximize V_2^2 subject to the constraining equation $G_1 = 0$, we determine all extreme values by solving the system

$$\frac{\partial V_2^2}{\partial x} - \lambda_1 \frac{\partial G_1}{\partial x} = 0$$

$$\frac{\partial V_2^2}{\partial y} - \lambda_1 \frac{\partial G_1}{\partial y} = 0$$

$$\frac{\partial V_2^2}{\partial z} - \lambda_1 \frac{\partial G_1}{\partial z} = 0$$

$$G_1 = 0$$

where λ_1 is the undetermined Lagrange multiplier. All solutions of this system will extremize V_2^2 and satisfy $G_1 = 0$. The first three equations yield

$$x = \lambda_0 u_1$$

$$y = \lambda_0 u_2$$

$$z = \lambda_0 u_3$$

where $\lambda_0 = \lambda_1/(\lambda_1 - 1)$. Substituting these equations into $G_1 = 0$, we obtain a quadratic equation in λ_0, the solution of which is

$$\lambda_0 = 1 \pm \frac{V'}{V_p}.$$

Consequently the vectors which extremize V_2^2 are

$$\mathbf{V}_2 = \left(1 + \frac{V'}{V_p}\right)\mathbf{V}_p$$

and

$$\mathbf{V}_2 = \left(1 - \frac{V'}{V_p}\right)\mathbf{V}_p$$

The magnitudes of these vectors are $|V_p + V'|$ and $|V_p - V'|$, respectively. Thus, the solution we seek is

$$\mathbf{V}_2 = \left(1 + \frac{V'}{V_p}\right)\mathbf{V}_p \tag{23}$$

The total trajectory can now be calculated by referring to Section II.

Let $\sigma = \measuredangle\, \mathbf{V}_p, \mathbf{V}_1$. Then the length of the total velocity change $\Delta\mathbf{V}$ with respect to the Sun after encounter can be calculated by

$$\Delta V = [(\mathbf{V}_2 - \mathbf{V}_1)^2]^{1/2} = V'[2(1 - \cos\sigma)]^{1/2} \tag{24}$$

The actual velocity increase δV is given by

$$\delta V = V_p + V' - (V_p^2 + 2V_p V' \cos\sigma + V'^2)^{1/2}$$

This increase is generally very great and can easily result in a hyperbolic postencounter trajectory. This can be determined by examining the sign of the resulting semimajor axis a_3 given by

$$a_3 = \frac{\mu_s R_p}{2\mu_s - R_p(V_p + V')^2} \tag{25}$$

This highest energy postencounter trajectory will be elliptical or hyperbolic according to whether $a_3 > 0$ or $a_3 < 0$, respectively. It will be parabolic if the denominator vanishes.

We digress a moment to consider the following problem. Suppose P_1 and P_2 have circular co-planar motion. Suppose also that the $P_1 - P_2$ transfer is Hohmann (see Fig. 4), that is, one having minimum energy. What is the launch trajectory's minimum hyperbolic excess velocity V_h at P_1 such that after encountering P_2 it will escape the entire solar system? The radius of P_2's orbit is also to be determined.

First of all we use the fact that a minimum energy escape trajectory is parabolic. In view of the above equation, this means that

$$2\mu_s = R_p(V_p + V')^2$$

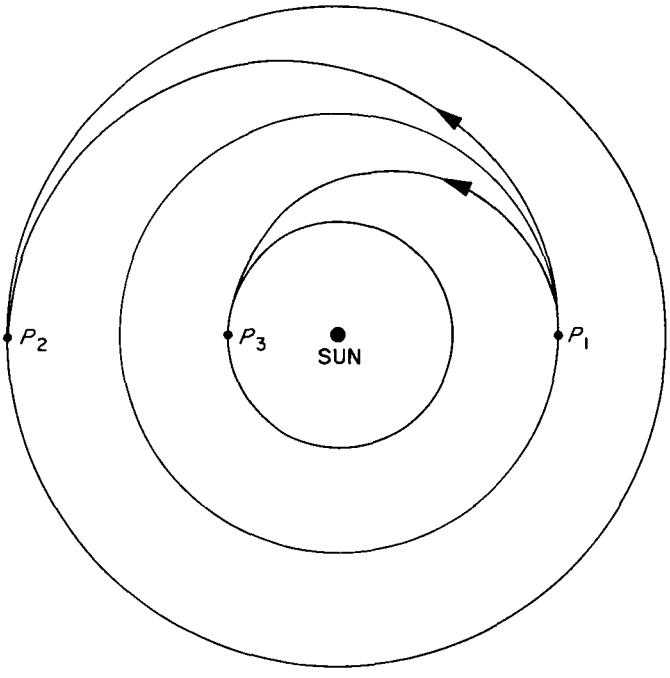

Fig. 4. Hohmann's transfer to P_2 when the orbit of P_2 lies inside or outside the orbit of P_1

From Eq. (24) we observe that the orbit of P_2 must be outside of the orbit of P_1. Consequently, this equation becomes

$$2\mu_s = R_p(2V_p - V_1)^2$$

By employing the energy equation, we obtain

$$\sqrt{2\mu_s} = \sqrt{R_p}\left\{2\left(\frac{\mu_s}{R_p}\right)^{1/2} - \left[\mu_s\left(\frac{2}{R_p} - \frac{2}{R_1 + R_p}\right)\right]^{1/2}\right\}$$

where R_1 is the radius of P_1's orbit. Thus, we have

$$1 = \sqrt{2} - \left(\frac{R_1}{R_1 + R_p}\right)^{1/2}$$

The solution is

$$R_p = 2(1 + \sqrt{2})R_1$$

Consequently the minimum launch hyperbolic excess velocity is

$$V_h = \left(\frac{\mu_s}{R_1}\right)^{1/2}\left\{2(\sqrt{2} - 1)^{1/2} - 1\right\}$$

For the case P_1 = Earth, this required launch hyperbolic excess velocity is 8.58 km/sec. The radius of P_2's orbit would be 4.83 A.U. This means that when P_2 is Jupiter, there will *always* exist hyperbolic postencounter trajectories.

These results are general and can obviously be applied to regions in the vicinity of the Earth. Thus, we can view P_1 as a rocket in a 200-km high parking orbit. In this case ΔV_0 = 1.415 km/sec and the radius of P_2 would be 31,800 km. Since escape velocity for such a vehicle in a 200-km parking orbit is 11.0 km/sec, this represents a savings of about 1.0 km/sec. In the case of escaping the entire solar system, the savings in injection velocity would be about 2.72 km/sec.

The above analysis shows that for deep space postencounter trajectories, P_2 should lie outside the orbit of P_1. Notice that if the $P_1 - P_2$ transfer is Hohmann, Eq. (24) shows that $\Delta V = \delta V = 0$ when P_2 is inside P_1's orbit while $\Delta V = \delta V = 2V'$ when P_2 is outside P_2's orbit.

We shall now consider numerical examples of these cases when P_1 = Earth and P_2 = Venus and Mars. The tables of trajectories will adhere to the following notations, which will also be used in other tables.

$T_{12} = T_2 - T_1$

HEV_1 = launch hyperbolic excess velocity

θ_{12} = heliocentric transfer angle from P_1 to P_2

ϕ_{12} = inclination of $P_1 - P_2$ transfer trajectory

$\mathbf{B} \cdot \hat{\mathbf{T}}$ = projection of $\mathbf{B}$ vector on $\hat{\mathbf{T}}$ axis (see Ref. 1)

$\mathbf{B} \cdot \hat{\mathbf{R}}$ = projection of $\mathbf{B}$ vector on $\hat{\mathbf{R}}$ axis (see Ref. 1)

TISI = total time vehicle spends in τ

DOCA = distance of closest approach to P_2's surface

V_∞ = hyperbolic excess velocity

All launch dates have 1200_h GMT as launch times.

Table 5 describes a set of Earth–Venus–Deep Space trajectories having a fixed launch date with varying flight times. One notices that the set begins with trajectories which penetrate deeply into the Venus surface. As the flight times begin to increase, the vector $\mathbf{V}_1$ becomes

more parallel to V_p; hence, less deflections are necessary. It is not until the transfers become greater than 127 deg that the surface penetrations stop.

Table 6 contains a similar set of Earth–Mars–Deep Space trajectories. One notices that the deflections are much higher than those occurring when P_2 is Venus.

Table 5. Earth–Venus deep space (launch date Aug. 22, 1970)

T_{12}, days	HEV_1, km/sec	θ_{12}, deg	ϕ_{12}, deg	a_1, AU	e_1	Aphelion, AU	$B \cdot \hat{T}$, km	$B \cdot \hat{R}$, km	V_1, km/sec	TISI, days	DOCA, km	DA, deg	V_2, km/sec	a_3, AU	e_3	Aphelion$_3$, AU	V_∞, km/sec
70.0	7.504	62.80	2.68	0.7019	0.4421	1.0122	−1019.	19.	34.444	0.90	−5754.	104.94	50.629	−7.854	1.0922	—	10.628
74.0	6.630	69.19	2.25	0.7238	0.3983	1.0122	−1320.	33.	35.020	1.00	−5630.	101.63	49.168	25.614	0.9718	50.507	—
78.0	5.872	75.59	1.85	0.7442	0.3595	1.0122	−1715.	56.	35.525	1.10	−5461.	98.29	47.832	5.340	0.8646	9.957	—
82.0	5.218	81.99	1.47	0.7632	0.3255	1.0122	−2234.	93.	35.964	1.21	−5229.	94.91	46.609	3.129	0.7692	5.5358	—
86.0	4.659	88.41	1.11	0.7804	0.2960	1.0122	−2922.	154.	36.345	1.34	−4910.	91.46	45.491	2.285	0.6841	3.8482	—
90.0	4.185	94.84	0.74	0.7959	0.2707	1.0122	−3839.	256.	36.672	1.48	−4465.	87.89	44.473	1.842	0.6084	2.9627	—
94.0	3.793	101.28	0.37	0.8096	0.2492	1.0122	−5062.	434.	36.951	1.64	−3843.	84.18	43.551	1.572	0.5413	2.4229	—
98.0	3.476	107.72	0.02	0.8216	0.2312	1.0122	−6686.	750.	37.188	1.81	−2974.	80.32	42.724	1.392	0.4824	2.0635	—
102.0	3.231	114.17	0.44	0.8319	0.2164	1.0122	−8807.	1321.	37.386	2.00	−1770.	76.29	41.995	1.266	0.4314	1.8122	—
106.0	3.057	120.63	0.90	0.8405	0.2044	1.0122	−11462.	2356.	37.551	2.19	− 149.	72.18	41.370	1.177	0.3884	1.6341	—
110.0	2.955	127.09	1.43	0.8477	0.1948	1.0122	−14460.	4174.	37.685	2.38	1890.	68.15	40.864	1.113	0.3540	1.5070	—
114.0	2.933	133.56	2.07	0.8535	0.1872	1.0122	−17082.	7101.	37.791	2.54	4090.	64.61	40.500	1.072	0.3294	1.4251	—
118.0	3.010	140.02	2.85	0.8580	0.1815	1.0122	−17811.	10926.	37.874	2.63	5695.	62.22	40.317	1.052	0.3170	1.3855	—

Table 6. Unrealizable Earth–Mars deep space (launch date May 19, 1971)

T_{12}, days	HEV_1, km/sec	θ_{12}, deg	ϕ_{12}, deg	a_1, AU	e_1	Aphelion, AU	$B \cdot \hat{T}$, km	$B \cdot \hat{R}$, km	V_1, km/sec	TISI, days	DOCA, km	DA, deg	V_2, km/sec	a_3, AU	e_3	Aphelion$_3$, AU	V_∞, km/sec
100.0	5.347	90.01	1.83	1.607	0.3706	2.2026	400.	0.	27.045	1.24	−3264.	97.18	36.216	−31.398	1.0440	—	5.316
106.0	4.879	93.82	1.81	1.519	0.3338	2.0260	466.	0.	26.456	1.37	−3245.	99.80	35.303	23.489	0.9412	45.5968	—
112.0	4.490	97.62	1.79	1.453	0.3037	1.8943	541.	−1.	25.956	1.51	−3225.	102.57	34.478	9.282	0.8512	17.1828	—
118.0	4.167	101.43	1.77	1.403	0.2789	1.7943	624.	−1.	25.529	1.66	−3205.	105.50	33.729	6.059	0.7720	10.7365	—
124.0	3.901	105.24	1.75	1.364	0.2586	1.7167	715.	−3.	25.162	1.83	−3185.	108.63	33.048	4.640	0.7021	7.8977	—
130.0	3.682	109.03	1.74	1.334	0.2419	1.6567	813.	−5.	24.844	2.01	−3166.	112.00	32.428	3.847	0.6404	6.3106	—
136.0	3.502	112.82	1.71	1.311	0.2283	1.6103	915.	−8.	24.567	2.20	−3151.	115.62	31.862	3.344	0.5859	5.3032	—
142.0	3.355	116.60	1.69	1.292	0.2173	1.5728	1017.	−13.	24.323	2.41	−3140.	119.55	31.347	2.999	0.5378	4.6134	—
148.0	3.236	120.37	1.67	1.277	0.2083	1.5430	1112.	−20.	24.107	2.63	−3137.	123.79	30.878	2.752	0.4955	4.1156	—
154.0	3.139	124.12	1.64	1.266	0.2012	1.5207	1193.	−29.	23.913	2.86	−3142.	128.36	30.454	2.569	0.4586	3.7471	—
160.0	3.061	127.85	1.62	1.257	0.1955	1.5027	1247.	−43.	23.737	3.10	−3157.	133.28	30.072	2.429	0.4266	3.4652	—
166.0	2.999	131.56	1.59	1.249	0.1911	1.4877	1263.	−60.	23.576	3.33	−3184.	138.53	29.730	2.323	0.3991	3.2501	—
172.0	2.949	135.25	1.55	1.244	0.1877	1.4775	1231.	−82.	23.426	3.55	−3220.	144.05	29.427	2.242	0.3760	3.0850	—
178.0	2.911	138.91	1.52	1.241	0.1852	1.4708	1141.	−108.	23.285	3.76	−3263.	149.80	29.160	2.180	0.3568	2.9578	—
184.0	2.882	142.54	1.47	1.238	0.1835	1.4652	994.	−137.	23.152	3.93	−3308.	155.65	28.927	2.135	0.3413	2.8637	—
190.0	2.861	146.15	1.42	1.237	0.1824	1.4626	795.	−168.	23.025	4.08	−3349.	161.48	28.727	2.102	0.3291	2.7938	—
196.0	2.847	149.73	1.36	1.236	0.1819	1.4608	558.	−199.	22.903	4.19	−3382.	167.07	28.556	2.079	0.3198	2.7439	—
202.0	2.839	153.27	1.29	1.236	0.1819	1.4608	300.	−231.	22.784	4.26	−3402.	171.92	28.411	2.065	0.3132	2.7118	—
208.0	2.837	156.79	1.19	1.237	0.1822	1.4624	41.	−265.	22.669	4.30	−3408.	174.34	28.289	2.059	0.3089	2.6950	—
214.0	2.840	160.27	1.07	1.238	0.1830	1.4645	−204.	−301.	22.556	4.30	−3403.	172.25	28.187	2.060	0.3064	2.6912	—
220.0	2.847	163.72	0.89	1.240	0.1840	1.4682	−423.	−344.	22.445	4.28	−3387.	168.12	28.103	2.066	0.3057	2.6976	—
226.0	2.858	16713.	0.63	1.242	0.1854	1.4723	−609.	−403.	22.336	4.22	−3362.	163.52	28.038	2.077	0.3068	2.7142	—
232.0	2.879	170.51	0.19	1.244	0.1870	1.4766	−754.	−494.	22.229	4.13	−3330.	158.56	28.001	2.097	0.3103	2.7477	—

This is because $\mathbf{V}_1'$ and $\mathbf{V}_p$ point in almost opposite directions. The mass of Mars is not able to handle these large deflections without requiring negative distances of closest approach.

Earth–Jupiter-Escape, 1967–1978. Table 6 shows that the mass of Mars is too small to enable physically realizable trajectories to occur. The great planet Jupiter is over 317 times the mass of the Earth. We have already seen that for this planet, there will always exist hyperbolic postencounter trajectories. Thus there is a good chance for positive distances of closest approach.

Minimum energy transfers to Jupiter usually require flight times ranging from 750 to 850 days. The resulting hyperbolic excess velocities are from 8.5 to 9 km/sec. By raising the hyperbolic excess velocity to 11 km/sec one can obtain 450- to 550-day transfers. This launch hyperbolic excess velocity is well within the capabilities of second-generation liquid oxygen-hydrogen rocket engines. In particular the *Titan* II–*Centaur* vehicle equipped with an extra high-energy third stage could inject a payload of approximately 500 lb on these trajectories. By doing this, one could save about 300 days in the Earth–Jupiter transfer and raise the energy of the postencounter trajectory.

Preliminary calculations proved so remarkable that a systematic numerical study covering eleven launch opportunities from 1967 through 1978 was undertaken. The first six periods used Earth–Jupiter transfers requiring 11.0 km/sec while the last five used 11.5 km/sec transfers. The results are shown in Tables 7 through 17. Figures displaying the geometrical configuration of the trajectories are also given. The total time required for the vehicle to cross the orbit of Saturn is given by TTS. All the trajectories have positive distances of closest approach and hence all are physically realizable.

The trajectories clearly display the great influence Jupiter can have on postencounter trajectories. The encounter takes rather moderate energy elliptical trajectories and transforms them into very high energy escape trajectories with hyperbolic excess velocities in the neighborhood of 20 km/sec. These encounters add more than 12 km/sec to the vehicle's velocity at encounter. All this velocity increase is free. The only penalty is a few extra pounds for planetary approach guidance.

There are some very interesting general characteristics about these trajectories which should be carefully noted as they may suggest possible techniques for approach guidance. The possibility of performing scientific observations or dropping off secondary payloads should also be considered. First of all, one notices that all the trajectories approach Jupiter from the sunny side. The vehicle will spend a rather long time in τ as its radius is almost 47 million miles. The distances of closest approach are well outside its atmosphere.

The positions of Saturn, Uranus, Neptune, and Pluto make trips to these planets by this technique unfavorable during most of this eleven-year period. One has to wait until 1976 before trips to Saturn become possible. After that the next opportunity will be in 1996 because

Table 7. Earth–Jupiter escape, 1967 (launch HEV = 11.0 km/sec)

Launch date, 1967	T_{12}, days	θ_{12}, deg	ϕ_{12}, deg	a_1, AU	e_1	$B \cdot \hat{T}$, km	$B \cdot \hat{R}$, km	V_1, km/sec	TISI, days	DOCA, km	DA, deg	V_2, km/sec	a_2, AU	e_2	V_∞, km/sec	TTS, yr
10/21	556.0	156.60	3.27	5.714	0.8277	571286.	−2245.	13.050	92.21	94685.	115.17	24.326	−3.333	2.635	16.315	3.342
10/23	544.0	153.86	2.94	6.097	0.8382	548254.	−696.	13.420	89.73	90604.	114.16	24.692	−3.123	2.745	16.855	3.270
10/25	532.0	151.11	2.68	6.571	0.8497	525266.	433.	13.807	87.26	86251.	113.18	25.075	−2.927	2.862	17.411	3.198
10/27	524.0	148.67	2.49	6.930	0.8573	511128.	1106.	14.059	85.73	83493.	112.57	25.324	−2.811	2.938	17.766	3.152
10/29	516.0	146.22	2.32	7.349	0.8653	497049.	1635.	14.317	84.21	80635.	111.98	25.579	−2.700	3.018	18.127	3.106
10/31	510.0	143.92	2.19	7.686	0.8711	487304.	2007.	14.502	83.15	78607.	111.57	25.761	−2.625	3.075	18.383	3.073
11/2	506.0	141.77	2.09	7.896	0.8744	481846.	2278.	14.607	82.56	77455.	111.34	25.865	−2.584	3.108	18.528	3.052
11/4	504.0	139.77	2.00	7.943	0.8752	480633.	2482.	14.630	82.43	77193.	111.29	25.888	−2.575	3.115	18.560	3.045
11/6	504.0	137.91	1.93	7.820	0.8733	483656.	2643.	14.570	82.76	77821.	111.43	25.829	−2.598	3.096	18.478	3.050
11/8	506.0	136.21	1.87	7.546	0.8688	490939.	2776.	14.427	83.56	79323.	111.74	25.690	−2.654	3.052	18.283	3.069
11/10	512.0	134.81	1.82	7.037	0.8596	506846.	2869.	14.128	85.29	82552.	112.43	25.395	−2.779	2.961	17.868	3.113
11/12	522.0	133.70	1.79	6.415	0.8464	531616.	2918.	13.686	87.98	87366.	113.50	24.961	−2.982	2.827	17.247	3.183
11/14	538.0	133.05	1.78	5.721	0.8285	569895.	2871.	13.056	92.12	94281.	115.17	24.340	−3.324	2.639	16.336	3.291

the synodic period of Saturn relative to Jupiter is about 20 years. Earth–Jupiter–Pluto transfers come in 1977. The total flight time to Pluto will be about 7 years. Ordinarily this would require 40 to 50 years on direct minimum energy Earth–Pluto transfer when the hyperbolic excess velocity is about 11.6 km/sec.

The trajectory's departing hyperbolic asymptote sweeps out a complete revolution of the solar system in about 12 years, which is approximately Jupiter's synodic period relative to the Earth.

For truly deep space exploration near the ecliptic plane, these trajectories are most economical. One interesting possibility is that of utilizing a Jupiter encounter together with ion propulsion. This would increase the approach velocity V' and hence the velocity after encounter $V_p + V'$. The engine could also be turned on after encounter until its propellant or energy has been exhausted.

Tables 7 through 17 and Fig. 5 through 26 relate to the above discussion.

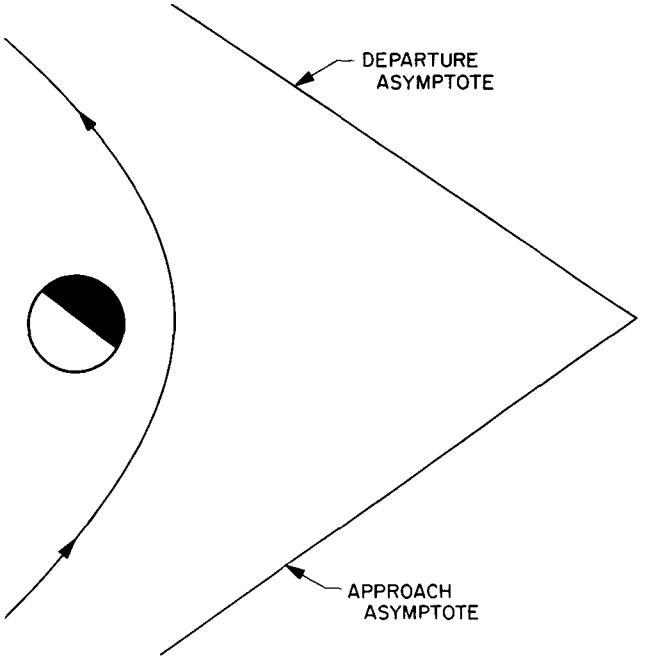

Fig. 6. November 4, 1967, Earth–Jupiter-escape trajectory during its closest approach to Jupiter

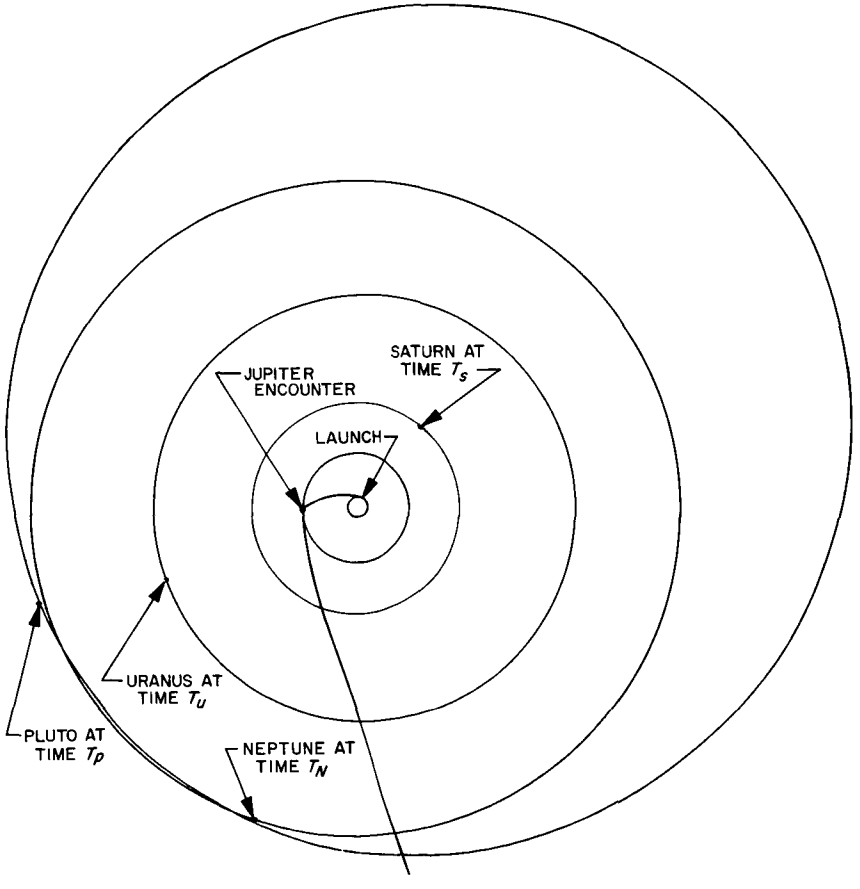

Fig. 5. Planetary configuration for Earth–Jupiter-escape, 1967 (Nov. 4 trajectory)

Table 8. Earth–Jupiter escape, 1968 (launch HEV = 11.0 km/sec)

Launch date, 1968	T_{12}, days	θ_{12}, deg	ϕ_{12}, deg	a_1, AU	e_1	$B \cdot \hat{T}$, km	$B \cdot \hat{R}$, km	V_1, km/sec	TISI, days	DOCA, km	DA, deg	V_2, km/sec	a_3, AU	e_3	V_∞, km/sec	TTS, yr
11/22	532.0	152.06	2.58	6.481	0.8488	492941.	−3748.	13.759	85.45	73899.	114.32	25.365	−2.797	2.944	17.809	3.208
11/24	522.0	149.44	2.39	6.957	0.8589	475565.	−2994.	14.094	83.51	70538.	113.54	25.694	−2.656	3.048	18.276	3.148
11/26	514.0	146.96	2.23	7.398	0.8671	462353.	−2467.	14.359	82.03	67896.	112.95	25.955	−2.553	3.131	18.643	3.102
11/28	508.0	144.63	2.11	7.756	0.8731	453241.	−2092.	14.550	81.01	66036.	112.54	26.142	−2.483	3.191	18.903	3.069
11/30	504.0	142.46	2.01	7.980	0.8766	448148.	−1822.	14.659	80.43	64986.	112.31	26.249	−2.444	3.226	19.051	3.048
12/2	500.0	140.28	1.91	8.217	0.8801	443052.	−1585.	14.768	79.86	63903.	112.08	26.356	−2.407	3.261	19.199	3.028
12/4	498.0	138.25	1.84	8.269	0.8808	441921.	−1412.	14.791	79.73	63650.	112.04	26.380	−2.399	3.268	19.231	3.020
12/6	498.0	136.37	1.77	8.126	0.8788	444744.	−1286.	14.727	80.06	64226.	112.18	26.318	−2.420	3.248	19.146	3.026
12/8	502.0	134.80	1.72	7.648	0.8714	455552.	−1222.	14.495	81.28	66460.	112.66	26.092	−2.501	3.175	18.833	3.057
12/10	508.0	133.37	1.67	7.102	0.8618	470475.	−1176.	14.186	82.96	69445.	113.35	25.790	−2.617	3.078	18.411	3.102
12/12	518.0	132.25	1.63	6.442	0.8482	493682.	−1171.	13.730	85.57	73889.	114.42	25.345	−2.806	2.938	17.780	3.172
12/14	536.0	131.74	1.60	5.647	0.8276	533761.	−1235.	13.012	90.04	81007.	116.27	24.640	−3.160	2.720	16.755	3.296
12/16	566.0	132.14	1.57	4.843	0.8003	599175.	−1420.	11.978	97.38	90880.	119.39	23.619	−3.837	2.415	15.206	3.499

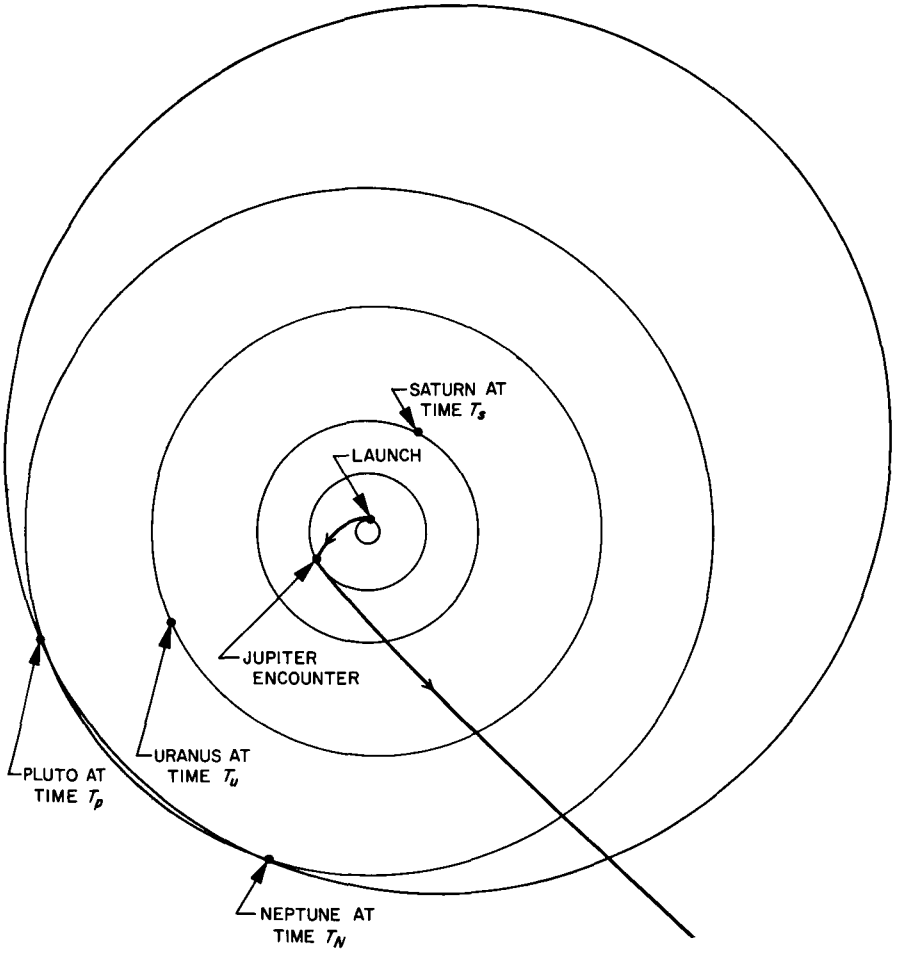

Fig. 7. Planetary configuration for Earth–Jupiter-escape, 1968 (Dec. 4 trajectory)

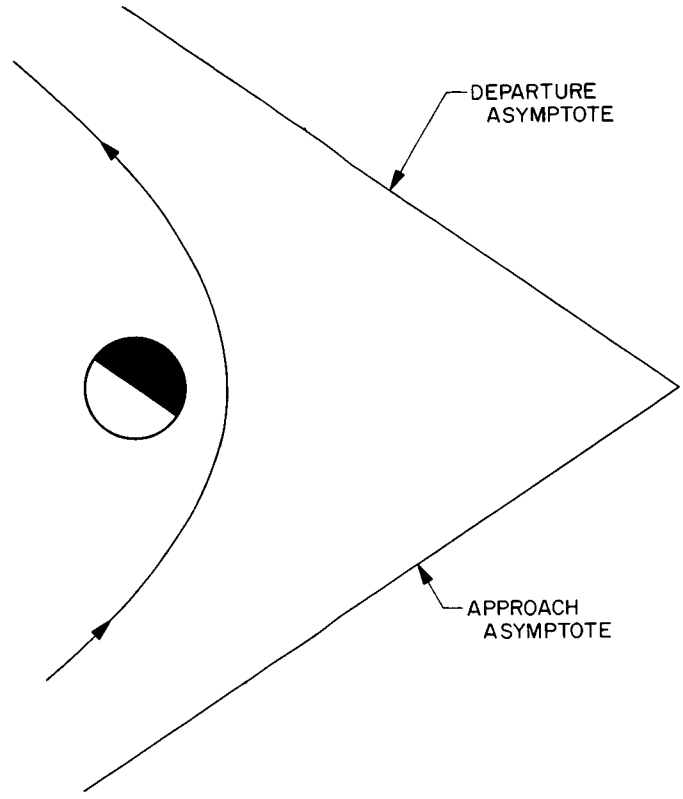

Fig. 8. December 4, 1968, Earth–Jupiter-escape trajectory during its closest approach to Jupiter

Table 9. Earth–Jupiter escape, 1969–70 (launch HEV = 11.0 km/sec)

Launch date, 1969–70	T_{12}, days	θ_{12}, deg	ϕ_{12}, deg	a_1, AU	e_1	$B \cdot \hat{T}$, km	$B \cdot \hat{R}$, km	V_1, km/sec	TISI, days	DOCA, km	DA, deg	V_2, km/sec	a_2, AU	e_2	V_∞, km/sec	TTS, yr
12/17	544.0	157.89	2.08	5.600	0.8266	495847.	−7663.	13.142	86.41	68278.	117.09	25.182	−2.928	2.828	17.407	3.308
12/19	532.0	155.08	1.89	6.008	0.8330	475084.	−6751.	13.538	84.04	64694.	116.08	25.572	−2.747	2.950	17.972	3.234
12/21	522.0	152.42	1.75	6.415	0.8479	458400.	−6113.	13.875	82.14	61669.	115.27	25.903	−2.608	3.055	18.443	3.174
12/23	514.0	149.91	1.63	6.790	0.8560	445702.	−5658.	14.144	80.68	59286.	114.65	26.166	−2.506	3.139	18.814	3.128
12/25	506.0	147.41	1.53	7.232	0.8646	433103.	−5275.	14.420	79.23	56830.	114.05	26.437	−2.409	3.226	19.191	3.081
12/27	498.0	144.90	1.45	7.758	0.8736	420590.	−4949.	14.703	77.79	54299.	113.46	26.715	−2.315	3.317	19.575	3.034
12/29	492.0	142.55	1.38	8.192	0.8801	411969.	−4713.	14.905	76.80	52520.	113.05	26.914	−2.252	3.382	19.847	3.001
12/31	488.0	140.36	1.32	8.467	0.8839	407158.	−4544.	15.021	76.24	51518.	112.82	27.028	−2.217	3.420	20.002	2.980
1/2	486.0	138.32	1.27	8.532	0.8848	406108.	−4429.	15.048	76.11	51302.	112.77	27.054	−2.209	3.428	20.037	2.973
1/4	484.0	136.28	1.22	8.591	0.8856	405042.	−4323.	15.072	75.99	51061.	112.73	27.078	−2.202	3.436	20.070	2.965
1/6	486.0	134.56	1.17	8.214	0.8804	411499.	−4290.	14.916	76.74	52413.	113.03	26.926	−2.249	3.385	19.862	2.983
1/8	488.0	132.83	1.13	7.870	0.8754	417968.	−4252.	14.759	77.49	53718.	113.36	26.774	−2.296	3.335	19.655	3.002
1/10	494.0	131.42	1.09	7.248	0.8649	432109.	−4265.	14.432	79.13	56539.	114.04	26.456	−2.403	3.231	19.215	3.047

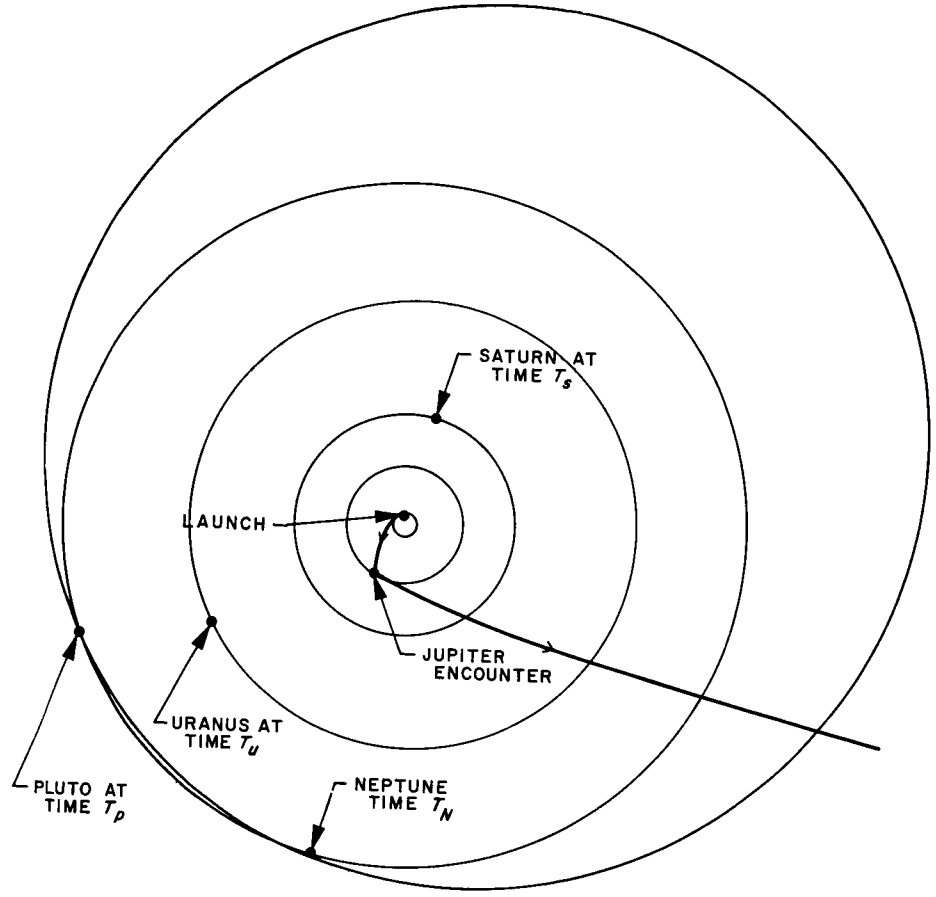

Fig. 9. Planetary configuration for Earth–Jupiter-escape, 1969–70 (Jan. 4 trajectory)

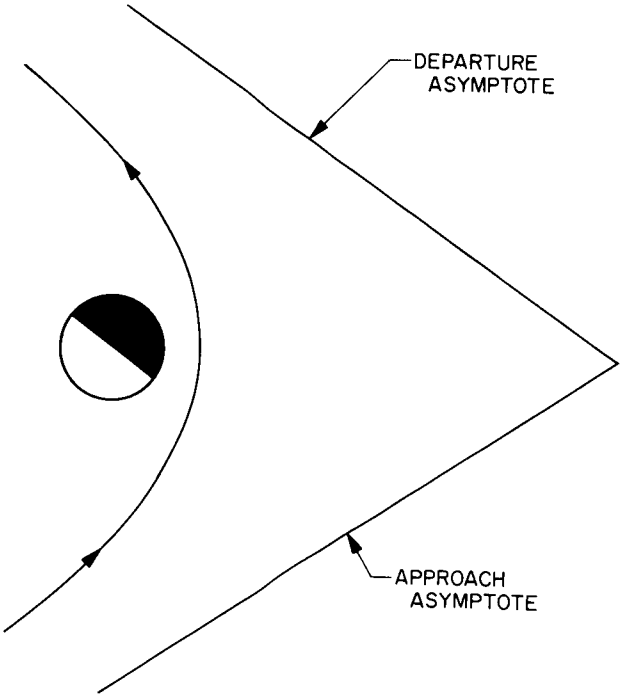

Fig. 10. January 4, 1970, Earth–Jupiter-escape trajectory during its closest approach to Jupiter

Table 10. Earth–Jupiter escape, 1971 (launch HEV = 11.0 km/sec)

Launch date, 1971	T_{12}, days	θ_{12}, deg	ϕ_{12}, deg	a_1, AU	e_1	$B \cdot \hat{T}$, km	$B \cdot \hat{R}$, km	V_1, km/sec	TISI, days	DOCA, km	DA, deg	V_2, km/sec	a_3, AU	e_3	V_∞, km/sec	TTS, yr
1/23	496.0	148.75	0.38	6.832	0.8568	416843.	−6328.	14.438	76.70	49962.	115.09	26.864	−2.314	3.263	19.579	3.055
1/25	490.0	146.39	0.37	7.168	0.8632	408320.	−6241.	14.644	75.70	48338.	114.65	27.065	−2.250	3.328	19.856	3.021
1/27	482.0	143.86	0.36	7.725	0.8728	396107.	−6123.	14.942	74.29	45890.	114.04	27.358	−2.162	3.424	20.258	2.974
1/29	478.0	141.67	0.35	7.985	0.8768	391419.	−6059.	15.064	73.73	44966.	113.79	27.477	−2.128	3.463	20.419	2.953
1/31	474.0	139.48	0.34	8.262	0.8808	386723.	−5997.	15.186	73.18	44008.	113.56	27.596	−2.095	3.503	20.580	2.935
2/2	470.0	137.28	0.33	8.560	0.8849	382033.	−5935.	15.307	72.64	43023.	113.33	27.716	−2.062	3.542	20.742	2.912
2/4	468.0	135.25	0.32	8.628	0.8858	381014.	−5904.	15.334	72.52	42805.	113.28	27.743	−2.055	3.551	20.777	2.904
2/6	468.0	133.39	0.30	8.448	0.8834	383656.	−5903.	15.264	72.82	43352.	113.41	27.675	−2.073	3.528	20.685	2.910
2/8	470.0	131.69	0.29	8.057	0.8779	389970.	−5928.	15.099	73.56	44646.	113.73	27.514	−2.118	3.475	20.468	2.929
2/10	474.0	130.15	0.26	7.525	0.8695	400048.	−5973.	14.843	74.73	46670.	114.25	27.264	−2.189	3.392	20.128	2.960
2/12	482.0	128.95	0.24	6.793	0.8559	417756.	−6043.	14.418	76.78	50123.	115.14	26.847	−2.321	3.256	19.552	3.018
2/14	494.0	128.07	0.20	6.029	0.8383	443323.	−6113.	13.844	79.73	54821.	116.45	26.284	−2.519	3.075	18.763	3.103
2/16	514.0	127.86	0.15	5.214	0.8141	484748.	−6092.	13.006	84.49	61715.	118.59	25.456	−2.874	2.817	17.571	3.240

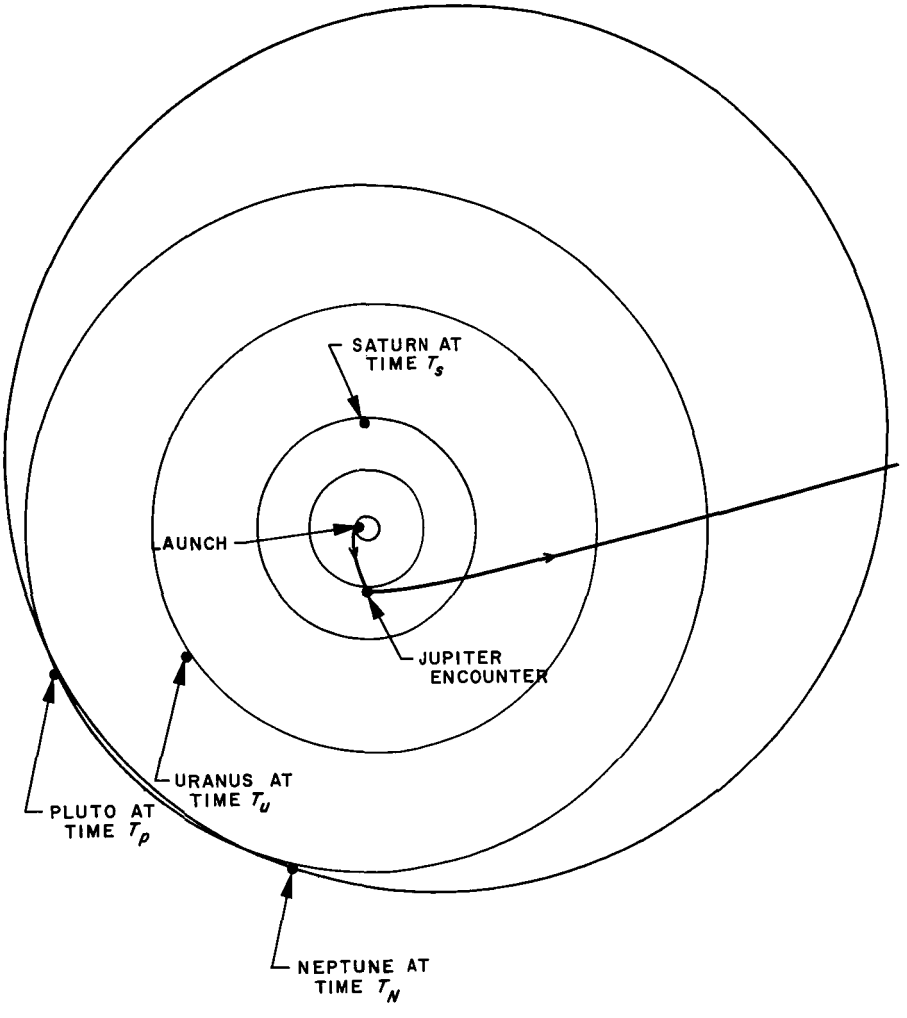

Fig. 11. Planetary configuration for Earth–Jupiter-escape, 1971 (Feb. 4 trajectory)

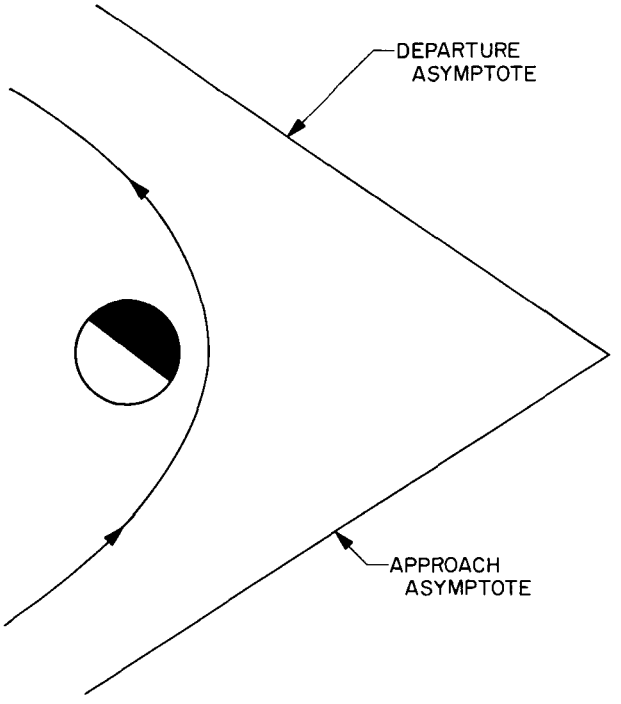

Fig. 12. Feb. 4, 1971, Earth–Jupiter-escape trajectory during its closest approach to Jupiter

Table 11. Earth–Jupiter escape, 1972 (launch HEV = 11.0 km/sec)

Launch date, 1972	T_{12}, days	θ_{12}, deg	ϕ_{12}, deg	a_1, AU	e_1	$B \cdot \hat{T}$, km	$B \cdot \hat{R}$, km	V_1, km/sec	TISI, days	DOCA, km	DA, deg	V_2, km/sec	a_2, AU	e_2	V_∞, km/sec	TTS, yr
2/23	492.0	150.51	1.09	6.047	0.8375	428459.	−5185.	14.174	76.33	50843.	116.32	26.865	−2.371	3.150	19.342	3.067
2/25	484.0	147.98	0.99	6.416	0.8465	415915.	−5445.	14.464	74.90	48567.	115.66	27.151	−2.276	3.240	19.742	3.020
2/27	476.0	145.46	0.91	6.854	0.8560	403429.	−5624.	14.761	73.47	46199.	115.01	27.446	−2.185	3.335	20.149	2.973
2/29	470.0	143.10	0.85	7.215	0.8629	394839.	−5736.	14.976	72.43	44540.	114.56	27.658	−2.124	3.403	20.439	2.939
3/2	464.0	140.75	0.79	7.629	0.8702	386287.	−5815.	15.194	71.50	42835.	114.12	27.874	−2.064	3.473	20.732	2.905
3/4	460.0	138.58	0.75	7.894	0.8744	381536.	−5875.	15.320	70.95	41886.	113.87	27.998	−2.031	3.514	20.899	2.885
3/6	456.0	136.40	0.72	8.179	0.8787	376816.	−5920.	15.446	70.40	40918.	113.63	28.122	−1.999	3.554	21.066	2.864
3/8	454.0	134.40	0.69	8.245	0.8796	375803.	−5968.	15.474	70.28	40714.	113.58	28.150	−1.992	3.563	21.103	2.857
3/10	454.0	132.58	0.68	8.077	0.8772	378489.	−6028.	15.403	70.58	41274.	113.71	28.080	−2.010	3.540	21.009	2.862
3/12	456.0	130.92	0.67	7.709	0.8714	384962.	−6100.	15.235	71.32	42605.	114.04	27.913	−2.054	3.485	20.783	2.881
3/14	458.0	129.27	0.66	7.375	0.8658	391445.	−6170.	15.066	72.07	43889.	114.38	27.747	−2.099	3.431	20.558	2.899
3/16	464.0	127.97	0.67	6.776	0.8543	405605.	−6261.	14.715	73.68	46654.	115.11	27.401	−2.199	3.319	20.083	2.944
3/18	474.0	127.02	0.69	6.075	0.8382	427651.	−6344.	14.202	76.19	50760.	116.25	26.892	−2.363	3.157	19.376	3.015

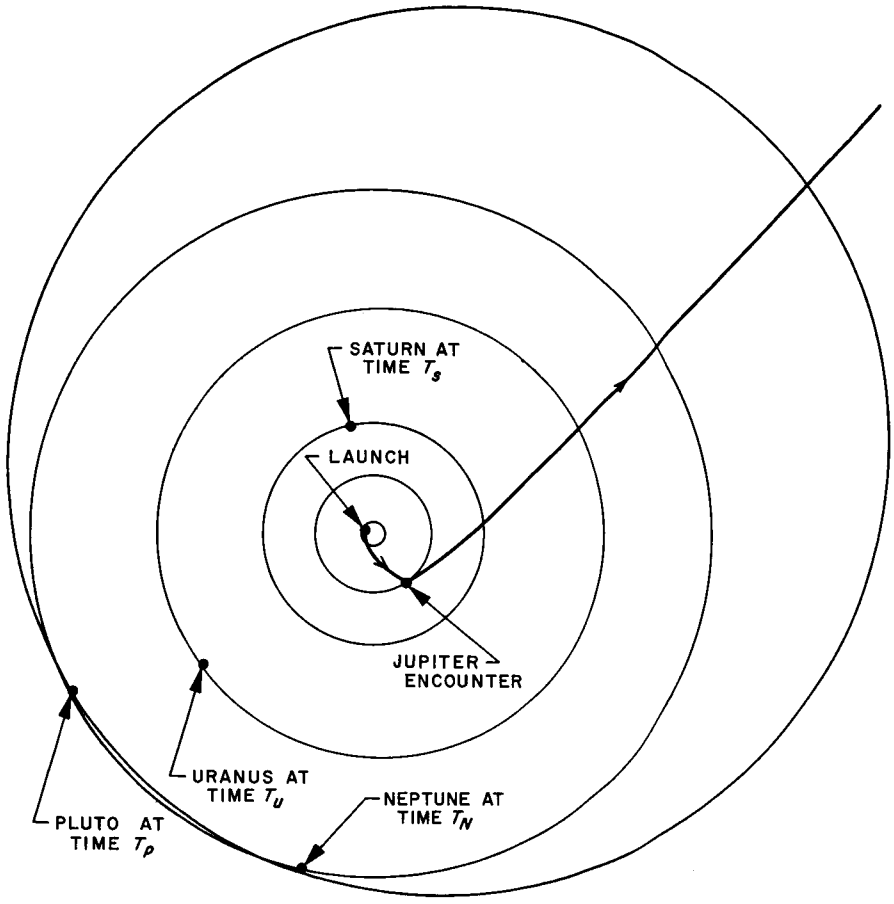

Fig. 13. Planetary configuration for Earth–Jupiter-escape, 1972 (March 8 trajectory)

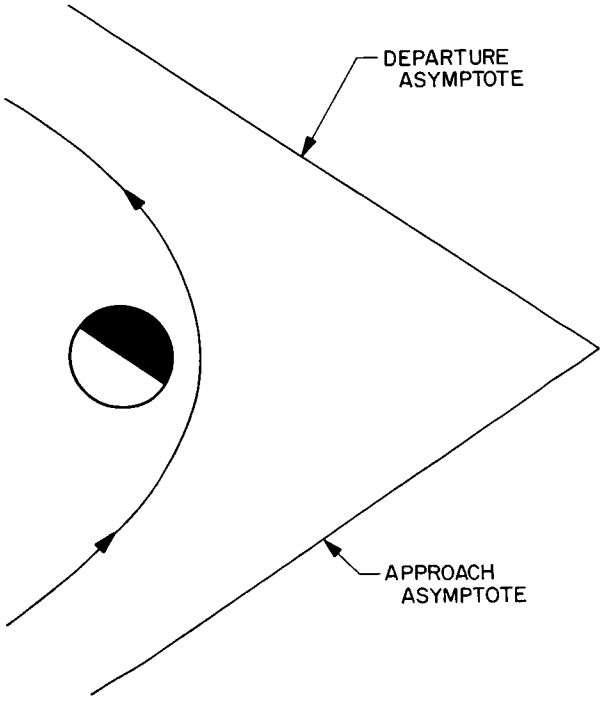

Fig. 14. March 8, 1972, Earth–Jupiter-escape trajectory during its closest approach to Jupiter

Table 12. Earth–Jupiter escape, 1973 (launch HEV = 11.0 km/sec)

Launch date, 1973	T_{12}, days	θ_{12}, deg	ϕ_{12}, deg	a_1, AU	e_1	$B \cdot \hat{T}$, km	$B \cdot \hat{R}$, km	V_1, km/sec	TISI, days	DOCA, km	DA, deg	V_2, km/sec	a_2, AU	e_2	V_∞, km/sec	TTS, yr
3/29	488.0	150.80	2.30	5.572	0.8220	455051.	−2033.	14.006	76.95	57502.	116.75	26.697	−2.482	3.010	18.904	3.072
3/31	478.0	148.11	2.11	5.966	0.8333	437723.	−2776.	14.372	75.04	54441.	115.86	27.066	−2.351	3.123	19.425	3.012
4/2	470.0	145.60	1.96	6.334	0.8427	424557.	−3263.	14.666	73.58	52025.	115.17	27.360	−2.255	3.214	19.835	2.965
4/4	464.0	143.27	1.85	6.635	0.8495	415485.	−3593.	14.879	72.57	50328.	114.70	27.572	−2.190	3.280	20.127	2.931
4/6	458.0	140.94	1.74	6.976	0.8567	406455.	−3860.	15.095	71.56	48580.	114.23	27.787	−2.127	3.348	20.422	2.897
4/8	454.0	138.79	1.67	7.193	0.8608	401433.	−4050.	15.221	71.00	47608.	113.96	27.911	−2.092	3.388	20.592	2.876
4/10	450.0	136.65	1.59	7.425	0.8650	396403.	−4211.	15.346	70.44	46601.	113.71	28.036	−2.058	3.427	20.761	2.856
4/12	448.0	134.69	1.54	7.481	0.8660	395346.	−4339.	15.375	70.31	46403.	113.65	28.064	−2.051	3.436	20.799	2.848
4/14	446.0	132.73	1.49	7.532	0.8669	394262.	−4456.	15.401	70.19	46177.	113.59	28.091	−2.044	3.445	20.835	2.841
4/16	446.0	130.96	1.45	7.392	0.8645	397135.	−4561.	15.330	70.51	46759.	113.74	28.019	−2.063	3.422	20.738	2.846
4/18	450.0	129.54	1.43	6.928	0.8556	408001.	−4657.	15.068	71.70	48951.	114.28	27.756	−2.136	3.338	20.379	2.878
4/20	454.0	128.13	1.41	6.530	0.8472	418941.	−4757.	14.810	72.91	51067.	114.84	27.498	−2.212	3.257	20.024	2.909
4/22	462.0	127.08	1.40	5.974	0.8335	438116.	−4842.	14.382	75.03	54645.	115.81	27.069	−2.351	3.123	19.426	2.968

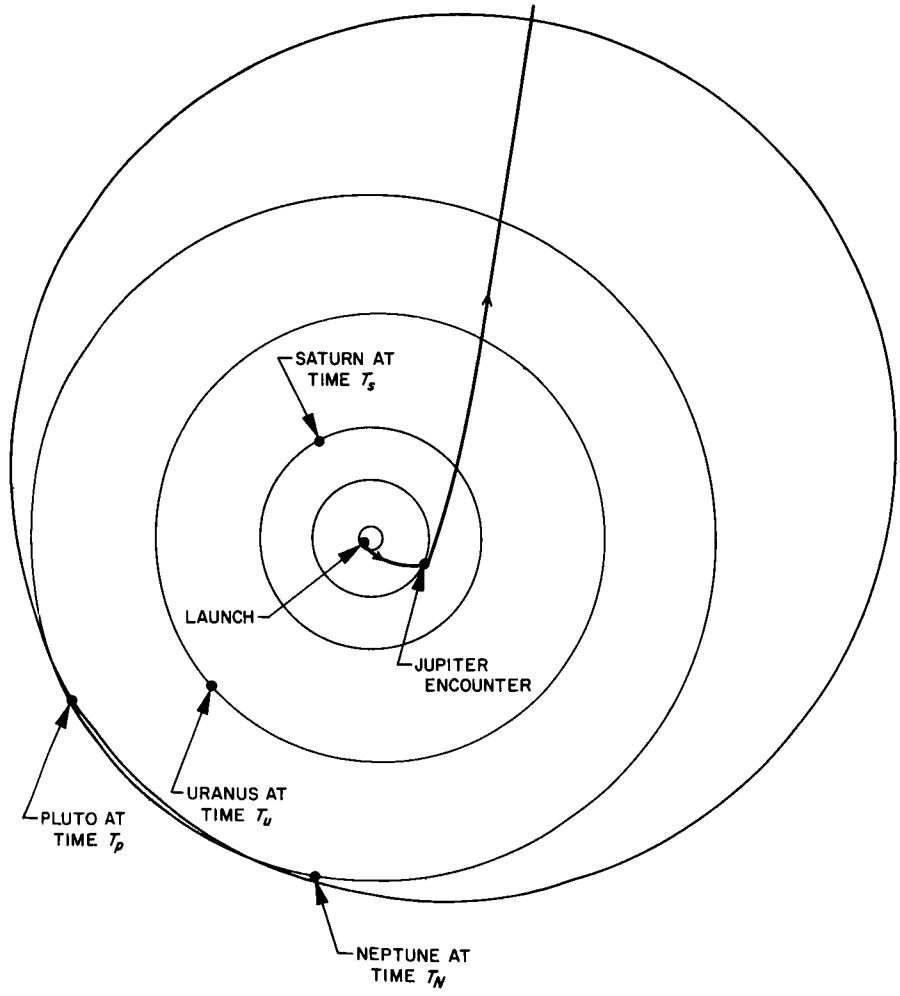

Fig. 15. Planetary configuration for Earth–Jupiter-escape, 1973 (April 14 trajectory)

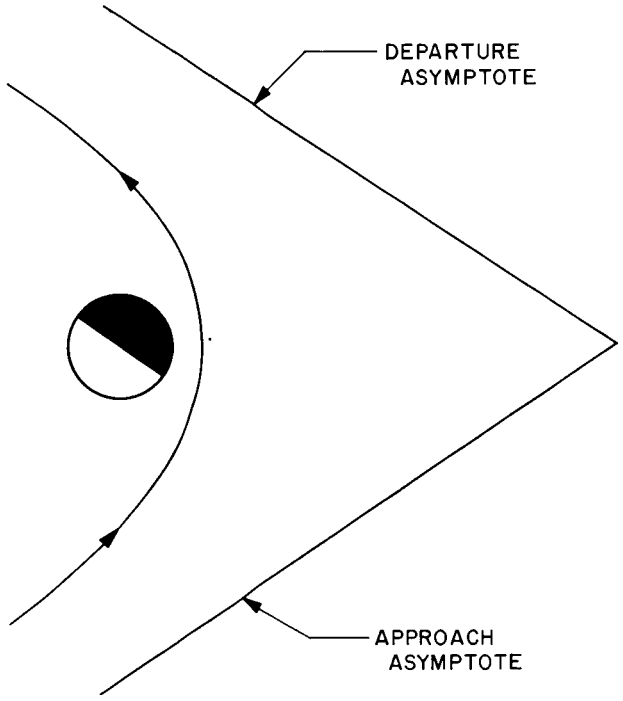

Fig. 16. April 14, 1973, Earth–Jupiter-escape trajectory during its closest approach to Jupiter

Table 13. Earth–Jupiter escape, 1974 (launch HEV = 11.5 km/sec)

Launch date, 1974	T_{12}, days	θ_{12}, deg	ϕ_{12}, deg	a_1, AU	e_1	$B \cdot \hat{T}$, km	$B \cdot \hat{R}$, km	V_1, km/sec	TISI, days	DOCA, km	DA, deg	V_2, km/sec	a_3, AU	e_3	V_∞, km/sec	TTS, yr
5/11	440.0	141.85	2.11	8.404	0.8803	399578.	−521.	15.896	68.93	51016.	111.88	28.349	−1.992	3.487	21.105	2.784
5/13	436.0	139.74	2.02	8.777	0.8851	394311.	−729.	16.037	68.34	49937.	111.60	28.486	−1.958	3.530	21.288	2.763
5/15	430.0	137.44	1.93	9.513	0.8939	384920.	−937.	16.278	67.32	47882.	111.14	28.729	−1.899	3.608	21.612	2.730
5/17	426.0	135.33	1.86	10.010	0.8990	379685.	−1087.	16.420	66.75	46737.	110.88	28.869	−1.867	3.653	21.798	2.709
5/19	422.0	133.23	1.79	10.565	0.9042	374476.	−1218.	16.561	66.18	45571.	110.63	29.010	−1.835	3.698	21.985	2.688
5/21	420.0	131.30	1.74	10.708	0.9055	373318.	−1320.	16.595	66.05	45323.	110.56	29.043	−1.828	3.709	22.028	2.680
5/23	420.0	129.56	1.69	10.395	0.9027	376201.	−1405.	16.520	66.36	45992.	110.69	28.966	−1.845	3.684	21.926	2.685
5/25	420.0	127.83	1.65	10.091	0.8998	379088.	−1490.	16.441	66.67	46638.	110.83	28.888	−1.863	3.659	21.823	2.691
5/27	422.0	126.27	1.62	9.441	0.8931	386084.	−1571.	16.257	67.43	48193.	111.17	28.702	−1.905	3.599	21.577	2.709
5/29	426.0	124.90	1.59	8.595	0.8828	397259.	−1652.	15.970	68.64	50624.	111.71	28.415	−1.975	3.508	21.193	2.741
5/31	432.0	123.72	1.57	7.699	0.8696	412754.	−1739.	15.589	70.32	53893.	112.47	28.034	−2.075	3.387	20.679	2.785
6/2	442.0	122.90	1.55	6.709	0.8510	437023.	−1830.	15.034	72.92	58800.	113.65	27.475	−2.237	3.214	19.915	2.856
6/4	458.0	122.64	1.54	5.718	0.8263	474766.	−1925.	14.251	76.95	65875.	115.50	26.683	−2.508	2.975	18.809	2.967

Table 14. Earth–Jupiter escape, 1975 (launch HEV = 11.5 km/sec)

Launch date, 1975	T_{12}, days	θ_{12}, deg	ϕ_{12}, deg	a_1, AU	e_1	$B \cdot \hat{T}$, km	$B \cdot \hat{R}$, km	V_1, km/sec	TISI, days	DOCA, km	DA, deg	V_2, km/sec	a_3, AU	e_3	V_∞, km/sec	TTS, yr
6/15	458.0	146.58	1.81	7.432	0.8644	455925.	4283.	15.352	73.77	68795.	111.64	27.327	−2.265	3.206	19.792	2.873
6/17	452.0	144.31	1.72	7.886	0.8719	445630.	3972.	15.576	72.69	66663.	111.16	27.551	−2.196	3.274	20.098	3.839
6/19	444.0	141.87	1.64	8.661	0.8831	430939.	3656.	15.899	71.16	63461.	110.50	27.877	−2.103	3.375	20.541	2.793
6/21	440.0	139.78	1.57	9.042	0.8879	425241.	3474.	16.035	70.56	62246.	110.23	28.011	−2.066	3.416	20.721	2.772
6/23	434.0	137.51	1.51	9.793	0.8964	415143.	3268.	16.270	69.50	59965.	109.78	28.248	−2.004	3.491	21.040	2.738
6/25	432.0	135.60	1.46	9.923	0.8976	413875.	3163.	16.306	69.36	59719.	109.70	28.281	−1.996	3.501	21.084	2.730
6/27	428.0	133.52	1.41	10.435	0.9026	408221.	3028.	16.441	68.77	58414.	109.45	28.418	−1.962	3.544	21.266	2.709
6/29	426.0	131.61	1.37	10.563	0.9038	406922.	2939.	16.472	68.63	58114.	109.39	28.449	−1.954	3.554	21.308	2.702
7/1	426.0	129.88	1.33	10.271	0.9011	409960.	2886.	16.399	68.95	58817.	109.53	28.375	−1.972	3.531	21.209	2.707
7/3	428.0	128.34	1.29	9.634	0.8947	417404.	2859.	16.222	69.73	60521.	109.86	28.196	−2.017	3.475	20.970	2.725
7/5	432.0	126.97	1.26	8.795	0.8848	429314.	2846.	15.946	70.98	63188.	110.39	27.917	−2.091	3.388	20.597	2.756
7/7	436.0	125.60	1.23	8.110	0.8755	441327.	2824.	15.674	72.25	65779.	110.95	27.645	−2.168	3.304	20.228	2.788
7/9	446.0	124.78	1.20	7.046	0.8572	467128.	2847.	15.131	74.92	71207.	112.11	27.096	−2.339	3.137	19.477	2.858

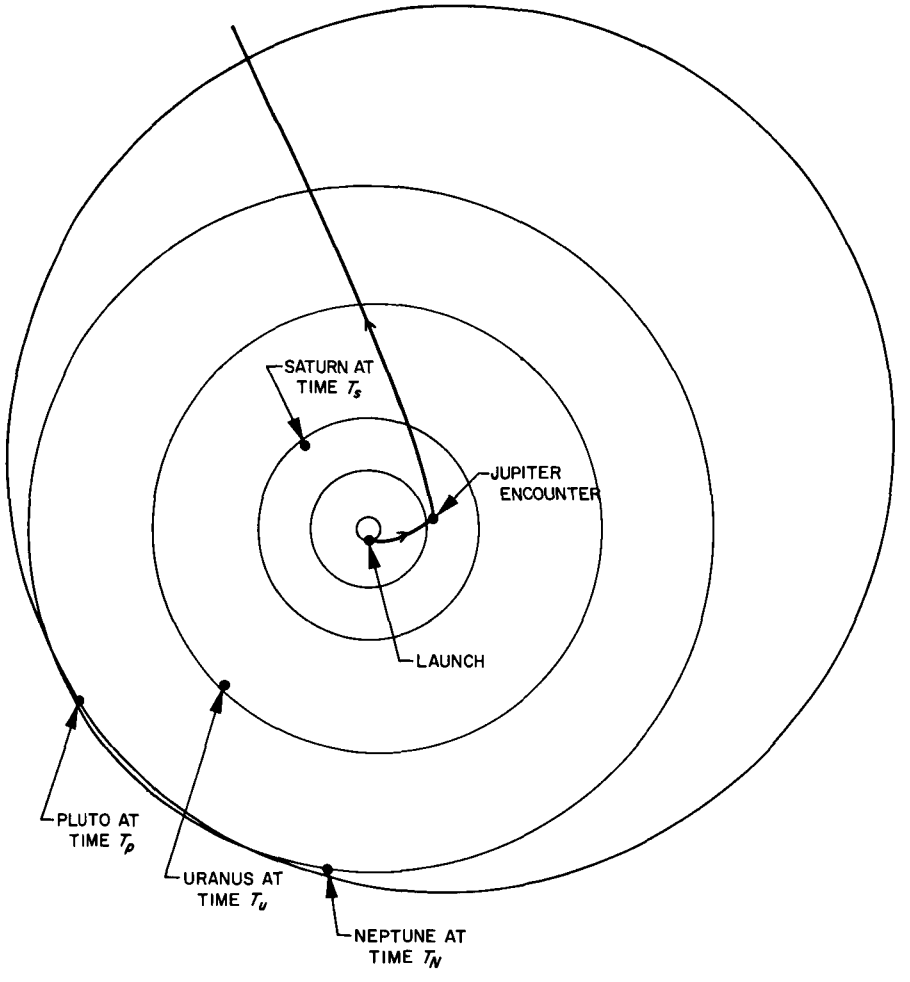

Fig. 17. Planetary configuration for Earth–Jupiter-escape, 1974 (May 21 trajectory)

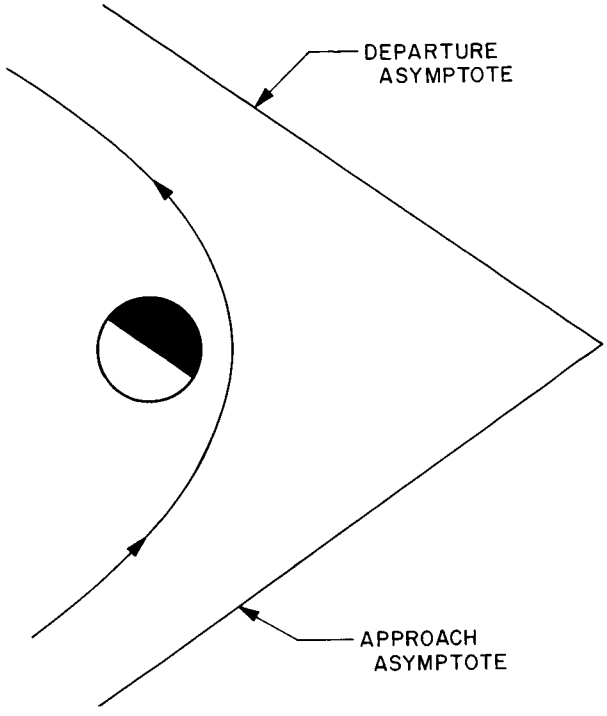

Fig. 18. May 21, 1974, Earth–Jupiter-escape trajectory during its closest approach to Jupiter

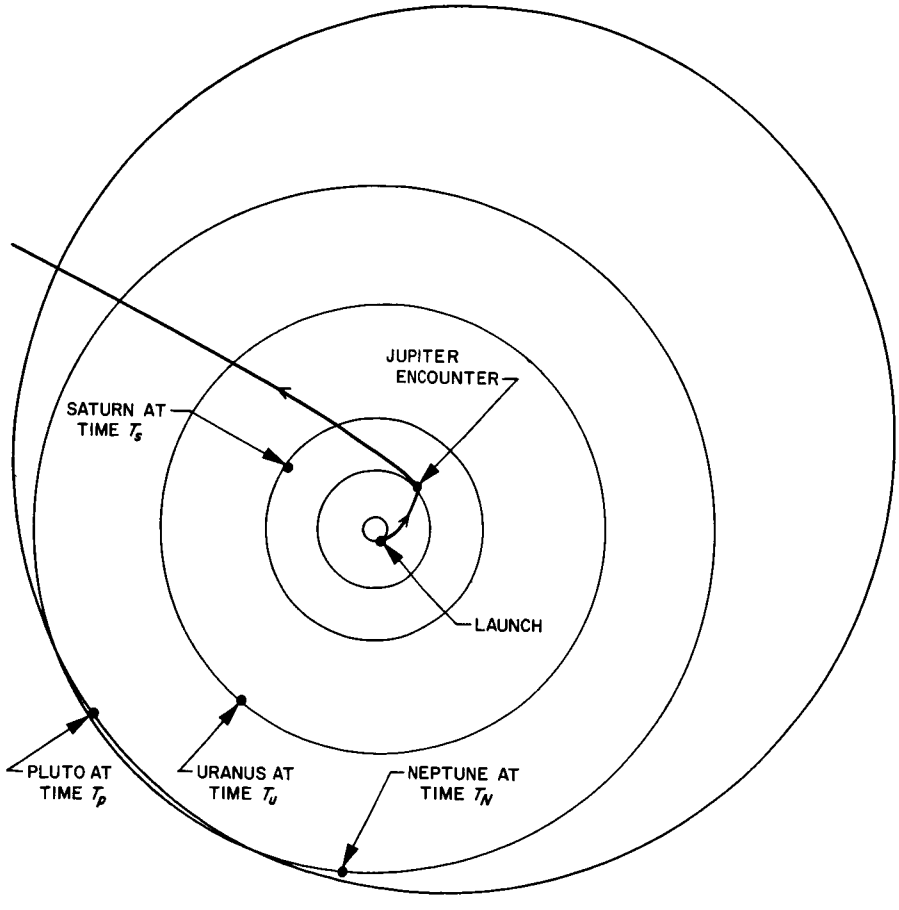

Fig. 19. Planetary configuration for Earth–Jupiter-escape, 1975 (June 29 trajectory)

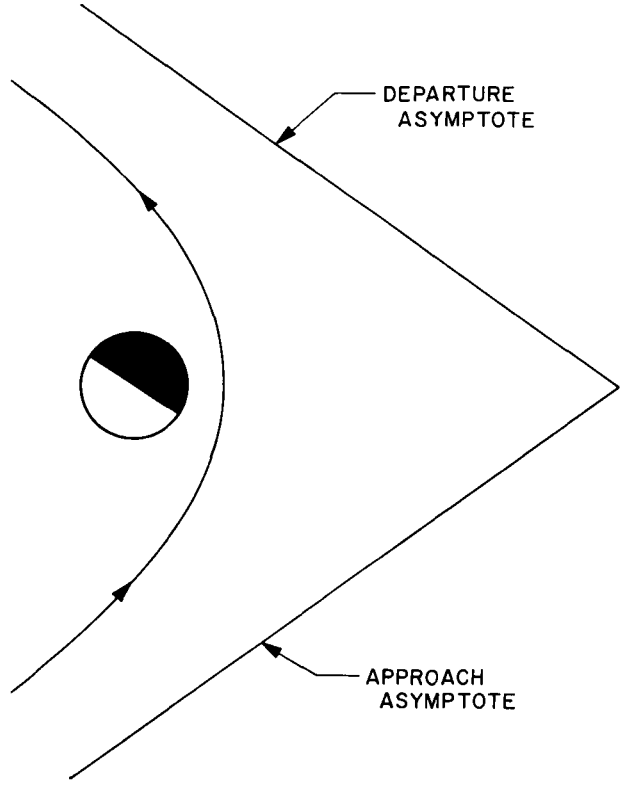

Fig. 20. June 29, 1975, Earth–Jupiter-escape trajectory during its closest approach to Jupiter

Table 15. Earth–Jupiter escape, 1976 (launch HEV = 11.5 km/sec)

Launch date, 1976	T_{12}, days	θ_{12}, deg	ϕ_{12}, deg	a_1, AU	e_1	$B \cdot \hat{T}$, km	$B \cdot \hat{R}$, km	V_1, km/sec	TISI, days	DOCA, km	DA, deg	V_2, km/sec	a_3, AU	e_3	V_∞, km/sec	TTS, yr
7/23	464.0	145.73	0.55	8.335	0.8790	471768.	7247.	15.504	75.70	77521.	109.94	27.003	−2.320	3.202	19.554	2.871
7/25	458.0	143.47	0.53	8.902	0.8865	461153.	7109.	15.724	74.60	75187.	109.48	27.223	−2.251	3.269	19.854	2.837
7/27	452.0	141.22	0.52	9.572	0.8943	450622.	6979.	15.947	73.52	72810.	109.04	27.447	−2.183	3.339	20.158	2.804
7/29	448.0	139.13	0.50	10.021	0.8989	444709.	6890.	16.078	72.90	71475.	108.78	27.576	−2.146	3.379	20.333	2.783
7/31	444.0	137.05	0.49	10.516	0.9036	438810.	6804.	16.208	72.29	70110.	108.53	27.707	−2.1092	3.421	20.509	2.763
8/2	442.0	135.14	0.47	10.649	0.9047	437444.	6763.	16.241	72.15	69806.	108.46	27.738	−2.101	3.431	20.551	2.755
8/4	440.0	133.22	0.46	10.774	0.9058	436060.	6723.	16.271	72.01	69475.	108.41	27.768	−2.092	3.440	20.591	2.747
8/6	440.0	131.48	0.44	10.488	0.9033	439182.	6727.	16.200	72.34	70202.	108.54	27.698	−2.112	3.418	20.497	2.752
8/8	442.0	129.91	0.42	9.863	0.8973	446841.	6764.	16.031	73.14	71972.	108.86	27.527	−2.159	3.365	20.269	2.770
8/10	446.0	128.50	0.40	9.035	0.8881	459142.	6839.	15.767	74.41	74765.	109.38	27.262	−2.238	3.283	19.911	2.801
8/12	452.0	127.27	0.37	8.142	0.8762	476174.	6936.	15.416	76.17	78514.	110.12	26.911	−2.349	3.176	19.431	2.845
8/14	462.0	126.38	0.34	7.138	0.8593	502889.	7065.	14.901	78.92	84178.	111.26	26.392	−2.533	3.020	18.715	2.914
8/16	478.0	125.99	0.29	6.115	0.8367	544441.	7176.	14.171	83.15	92402.	113.04	25.656	−2.841	2.803	17.673	3.023

Table 16. Earth–Jupiter escape, 1977 (launch HEV = 11.5 km/sec)

Launch date, 1977	T_{12}, days	θ_{12}, deg	ϕ_{12}, deg	a_1, AU	e_1	$B \cdot \hat{T}$, km	$B \cdot \hat{R}$, km	V_1, km/sec	TISI, days	DOCA, km	DA, deg	V_2, km/sec	a_2, AU	e_2	V_∞, km/sec	TTS, yr
8/23	498.0	152.07	1.05	7.297	0.8632	518786.	7431.	14.668	82.19	89963.	110.91	25.865	−2.669	2.971	18.229	3.025
8/25	488.0	149.49	0.94	8.000	0.8750	498799.	7621.	15.033	80.13	85708.	110.09	26.230	−2.526	3.082	18.739	2.967
8/27	480.0	147.07	0.86	8.685	0.8846	483607.	7718.	15.326	78.56	82382.	109.46	26.522	−2.421	3.171	19.142	2.921
8/29	474.0	144.82	0.80	9.271	0.8917	473133.	7774.	15.538	77.46	80059.	109.02	26.732	−2.350	3.236	19.429	2.887
8/31	468.0	142.56	0.74	9.960	0.8991	462716.	7797.	15.752	76.38	77684.	108.59	26.945	−2.281	3.303	19.719	2.854
9/2	462.0	140.30	0.70	10.785	0.9067	452377.	7795.	15.970	75.30	75266.	108.17	27.163	−2.215	3.372	20.013	2.821
9/4	458.0	138.20	0.66	11.336	0.9112	446558.	7803.	16.096	74.69	73895.	107.93	27.289	−2.178	3.412	20.183	2.801
9/6	456.0	136.26	0.64	11.482	0.9123	445206.	7836.	16.127	74.55	73586.	107.87	27.318	−2.169	3.421	20.223	2.793
9/8	454.0	134.32	0.62	11.619	0.9133	443838.	7864.	16.155	74.41	73248.	107.82	27.347	−2.161	3.431	20.262	2.785
9/10	454.0	132.54	0.61	11.296	0.9109	446914.	7926.	16.086	74.74	73969.	107.95	27.278	−2.181	3.409	20.170	2.790
9/12	458.0	131.08	0.61	10.241	0.9018	458962.	8060.	15.828	76.01	76806.	108.44	27.020	−2.258	3.328	19.823	2.821
9/14	462.0	129.62	0.61	9.387	0.8931	471099.	8189.	15.573	77.29	79569.	108.95	26.767	−2.338	3.249	19.479	2.852
9/16	470.0	128.48	0.62	8.261	0.8790	492546.	8371.	15.146	79.53	84332.	109.84	26.342	−2.484	3.118	18.897	2.908

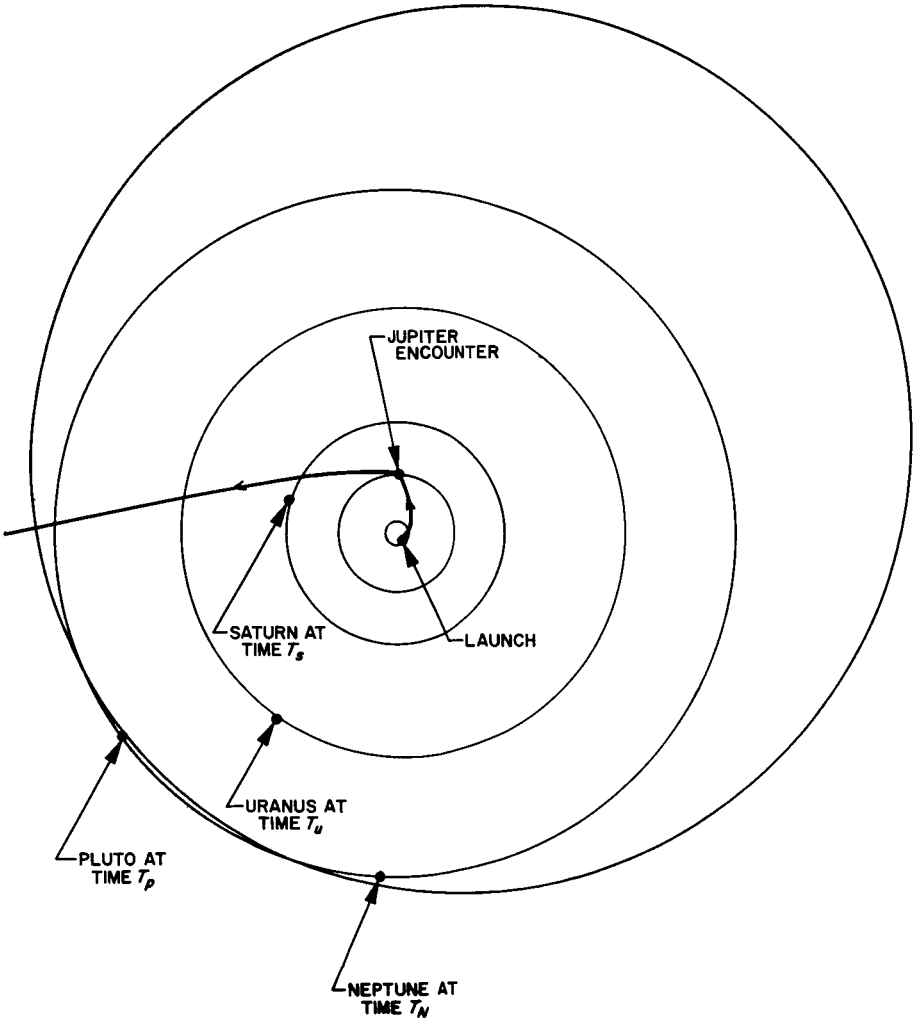

Fig. 21. Planetary configuration for Earth–Jupiter-escape, 1976 (Aug. 4 trajectory)

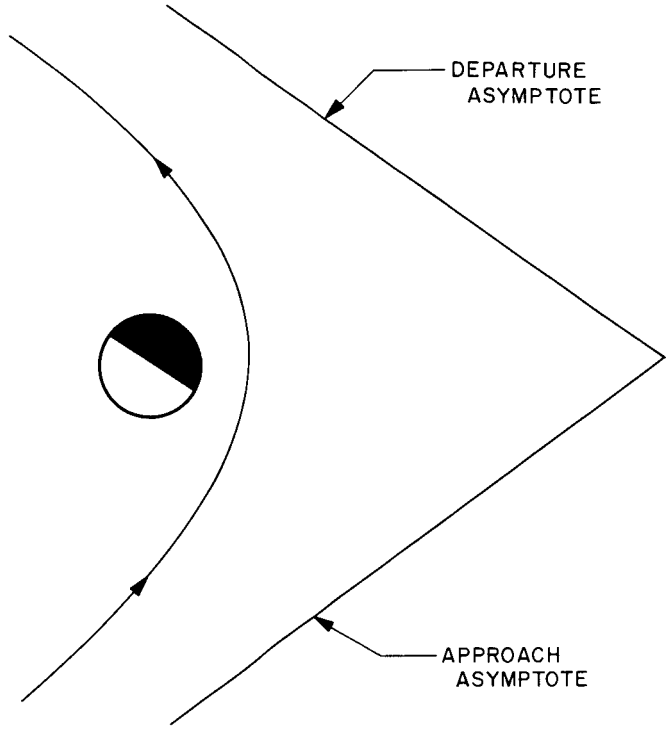

Fig. 22. August 4, 1976, Earth–Jupiter-escape trajectory during its closest approach to Jupiter

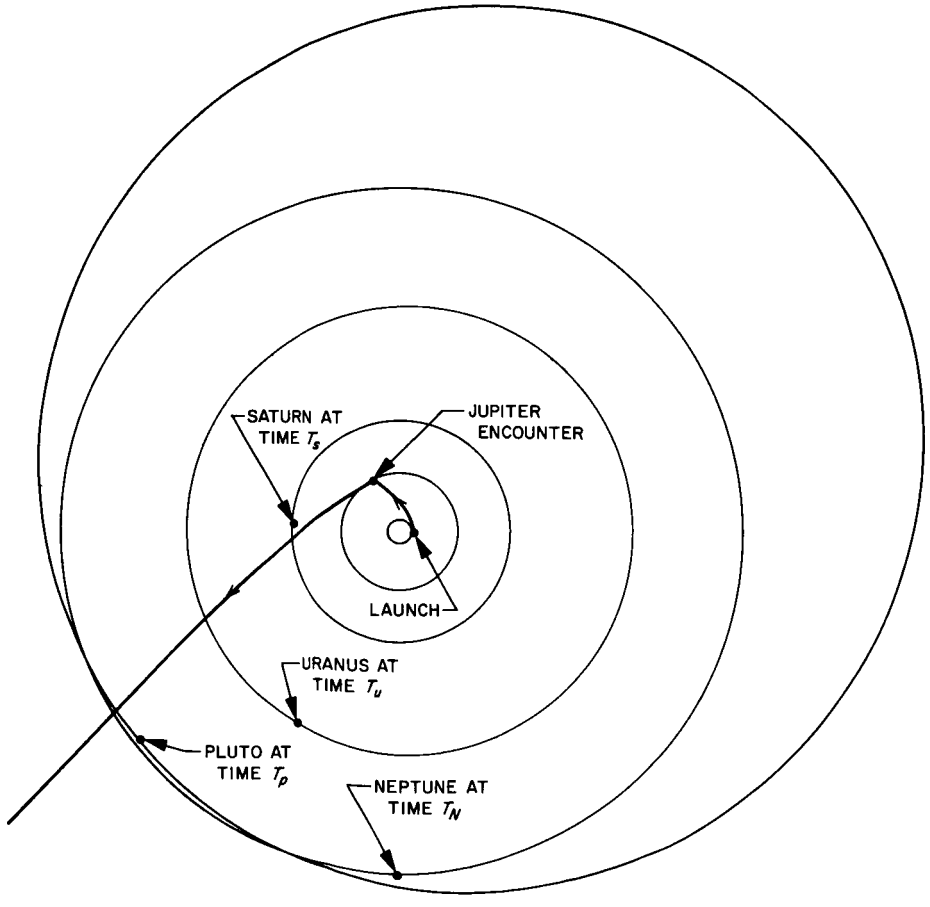

Fig. 23. Planetary configuration for Earth–Jupiter-escape, 1977 (September 8 trajectory)

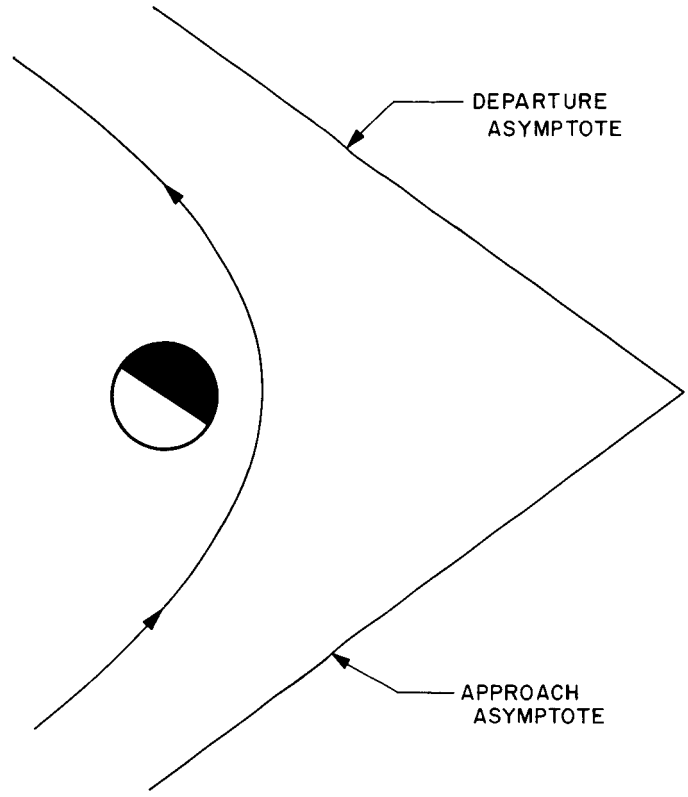

Fig. 24. September 8, 1977, Earth–Jupiter-escape trajectory during its closest approach to Jupiter

Table 17. Earth–Jupiter escape, 1978 (launch HEV = 11.5 km/sec)

Launch date, 1978	T_{12}, days	θ_{12}, deg	ϕ_{12}, deg	a_1, AU	e_1	$B \cdot \hat{T}$, km	$B \cdot \hat{R}$, km	V_1, km/sec	TISI, days	DOCA, km	DA, deg	V_2, km/sec	a_3, AU	e_3	V_∞, km/sec	TTS, yr
9/29	492.0	147.61	1.96	9.045	0.8902	473315.	5210.	15.208	79.79	78685.	109.64	26.348	−2.432	3.214	19.101	2.959
10/1	486.0	145.34	1.83	9.667	0.8970	436690.	5437.	15.416	78.72	76490.	109.21	26.551	−2.362	3.278	19.379	2.925
10/3	480.0	143.06	1.73	10.400	0.9042	453496.	5607.	15.626	77.65	74236.	108.80	26.758	−2.295	3.345	19.660	2.892
10/5	474.0	140.79	1.64	11.277	0.9115	443669.	5734.	15.839	76.60	71941.	108.40	26.969	−2.230	3.413	19.945	2.859
10/7	470.0	138.66	1.56	11.862	0.9159	438167.	5835.	15.962	76.00	70648.	108.17	27.091	−2.194	3.452	20.108	2.839
10/9	468.0	136.68	1.51	12.012	0.9169	436897.	5929.	15.991	75.87	70353.	108.11	27.119	−2.186	3.461	20.146	2.832
10/11	466.0	134.71	1.45	12.151	0.9179	435610.	6013.	16.017	75.73	70029.	108.07	27.146	−2.178	3.470	20.183	2.824
10/13	468.0	133.04	1.42	11.359	0.9122	442797.	6126.	15.856	76.52	71726.	108.37	26.986	−2.225	3.419	19.969	2.842
10/15	470.0	131.37	1.39	10.666	0.9066	450028.	6240.	15.693	77.31	73385.	108.68	26.827	−2.273	3.367	19.755	2.860
10/17	476.0	130.00	1.37	9.475	0.8952	465948.	6389.	15.352	79.03	77001.	109.35	26.492	−2.382	3.260	19.300	2.903
10/19	486.0	128.95	1.37	8.168	0.8788	490927.	6570.	14.851	81.71	82489.	110.40	25.996	−2.559	3.105	18.619	2.972

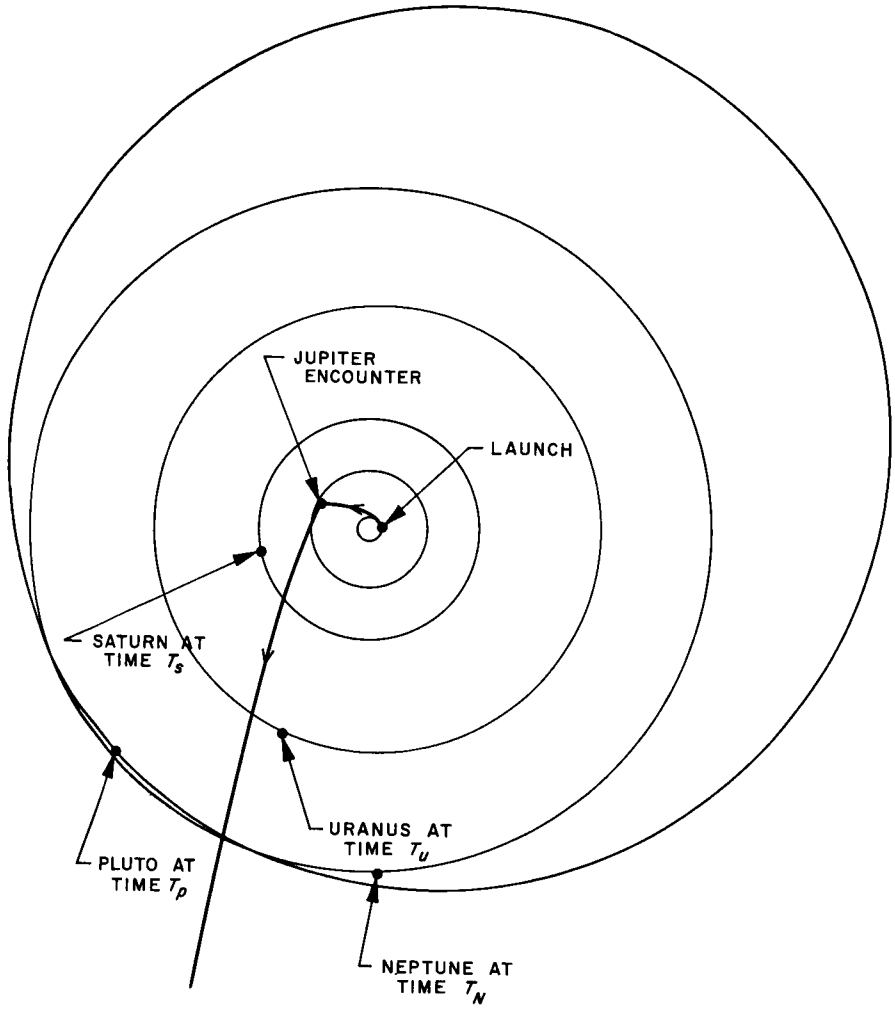

Fig. 25. Planetary configuration for Earth–Jupiter-escape, 1978 (October 11 trajectory)

B. The Determination of Deep Space Post-encounter Trajectories Corresponding to the Initial Conditions ($P_1, T_1; P_2, T_2; d$)

We have seen that when P_2 is Venus or Mars, the trajectories have negative distances of closest approach. We therefore give d a specified value and include it along with the other initial conditions. In this case V_2 must satisfy two equations $G_1 = 0$ and $G_2 = 0$, where G_1 and G_2 are defined by Eq. (16) and (20), respectively. We therefore proceed by solving the system.

$$\frac{\partial V_2^2}{\partial x} - \lambda_1 \frac{\partial G_1}{\partial x} - \lambda_2 \frac{\partial G_2}{\partial x} = 0$$

$$\frac{\partial V_2^2}{\partial y} - \lambda_1 \frac{\partial G_1}{\partial y} - \lambda_2 \frac{\partial G_2}{\partial y} = 0$$

$$\frac{\partial V_2^2}{\partial z} - \lambda_1 \frac{\partial G_1}{\partial z} - \lambda_2 \frac{\partial G_2}{\partial z} = 0$$

$$G_1 = 0$$

$$G_2 = 0$$

The first three equations yield the relations

$$\begin{aligned} x &= \nu_1 \eta_2 - u_1 \eta_1 \\ y &= \nu_2 \eta_2 - u_2 \eta_1 \\ z &= \nu_3 \eta_2 - u_3 \eta_1 \end{aligned} \tag{26}$$

where

$$\eta_1 = \frac{\lambda_1}{1 - \lambda_1} \qquad \eta_2 = \frac{\lambda_2}{2(1 - \lambda_1)}$$

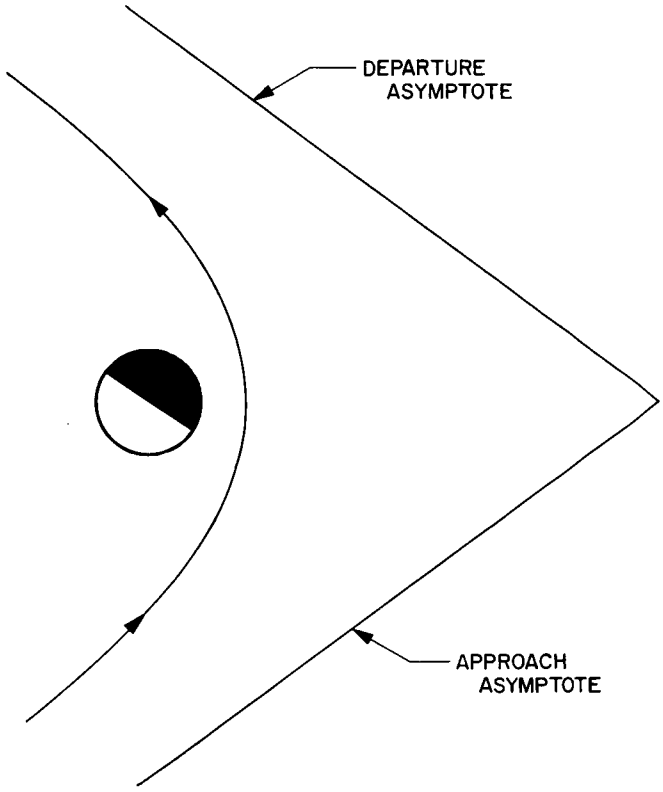

Fig. 26. October 11, 1978, Earth–Jupiter-escape trajectory during its closest approach to Jupiter

Substituting these equations into the second constraining equation, one finds

$$\eta_2 = \frac{K + (\mathbf{V}_1' \cdot \mathbf{V}_p)\,\eta_1}{V'^2}$$

When these results are substituted into the first constraining equations, we obtain the solutions

$$\eta_1 = \frac{2V'\left(e_2^2 - 1\right)^{1/2}}{V_p e_2^2 \sin\omega} - 1$$

$$\eta_2 = \frac{V'^2}{e_2^2}\left[e_2^2 - 2 + \left(e_2^2 - 1\tan\omega\right)^{1/2}\right]$$

and

$$\eta_1 = \frac{-2V'\left(e_2^2 - 1\right)^{1/2}}{V_p e_2^2 \sin\omega} - 1$$

$$\eta_2 = \frac{V'^2}{e_2^2}\left[e_2^2 - 2 - \left(e_2^2 - 1\tan\omega\right)^{1/2}\right]$$

where

$$\omega = \measuredangle\,\mathbf{V}_1, \mathbf{V}_p \quad \text{and} \quad e_2 = 1 + (d + r_p)\frac{V'^2}{\mu_p}$$

The solution vectors are then obtained by substituting these quantities back into Eq. (26). The total trajectory is now calculated by the method of Section II.

Table 18 shows some Earth–Venus–Deep Space trajectories for varying values of d. The first important fact to be noticed is that the postencounter trajectories all pass beyond the orbit of Mars. This means that trips to Mars can be carried out by using Venus to perturb the postencounter trajectory, such that it intercepts Mars (see Ref. 1). One might think that Jupiter can also be reached by such a technique. This is possible; however, it turns out to require more energy than direct Earth–Jupiter transfers. All these postencounter trajectories do not have very great aphelion values. Hence, they do not make good Deep Space trajectories. We expect this because Venus is inside the Earth's orbit.

Table 19 gives a similar set of trajectories when P_2 is Mars. These trajectories were constructed from Earth–Mars transfers having launch hyperbolic excess velocities slightly under 4 km/sec. The distances of closest

approach were all held at 1000 km. The table shows that this planet does not have enough mass to produce good deep space trajectories.

Before considering solar probes, let us view the concept of deep space relative to the region in the immediate vicinity of the Earth. Thus, deep space will be regions beyond the Moon. In this case we view P_1 as an orbiting point corresponding to a rocket in a 200-km-high parking orbit. We let P_2 be the center of the Moon. For these trajectories we use the additional notation:

ΔV_2 = velocity gained just after leaving τ of Moon

$\Delta\Delta V_1$ = velocity savings at injection if the postencounter trajectory resulted from a direct injection

ΔV_∞ = increase in hyperbolic excess velocity due to the Moon encounter

Tables 20 through 24 give five sets of Earth–Moon-Escape trajectories for fixed Earth–Moon transfers and varying distances of closest approach. From these tables we find that maximum increase in V_2 occurs for launch trajectories having approximately 4 km/sec hyperbolic excess velocity. The gain is almost 1.1 km/sec. The maximum increase in postencounter hyperbolic excess velocities occurs for parabolic launch trajectories. In this case the encounter transforms parabolic trajectories into hyperbolic trajectories with hyperbolic excess velocities in the neighborhood of 1.3 to 1.6 km/sec. The maximum increase in injection velocities is about 0.55 km/sec which occurs for launch trajectories having a hyperbolic excess velocity of about 8 km/sec. This method should not be very useful for going to other planets as the guidance restrictions would not be justified against the rather small velocity gains. However, for deep space in the immediate vicinity of the Earth, they could be quite useful. For example, an elliptical trajectory with aphelion just slightly more than the Moon's semimajor axis can be converted into an escape trajectory. The path of the trajectory having a distance of closest approach equal to 100 km is shown in Fig. 27.

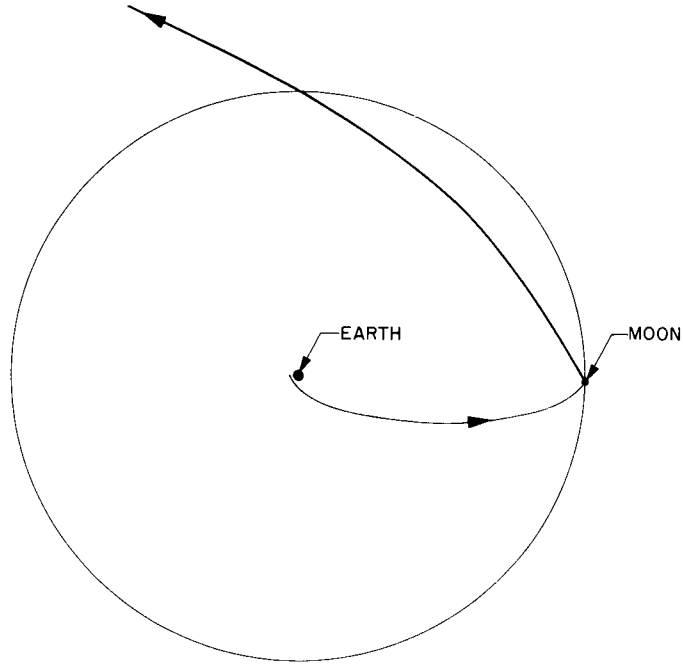

Fig. 27. Earth–Moon-escape, DOCA = 100 km

Table 18. Earth–Venus deep space (launch date Aug. 12, 1970)

T_{12}, days	HEV_1, km/sec	θ_{12}, deg	ϕ_{12}, deg	a_1, AU	e_1	Aphelion, AU	$B \cdot \hat{T}$, km	$B \cdot \hat{R}$, km	V_1, km/sec	TISI, days	DOCA, km	DA, deg	V_2, km/sec	a_2, AU	e_2	Aphelion$_2$, AU
104.0	3.747	110.89	0.39	0.8169	0.2417	1.0143	−9881.	1119.	37.083	1.72	0.	53.90	42.364	1.3312	0.4659	1.951
104.0	3.747	110.89	0.39	0.8169	0.2417	1.0143	−10436.	1182.	37.083	1.72	500.	51.41	42.221	1.3075	0.4575	1.906
104.0	3.747	110.89	0.39	0.8169	0.2417	1.0143	−10984.	1244.	37.083	1.72	1000.	49.16	42.082	1.2853	0.4495	1.863
104.0	3.747	110.89	0.39	0.8169	0.2417	1.0143	−11529.	1305.	37.083	1.72	1500.	47.09	41.947	1.2645	0.4418	1.823
104.0	3.747	110.89	0.39	0.8169	0.2417	1.0143	—	—	37.083	—	—	—	—	—	—	—
105.0	3.664	112.50	0.30	0.8197	0.2374	1.0143	−10039.	1163.	37.138	1.76	0.	55.54	42.316	1.3223	0.4610	1.9318
105.0	3.664	112.50	0.30	0.8197	0.2374	1.0143	−10597.	1228.	37.138	1.76	500.	53.02	42.186	1.3011	0.4533	1.891
105.0	3.664	112.50	0.30	0.8197	0.2374	1.0143	−11149.	1292.	37.138	1.76	1000.	50.73	42.058	1.2808	0.4459	1.852
105.0	3.664	112.50	0.30	0.8197	0.2374	1.0143	−11697.	1355.	37.138	1.76	1500.	48.64	41.933	1.2617	0.4387	1.815
105.0	3.664	112.50	0.30	0.8197	0.2374	1.0143	—	—	37.138	—	—	—	—	—	—	—
106.0	3.585	114.11	0.20	0.8223	0.2333	1.0143	−10201.	1211.	37.190	1.81	0.	57.19	42.257	1.3118	0.4554	1.909
106.0	3.585	114.11	0.20	0.8223	0.2333	1.0143	−10763.	1278.	37.190	1.81	500.	54.65	42.140	1.2930	0.4486	1.873

Table 19. Earth–Mars deep space, 1966–67

Launch date	T_{12}, days	HEV_1, km/sec	θ_{12}, deg	ϕ_{12}, deg	a_1, AU	e_1	Aphelion, AU	$B \cdot \hat{T}$, km	$B \cdot \hat{R}$, km	V_1, km/sec	TISI, days	DOCA, km	DA, deg	V_2, km/sec	a_3, AU	e_3	Aphelion$_3$, AU
12/13/66	198.0	3.883	160.85	1.23	1.304	0.2549	1.638	5190.	228.	22.078	1.86	1000.	18.56	24.372	1.5457	0.1953	1.8476
12/19/66	186.0	3.929	151.62	0.64	1.333	0.2687	1.691	5080.	84.	22.285	1.72	1000.	16.05	24.443	1.5715	0.2239	1.9234
12/25/66	180.0	3.785	145.51	0.54	1.341	0.2703	1.704	5049.	−356.	22.375	1.69	1000.	15.61	24.499	1.5791	0.2302	1.9426
12/31/66	168.0	3.953	136.29	0.30	1.380	0.2895	1.780	4959.	−176.	22.658	1.56	1000.	13.35	24.636	1.6154	0.2618	2.0383
1/6/67	162.0	3.894	130.18	0.27	1.389	0.2923	1.794	4944.	−141.	22.743	1.54	1000.	13.00	24.695	1.624	0.2673	2.0581
1/12/67	156.0	3.902	124.06	0.25	1.395	0.2952	1.807	4917.	392.	22.811	1.52	1000.	12.68	24.734	1.6298	0.2715	2.0723
1/18/67	150.0	3.997	117.95	0.24	1.400	0.2984	1.817	4920.	−88.	22.859	1.50	1000.	12.40	24.767	1.6347	0.2769	2.0874

Table 20. Earth–Moon-escape (ΔV_1 = 3.1316 km/sec, T_{12} = 112.28 hr, θ_{12} = 179.24 deg, $a_1 = 0.19598 \times 10^6$ km, e_1 = 0.9664, V_1 = 0.200 km/sec, injection altitude = 200 km)

DOCA, km	TISI, hr	ΔV_2, km/sec	$\Delta\Delta V_1$, km/sec	DA, deg	V_2, km/sec	a_3, km $\times 10^6$	e_3	V_∞, km/sec	ΔV_∞, km/sec
0.	35.22	1.413	0.1166	106.63	1.613	−0.7569	1.4217	0.7257	—
100.	35.26	1.405	0.1156	104.91	1.605	−0.7927	1.3998	0.7091	—
200.	35.31	1.399	0.1146	103.26	1.599	−0.8278	1.3804	0.6939	—
300.	35.35	1.393	0.1138	101.68	1.593	−0.8615	1.3633	0.6802	—
400.	35.39	1.387	0.1130	100.16	1.587	−0.8933	1.3486	0.6680	—
500.	35.44	1.383	0.1124	98.70	1.583	−0.9227	1.3360	0.6573	—
600.	35.48	1.379	0.1118	97.28	1.579	−0.9491	1.3253	0.6481	—
700.	35.52	1.376	0.1114	95.92	1.576	−0.9720	1.3166	0.6404	—
800.	35.56	1.374	0.1110	94.60	1.574	−0.9912	1.3097	0.6341	—
900.	35.60	1.372	0.1107	93.32	1.572	−1.0065	1.3044	0.6293	—
1000.	35.64	1.370	0.1105	92.09	1.570	−1.0177	1.3006	0.6259	—

Table 21. Earth–Moon-escape (ΔV_1 = 3.3493 km/sec, T_{12} = 38.23 hr, θ_{12} = 157.35 deg, $a_1 = -0.14410 \times 10^6$ km, e_1 = 1.0457, V_1 = 2.200 km/sec, injection altitude = 200 km, HEV_1 = 1.6631)

DOCA, km	TISI, hr	ΔV_2, km/sec	$\Delta\Delta V_1$, km/sec	DA, deg	V_2, km/sec	a_3, km $\times 10^6$	e_3	V_∞, km/sec	ΔV_∞, km/sec
0.	15.06	0.971	0.2318	39.68	3.171	−0.49935	7.5640	2.8253	1.1621
100.	15.07	0.978	0.2337	38.17	3.178	−0.4968	7.6390	2.8327	1.1695
200.	15.07	0.984	0.2354	36.77	3.184	−0.4944	7.7087	2.8395	1.1767
300.	15.08	0.989	0.2369	35.47	3.189	−0.49217	7.7736	2.8458	1.1826
400.	15.08	0.995	0.2384	34.26	3.195	−0.4902	7.8341	2.8517	1.1885
500.	15.09	1.000	0.2398	33.14	3.200	−0.4883	7.8905	2.8572	1.1940
600.	15.09	1.004	0.2411	32.08	3.204	−0.4866	7.9433	2.8622	1.1990
700.	15.10	1.008	0.2423	31.10	3.208	−0.4849	7.9928	2.8669	1.2037
800.	15.11	1.012	0.2434	30.17	3.212	−0.4835	8.0392	2.8714	1.2082
900.	15.11	1.016	0.2444	29.29	3.216	−0.4821	8.0827	2.8755	1.2123
1000.	15.12	1.019	0.2454	28.47	3.219	−0.4808	8.1237	2.8794	1.2162

Table 22. Earth–Moon-escape (ΔV_1 = 3.9100 km/sec, T_{12} = 22.94 hr, θ_{12} = 139.89 deg, $a_1 = -0.02561 \times 10^6$ km, e_1 = 1.2569, V_1 = 4.200 km/sec, injection altitude = 200 km, HEV_1 = 3.9454 km/sec)

DOCA, km	TISI, hr	ΔV_2, km/sec	$\Delta\Delta V_1$, km/sec	DA, deg	V_2, km/sec	a_3, km × 10^6	e_3	V_∞, km/sec	ΔV_∞, km/sec
0.	8.49	1.068	0.4245	15.37	5.268	−0.01553	25.250	5.0670	1.1216
100.	8.49	1.070	0.4256	14.63	5.270	−0.01551	25.327	5.0696	1.1242
200.	8.49	1.072	0.4265	13.97	5.272	−0.01549	25.393	5.0718	1.1264
300.	8.49	1.074	0.4273	13.36	5.274	−0.01548	25.450	5.0738	1.1284
400.	8.49	1.076	0.4281	12.80	5.276	−0.01547	25.501	5.0755	1.1304
500.	8.49	1.077	0.4287	12.29	5.277	−0.01546	25.545	5.0770	1.1316
600.	8.49	1.079	0.4292	11.82	5.279	−0.01546	25.584	5.0784	1.1330
700.	8.49	1.080	0.4297	11.38	5.280	−0.01545	25.619	5.0795	1.1341
800.	8.49	1.081	0.4302	10.97	5.281	−0.01544	25.649	5.0806	1.1352
900.	8.49	1.082	0.4306	10.59	5.282	−0.01544	25.677	5.0815	1.1361
1000.	8.49	1.082	0.4309	10.24	5.282	−0.01543	25.702	5.0824	1.1370

Table 23. Earth–Moon-escape (ΔV_1 = 4.7679 km/sec, T_{12} = 16.27 hr, θ_{12} = 126.66 deg, a_1 = −10961. km, e_1 = 1.6002, V_1 = 6.200 km/sec, injection altitude = 200 km, HEV_1 = 6.0304 km/sec)

DOCA, km	TISI, hr	ΔV_2, km/sec	$\Delta\Delta V_1$, km/sec	DA, deg	V_2, km/sec	a_3, km × 10^6	e_3	V_∞, km/sec	ΔV_∞, km/sec
0.	5.85	1.031	0.5400	7.73	7.231	−7938.	47.944	7.0862	1.056
100.	5.85	1.029	0.5390	7.33	7.229	−7942.	47.848	7.0844	1.054
200.	5.85	1.028	0.5381	6.98	7.228	−7946.	47.760	7.0828	1.052
300.	5.85	1.026	0.5373	6.65	7.226	−7949.	47.679	7.0813	1.051
400.	5.85	1.025	0.5366	6.36	7.225	−7952.	47.604	7.0799	1.050
500.	5.85	1.024	0.5359	6.09	7.224	−7955.	47.534	7.0786	1.048
600.	5.85	1.022	0.5353	5.84	7.222	−7958.	47.648	7.0774	1.047
700.	5.85	1.021	0.5346	5.61	7.221	−7960.	47.407	7.0763	1.046
800.	5.85	1.020	0.5340	5.40	7.220	−7963.	47.350	7.0752	1.045
900.	5.85	1.019	0.5335	5.21	7.219	−7965.	47.297	7.0742	1.044
1000.	5.85	1.018	0.5330	5.03	7.218	−7967.	47.247	7.0733	1.043

Table 24. Earth–Moon-escape (ΔV_1 = 5.867 km/sec, T_{12} = 12.56 hr, θ_{12} = 117.16 deg, a_1 = 6117. km, e_1 = 2.0754, V_1 = 8.200 km/sec, injection altitude = 200 km, HEV_1 = 8.073 km/sec)

DOCA, km	TISI, hr	ΔV_2, km/sec	$\Delta\Delta V_1$, km/sec	DA, deg	V_2, km/sec	a_3, km × 10^6	e_3	V_∞, km/sec	ΔV_∞, km/sec
0.	4.45	0.872	0.541	4.58	9.072	−4968.	65.926	8.957	0.884
100.	4.45	0.870	0.540	4.34	9.070	−4971.	65.731	8.955	0.882
200.	4.45	0.868	0.538	4.12	9.068	−4973.	65.554	8.953	0.880
300.	4.45	0.866	0.537	3.93	9.066	−4975.	65.394	8.951	0.878
400.	4.45	0.864	0.536	3.75	9.064	−4977.	65.248	8.949	0.876
500.	4.45	0.863	0.535	3.59	9.063	−4979.	65.113	8.947	0.874
600.	4.45	0.861	0.534	3.44	9.061	−4981.	64.989	8.946	0.873
700.	4.45	0.860	0.533	3.30	9.060	−4982.	64.876	8.945	0.872
800.	4.45	0.859	0.533	3.17	9.059	−4984.	64.770	8.943	0.870
900.	4.45	0.857	0.532	3.06	9.057	−4985.	64.672	8.942	0.869
1000.	4.45	0.856	0.531	2.95	9.056	−4986.	64.581	8.941	0.868

IV. SOLAR PROBE POSTENCOUNTER TRAJECTORIES

The main reason why solar probe trajectories require very high launch energies is because the probe not only has to escape the Earth's gravitational field but also counteract its high orbital velocity. For example, if one wishes to construct a minimum launch energy trajectory that will pass through the Sun's center, one has to shoot directly opposite the Earth's orbital velocity vector and completely nullify it. Since the Earth's orbital velocity is about 29.8 km/sec, this minimum energy trajectory which will have an eccentricity equal to 1 will require a launch hyperbolic excess velocity of 29.8 km/sec.

If our rocket is designed to deliver only 11 km/sec hyperbolic excess velocity, the closest distance it can come to the Sun will be about 0.25 AU. This is well within the orbit of Mercury, but to really probe the Sun's atmosphere, one has to come much closer than 23,200,000 miles.

Let V_h denote the hyperbolic excess velocity of a minimum energy solar probe trajectory from a direct Earth launch. This will be taken to mean that trajectory which takes a vehicle closest to the Sun for a given V_h.

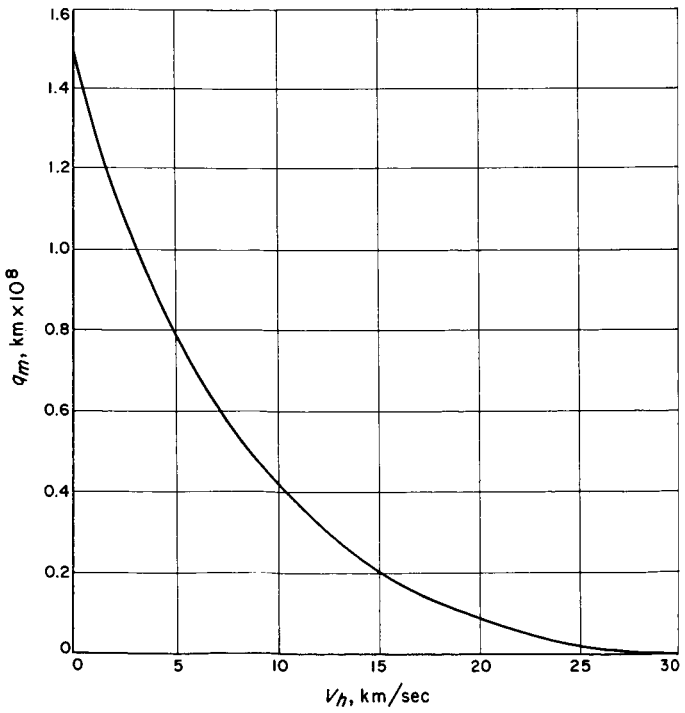

Fig. 28. Graph of the function of q_m in terms of orbital velocity at a distance R_1

If q_m denotes this minimum distance (i.e., perihelion distance), we shall see that it can be expressed as

$$q_m = \left[\frac{2\mu_s}{2\mu_s - R_1(V_0 - V_h)^2} - 1\right] R_1$$

where V_0 is the orbital velocity at a distance R_1. Figure 28 is a graph of this function.

To obtain really good solar probe trajectories it is highly desirable to come at least 10 million km from the surface. Figure 28 shows that hyperbolic excess velocities near 20 km/sec will be required. One way of achieving these close approaches is to spiral-in with an ion engine with its low thrust working continuously in the direction opposite its velocity vector. We shall replace the ion engine with planetary approach guidance and utilize the gravitational influence of a passing planet.

A. The Determination of Solar Probe Postencounter Trajectories Corresponding to the Initial Conditions (P_1, T_1; P_2, T_2)

Let us denote the perihelion distance of the postencounter trajectory by q and drop subscripts. Then, we have

$$q = a(1 - e)$$

Proceeding by the method of undetermined Lagrange multipliers, we seek the solutions to the following system of equations:

$$\frac{\partial q}{\partial x} - \lambda_1 \frac{\partial G_1}{\partial x} = 0$$

$$\frac{\partial q}{\partial y} - \lambda_1 \frac{\partial G_1}{\partial y} = 0$$

$$\frac{\partial q}{\partial z} - \lambda_1 \frac{\partial G_1}{\partial z} = 0$$

$$G_1 = 0$$

Among these solutions will be the vector V_2 which minimizes q and satisfies the constraining equation,

$G_1 = 0$. The first three equations become

$$\left[a\frac{\partial e}{\partial y} + 2\lambda_1(y - u_2)\right]\frac{\partial a}{\partial x} = \left[a\frac{\partial e}{\partial x} + 2\lambda_1(x - u_1)\right]\frac{\partial a}{\partial y}$$

$$\left[a\frac{\partial e}{\partial z} + 2\lambda_1(z - u_3)\right]\frac{\partial a}{\partial x} = \left[a\frac{\partial e}{\partial x} + 2\lambda_1(x - u_1)\right]\frac{\partial a}{\partial z}$$

$$\left[a\frac{\partial e}{\partial z} + 2\lambda_1(z - u_3)\right]\frac{\partial a}{\partial y} = \left[a\frac{\partial e}{\partial y} + 2\lambda_1(y - u_2)\right]\frac{\partial a}{\partial z}$$

From Eq. (9) it follows that

$$e^2 = 1 - \frac{h^2}{\mu a}$$

Thus we have the relations

$$\frac{\partial e}{\partial x} = \frac{h^2\dfrac{\partial a}{\partial x} - a\dfrac{\partial h^2}{\partial x}}{2e\mu a^2}$$

$$\frac{\partial e}{\partial y} = \frac{h^2\dfrac{\partial a}{\partial y} - a\dfrac{\partial h^2}{\partial y}}{2e\mu a^2}$$

$$\frac{\partial e}{\partial z} = \frac{h^2\dfrac{\partial a}{\partial z} - a\dfrac{\partial h^2}{\partial z}}{2e\mu a^2}$$

Substituting these equations into the above system we obtain

$$\left[2\lambda_1(y - u_2) - \frac{1}{2\mu e}\frac{\partial h^2}{\partial y}\right]\frac{\partial a}{\partial x} = \left[2\lambda_1(x - u_1) - \frac{1}{2\mu e}\frac{\partial h^2}{\partial x}\right]\frac{\partial a}{\partial y}$$

$$\left[2\lambda_1(z - u_3) - \frac{1}{2\mu e}\frac{\partial h^2}{\partial z}\right]\frac{\partial a}{\partial x} = \left[2\lambda_1(x - u_1) - \frac{1}{2\mu e}\frac{\partial h^2}{\partial x}\right]\frac{\partial a}{\partial z}$$

$$\left[2\lambda_1(z - u_3) - \frac{1}{2\mu e}\frac{\partial h^2}{\partial z}\right]\frac{\partial a}{\partial y} = \left[2\lambda_1(y - u_2) - \frac{1}{2\mu e}\frac{\partial h^2}{\partial y}\right]\frac{\partial a}{\partial z}$$

Now by the definition of the **h** vector, it follows that

$$h^2 = R^2V^2 - (\mathbf{R}\cdot\mathbf{V})^2$$

where we take $\mathbf{R} = \mathbf{R}_p$ and $\mathbf{V} = \mathbf{V}_2$. Thus, we obtain

$$\frac{\partial h^2}{\partial x} = 2R^2x - 2R_1(\mathbf{R}\cdot\mathbf{V})$$

$$\frac{\partial h^2}{\partial y} = 2R^2y - 2R_2(\mathbf{R}\cdot\mathbf{V})$$

$$\frac{\partial h^2}{\partial z} = 2R^2z - 2R_3(\mathbf{R}\cdot\mathbf{V})$$

From the energy equation, we also find

$$\frac{\partial a}{\partial x} = \frac{2xa^2}{\mu}$$

$$\frac{\partial a}{\partial y} = \frac{2ya^2}{\mu}$$

$$\frac{\partial a}{\partial z} = \frac{2za^2}{\mu}$$

Our system now becomes expressible as

$$[2\lambda_1\mu e u_2 - R_2(\mathbf{R}\cdot\mathbf{V})]\,x = [2\lambda_1\mu e u_1 - R_1(\mathbf{R}\cdot\mathbf{V})]\,y$$

$$[2\lambda_1\mu e u_3 - R_3(\mathbf{R}\cdot\mathbf{V})]\,x = [2\lambda_1\mu e u_1 - R_1(\mathbf{R}\cdot\mathbf{V})]\,z$$

$$[2\lambda_1\mu e u_3 - R_3(\mathbf{R}\cdot\mathbf{V})]\,y = [2\lambda_1\mu e u_2 - R_2(\mathbf{R}\cdot\mathbf{V})]\,z$$

If we set

$$\lambda^* = \frac{\mathbf{R}\cdot\mathbf{V}}{2\mu\lambda_1 e}$$

the system can be expressed as

$$(\mathbf{V}_p - \lambda^*\,\mathbf{R}_p)\times\mathbf{V}_2 = 0 \qquad (27)$$

If on the other hand we replaced the perihelion function $q = a\,(1 - e)$ by the aphelion function $q = a\,(1 + e)$ and repeated the above analysis we would obtain the equation

$$(\mathbf{V}_p + \lambda^*\,\mathbf{R}_p)\times\mathbf{V}_2 = 0 \qquad (28)$$

Hence the postencounter trajectory which will take the vehicle closest to the Sun (or farthest from the Sun when a hyperbolic postencounter trajectory is not possible) must lie in the orbital plane of P_2. This is a very interesting fact since the pre-encounter trajectory may have a very high inclination relative to P_2's orbital plane. It is also interesting to notice that in general the postencounter trajectory having least or maximum energy will not be the one having smallest perihelion or greatest aphelion distances respectively. This is because $\mathbf{V}_2$ must be parallel to $\mathbf{V}_p$ if the energy is to be maximum or minimum, but this will not in general satisfy Eq. (27) or (28). It will only satisfy these equations when P_2 is at its perihelion or aphelion when the encounter takes place. This is because $\mathbf{V}_p$ and $\mathbf{R}_p$ will be perpendicular.

In proceeding with the general case the vector $\mathbf{V}_2$ must satisfy

$$[\mathbf{V}_2\,\mathbf{R}_p\,\mathbf{V}_p] = 0$$

where the notation $[\mathbf{V}_2\,\mathbf{R}_p\,\mathbf{V}_p]$ stands for the determinant

$$[\mathbf{V}_2\,\mathbf{R}_p\,\mathbf{V}_p] \equiv \begin{vmatrix} x & y & z \\ R_1 & R_2 & R_3 \\ u_1 & u_2 & u_3 \end{vmatrix}$$

This is because $\mathbf{V}_2$ is a linear combination of $\mathbf{R}_p$ and $\mathbf{V}_p$. Hence

$$y = Ax + Cz$$

where

$$A = \frac{R_2 u_3 - R_3 u_2}{R_1 u_3 - R_3 u_1}$$

$$C = \frac{R_1 u_2 - R_2 u_1}{R_1 u_3 - R_3 u_1}$$

Substituting into the constraining equation yields

$$z = \frac{-E \pm (E^2 - DF)^{1/2}}{D}$$

where

$$D = 1 + C^2$$

$$E = AC\,x - U_2 C - u_3$$

$$F = (1 + A^2)\,x^2 - 2\,(u_1 + u_2 A)\,x + 2\,\mathbf{V}_p\cdot\mathbf{V}_1 - \mathbf{V}_1^2$$

Consequently

$$\mathbf{V}_2 = (x, y(x), z(x))$$

and the final solution is obtained by solving

$$\frac{d}{dx}\,[a\,(1 - e)] = 0$$

or in the case of maximum aphelion trajectories

$$\frac{d}{dx}\,[a\,(1 + e)] = 0$$

These equations become

$$(1 \mp e)^2\,\frac{da}{dx} = \frac{1}{\mu}\,\frac{dh^2}{dx}$$

where the negative or positive sign is chosen according to whether minimum perihelion or maximum aphelion trajectories are being calculated. The resulting expressions become very complicated and we omit the details.

Since planetary orbits are nearly circular, $\mathbf{V}_p$ will be nearly perpendicular to $\mathbf{R}_p$. Thus the solutions to Eq. (27) and (28) will be nearly parallel to $\mathbf{V}_p$. Substituting $\mathbf{V}_2 = k\,\mathbf{V}_p$ into the constraining equation where k is some undetermined scalar yields the solution

$$k = 1 \mp \frac{V'}{V_p}$$

which gives

$$\mathbf{V}_2 = \left(1 \mp \frac{V'}{V_p}\right)\mathbf{V}_p$$

These are the same vectors which maximized and minimized the postencounter energy. Hence if $V' < V_p$, we conclude that the asymptotic velocity vector $\mathbf{V}_2$ that will take the vehicle close to the closest possible distance to the Sun is

$$\mathbf{V}_2 = \left(1 - \frac{V'}{V_p}\right)\mathbf{V}_p$$

It should be noted that if it is possible to have $V' \geq V_p$, an actual Sun impact is possible. This vector will also minimize the postencounter energy.

By letting $\sigma = \measuredangle \mathbf{V}'_1, \mathbf{V}_p$, we may express the velocity decrease after encounter by the formulas:

$$\Delta V = V' \left[2(1 + \cos\sigma)\right]^2$$

$$\delta V = V' - V_p + (V_p^2 + 2V_p V' \cos\sigma + V'^2)^{1/2}$$

For Hohmann transfers we observe that when P_2 is inside the orbit of P_1, $\Delta V = \delta V = 2V'$; but when P_2 is outside, this velocity change is 0. Thus, we conclude that when $V' < V_p$, the orbit of the perturbing planet should be inside the orbit of P_1. This is just the opposite for the case of deep space trajectories.

Venus is almost eight times the mass of Mars. It is also inside the Earth's orbit. Thus, Venus should generate much better solar probe trajectories than deep space trajectories. Table 25 gives an example of these trajectories. These trajectories do pass further away from its center than those associated with deep space trajectories, but we still find negative distances of closest approach. Table 26 gives a sample of Earth-Mars solar-probe trajectories. This table clearly confirms the fact that P_2 should be inside the orbit of P_1 when $V' < V_p$. The table shows that the velocity loss is minimum when the launch energy is minimum. This is because the Earth-Mars transfers approach Hohmann and $\sigma \to 180$ deg.

Earth–Jupiter–Sun, 1967–1978. Let us now consider the possibility of actually impacting the Sun. We have

Table 25. Earth–Venus minimum perihelion (launch date Aug. 22, 1970)

T_{12}, days	HEV_1, km/sec	θ_{12}, deg	ϕ_{12}, deg	a_1, AU	e_1	Perihelion$_1$, AU	$B \cdot \hat{T}$, km	$B \cdot \hat{R}$, km	V_1, km/sec	TISI, hr	DOCA, km	DA, deg	V_2, km/sec	a_3, AU	e_3	Perihelion$_3$, AU
70.	7.504	62.80	2.68	0.7019	0.4421	2.393	1727.	−31.	34.444	0.90	−5249.	75.06	19.339	0.4273	0.6948	0.130
74.	6.630	69.19	2.25	0.7238	0.3983	0.436	1987.	−50.	35.020	1.00	−5156.	78.37	20.852	0.4398	0.6454	0.156
78.	5.872	75.59	1.85	0.7442	0.3595	0.477	2293.	−75.	35.525	1.10	−5051.	81.71	22.242	0.4528	0.5969	0.183
82.	5.218	81.99	1.47	0.7632	0.3255	0.514	2653.	−110.	35.964	1.21	−4933.	85.09	23.518	0.46624	0.5496	0.210
86.	4.659	88.41	1.11	0.7804	0.2960	0.549	3075.	−162.	36.345	1.34	−4802.	88.54	24.688	0.4800	0.5041	0.238
90.	4.185	94.84	0.74	0.7959	0.2707	0.581	3566.	−238.	36.672	1.48	−4658.	92.11	25.756	0.4939	0.4606	0.2664
94.	3.793	101.28	0.37	0.8096	0.2492	0.617	4130.	−354.	36.951	1.64	−4505.	95.82	26.726	0.5079	0.4196	0.2948
98.	3.476	107.72	0.02	0.8216	0.2312	0.632	4761.	−534.	37.188	1.81	−4349.	99.68	27.597	0.5215	0.3815	0.3225
102.	3.231	114.17	0.44	0.8319	0.2164	0.653	5433.	−815.	37.386	1.99	−4200.	103.71	28.367	0.5346	0.3469	0.3491
106.	3.057	120.63	0.90	0.8405	0.2044	0.669	6090.	−1252.	37.551	2.18	−4075.	107.82	29.029	0.5467	0.3164	0.3737
110.	2.955	127.09	1.43	0.8477	0.1948	0.683	6617.	−1910.	37.685	2.36	−3989.	111.85	29.569	0.5571	0.2911	0.3949
114.	2.933	133.56	2.07	0.8535	0.1872	0.695	6828.	−2838.	37.791	2.51	−3958.	115.39	29.961	0.5651	0.2725	0.4111
118.	3.010	140.02	2.85	0.8580	0.1815	0.703	6487.	−3979.	37.874	2.60	−3982.	117.78	30.167	0.5693	0.2627	0.4197

Table 26. Earth–Mars minimum perihelion (launch date May 19, 1971)

T_{12}, days	HEV_1, km/sec	θ_{12}, deg	ϕ_{12}, deg	a_1, AU	e_1	q, AU	$B \cdot \hat{T}$, km	$B \cdot \hat{R}$, km	V_1, km/sec	TISI, days	DOCA, km	DA, deg	V_2, km/sec	a_3, AU	e_3	q, AU
100.	5.347	90.01	1.83	1.607	0.3706	1.0114	−514.	0.	27.045	1.24	−3183.	82.82	16.739	0.8844	0.5634	0.3861
106.	4.879	93.82	1.81	1.519	0.3338	1.0114	−657.	0.	26.456	1.37	−3109.	80.20	17.680	0.9132	0.5132	0.4446
112.	4.490	97.62	1.79	1.453	0.3037	1.0114	−842.	1.	25.956	1.51	−3011.	77.43	18.514	0.9422	0.4662	0.5030
118.	4.167	101.43	1.77	1.403	0.2789	1.0114	−1079.	2.	25.529	1.66	−2880.	74.50	19.254	0.9713	0.4226	0.5608
124.	3.901	105.24	1.75	1.364	0.2586	1.0114	−1386.	5.	25.162	1.83	−2704.	71.37	19.908	1.0001	0.3825	0.6176
130.	3.682	109.03	1.74	1.334	0.2419	1.0114	−1786.	10.	24.844	2.01	−2465.	68.00	20.484	1.0285	0.3459	0.6728
136.	3.502	112.82	1.71	1.311	0.2283	1.0114	−2309.	20.	24.567	2.21	−2140.	64.38	20.987	1.0560	0.3128	0.7257
142.	3.355	116.60	1.69	1.292	0.2173	1.0114	−2995.	37.	24.323	2.42	−1694.	60.45	21.422	1.0826	0.2833	0.7758
148.	3.236	120.37	1.67	1.277	0.2083	1.0114	−3899.	68.	24.107	2.64	−1077.	56.21	21.793	1.1077	0.2575	0.8225
154.	3.139	124.12	1.64	1.266	0.2012	1.0114	−5095.	126.	23.913	2.87	−219.	51.64	22.104	1.1312	0.2352	0.8651
160.	3.061	127.85	1.62	1.257	0.1955	1.0114	−6685.	230.	23.737	3.11	982.	46.72	22.358	1.1527	0.2166	0.9030
166.	2.999	131.56	1.59	1.249	0.1911	1.0114	−8813.	422.	23.576	3.35	2679.	41.47	22.556	1.1720	0.2017	0.9357
172.	2.949	135.25	1.55	1.244	0.1877	1.0114	−11694.	782.	23.426	3.58	5105.	35.95	22.702	1.1889	0.1902	0.9628
178.	2.911	138.91	1.52	1.241	0.1852	1.0114	−15675.	1484.	23.285	3.80	8644.	30.20	22.799	1.2031	0.1821	0.9841
184.	2.882	142.54	1.47	1.238	0.1835	1.0114	−21360.	2941.	23.152	3.99	13991.	24.35	22.848	1.2146	0.1771	0.9995
190.	2.861	146.15	1.42	1.237	0.1824	1.0114	−29915.	6312.	23.025	4.15	22577.	18.52	22.854	1.2235	0.1749	1.0095
196.	2.847	149.73	1.36	1.236	0.1819	1.0114	−43419.	15523.	22.903	4.27	37764.	12.93	22.821	1.2299	0.1754	1.0142
202.	2.839	153.27	1.29	1.236	0.1819	1.0114	−60218.	46419.	22.784	4.34	67437.	8.08	22.753	1.2339	0.1779	1.0143
208.	2.837	156.79	1.19	1.237	0.1822	1.0114	−16779.	108127.	22.669	4.34	100727.	5.66	22.653	1.2359	0.1824	1.0104
214.	2.840	160.27	1.07	1.238	0.1830	1.0114	44515.	65560.	22.556	4.37	70645.	7.75	22.527	1.2360	0.1885	1.0030
220.	2.847	163.72	0.89	1.240	0.1840	1.0114	39075.	31757.	22.445	4.35	41969.	11.88	22.376	1.2346	0.1960	0.9926
226.	2.858	167.13	0.63	1.242	0.1854	1.0114	29050.	19222.	22.336	4.29	26737.	16.48	22.201	1.2316	0.2049	0.9792
232.	2.879	170.51	0.19	1.244	0.1870	1.0114	21044.	13791.	22.229	4.19	17429.	21.44	21.994	1.2264	0.2158	0.9617

already seen from Fig. 28 that the minimum launch hyperbolic excess velocity required for a trajectory to have unit eccentricity and therefore pass through the Sun's center is 29.8 km/sec. The trajectory is simply a straight line. After escaping the Earth, the probe becomes stationary and then simply falls directly into the Sun.

Suppose P_2 is a hypothetical planet moving in a circular coplanar orbit with P_1 which also has circular motion with radius R_1. We assume P_2 is outside the orbit of P_1. We shall consider the problem of determining the radius of P_2's orbit and also the minimum launch energy, such that after encounter, the probe becomes stationary and falls directly into the Sun.

For this to be true we must have $\mathbf{V}_2$ equal to $\mathbf{0}$. Hence, in this case, we have

$$V_p = V'$$

This means that the transfer must be less than 180 deg. For minimum energy, it is clear that the transfer $P_1 - P_2$ must begin at perihelion. Thus, we have

$$R_1 = a(1 - e)$$

According to Fig. 29, we have

$$\mathbf{V}_p = (\sin\theta, -\cos\theta, 0)V_p$$

$$\mathbf{e} = (-e, 0, 0)$$

$$\mathbf{h} = (0, 0, h)$$

$$\mathbf{R}_p = (-\cos\theta, -\sin\theta, 0)R_p$$

By employing Eq. (4), we find

$$\mathbf{V}_1 = \frac{h}{l}\,(\sin\theta, -e - \cos\theta, 0)$$

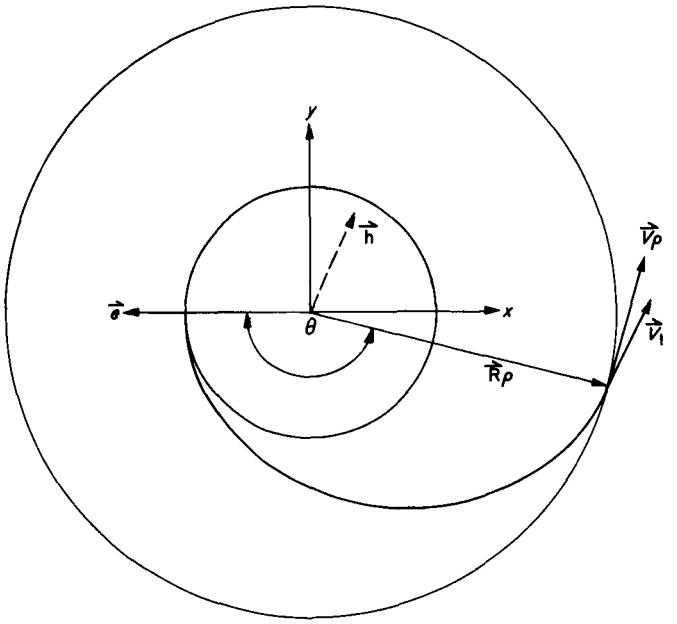

Fig. 29. Description of the functions of V_p, e, h, and R_p

Now we have

$$\mathbf{V}_1' = \mathbf{V}_1 - \mathbf{V}_p$$

Hence

$$V'^2 = V_1^2 - 2\mathbf{V}_1 \cdot \mathbf{V}_p + V_p^2$$

Since $V' = V_p$, we obtain the relation

$$V_1^2 = 2\mathbf{V}_1 \cdot \mathbf{V}_p$$

From this equation, we obtain

Making use of the relations

$$R_1 = a(1 - e),\ h^2 = \mu l,\ l = a(1 - e^2),\ \text{and}\ V_p^2 = \frac{\mu}{R_p}$$

enables our equation to be written as

$$4(R_p - 2R_1)\,a^2 + 4(R_1^2 - R_p^2)\,a + R_p^3 = 0 \qquad (29)$$

We now solve this quadratic equation and obtain

$$a = f(R_p)$$

The solution of $f'(R_p) = 0$ will then give us the solution to our problem. The solution corresponding to the case when $R_1 = 1$ is $R_p = 4.1$. Thus, the minimum launch hyperbolic excess velocity is only 5.0 km/sec. By substituting Jupiter's semimajor axis for R_p into Eq. (29), we find a = 6.4 AU. This corresponds to a launch hyperbolic excess velocity of 10.5 km/sec. This means that whenever our launch hyperbolic excess velocity is just a little greater than 10.5 km/sec, we can actually aim the departing asymptotic velocity vector V_2 directly at the Sun.

Let $\hat{\mathbf{R}}$ denote any arbitrary unit vector. By setting $\mathbf{V}_2 = V_2\hat{\mathbf{R}}$ and substituting it into Eq. (15), we find

$$V_2 = \mathbf{V}_p \cdot \hat{\mathbf{R}} \pm [(\mathbf{V}_p \cdot \hat{\mathbf{R}})^2 + V'^2 - V_p^2]^{1/2} \qquad (30)$$

The vector $\hat{\mathbf{R}}$ denotes a unit direction vector. Consequently, we observe that if $V' > V_p$, the direction of $\hat{\mathbf{R}}$

$$\frac{h^2}{l^2}(\sin^2\theta + e^2 + 2e\cos\theta + \cos^2\theta) = \frac{2hV_p}{l}(\sin^2\theta + e\cos\theta + \cos^2\theta)\,\frac{h}{l}\,[2(1 + e\cos\theta) + e^2 - 1]$$

$$= 2V_p(1 + e\cos\theta)$$

But

$$R_p = \frac{l}{1 + e\cos\theta}$$

Hence, we have

$$\frac{h}{l}\left[\frac{2l}{R_p} + e^2 - 1\right] = \frac{2V_p l}{R_p}$$

can be arbitrarily chosen. In particular, we can choose $\hat{\mathbf{R}} = -\hat{\mathbf{R}}_p$ in the case of solar impact postencounter trajectories, or we can choose $\hat{\mathbf{R}}$ so that 90-deg postencounter trajectories result. We shall consider this case later.

Let $\measuredangle\, \mathbf{V}_p, \hat{\mathbf{R}} = \theta$. Then Eq. (30) becomes

$$V_2 = V_p \cos\theta \pm [V'^2 - V_p^2 \sin^2\theta]^{1/2}$$

Hence, when $\theta = 0$, we find

$$\mathbf{V}_2 = \left(1 \pm \frac{V'}{V_p}\right)\mathbf{V}_p$$

which we have already discovered as the solution extremizing the energy.

By taking

$$\mathbf{R} = -\frac{\mathbf{R}_p}{R_p}$$

we obtain

$$\mathbf{V}_2 = \left\{\mathbf{V}_p \cdot \hat{\mathbf{R}}_p - [(\mathbf{V}_p \cdot \hat{\mathbf{R}}_p)^2 + V'^2 - V_p^2]^{1/2}\right\}\hat{\mathbf{R}}_p$$

Tables 27 through 37 represent a very detailed study of Earth-Jupiter-Sun trajectories. The Earth-Jupiter transfers were those used for the escape trajectories. The column labeled VAP gives the velocity of the probe as it becomes enveloped in the Sun's photosphere. The total flight time beginning from injection is labeled TFT.

These trajectories may be ideal for carrying out extensive solar measurements. Recent studies have shown that the Sun's atmosphere may extend well beyond the orbit of Mars. These trajectories will enable highly instrumented solar probes to continuously monitor solar phe-

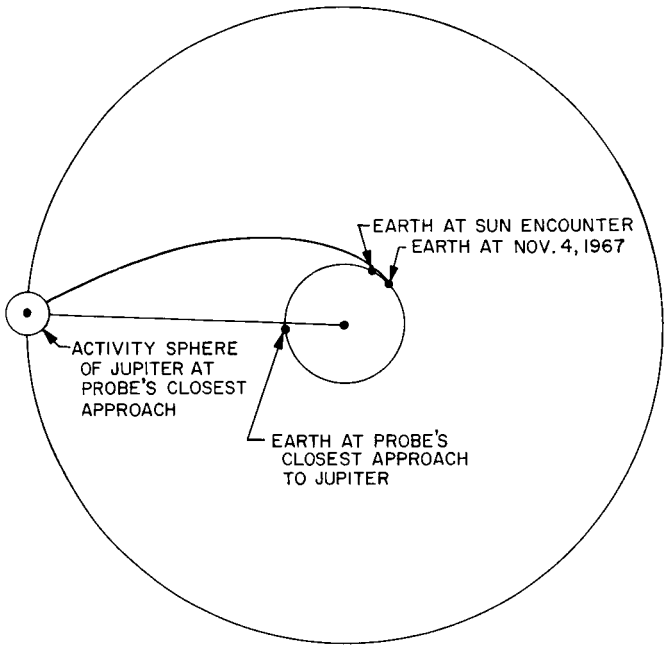

Fig. 30. Planetary configuration for Earth–Jupiter–Sun, 1967 (Nov. 4 trajectory)

Table 27. Earth–Jupiter–Sun, 1967 (launch HEV = 11.0 km/sec)

Launch date, 1967	T_{12}, days	θ_{12}, deg	ϕ_{12}, deg	$B \cdot \hat{T}$, km	$B \cdot \hat{R}$, km	V_1, km/sec	TISI, days	DOCA, km	DA, deg	V_2, km/sec	T_{23}, days	VAP, km/sec	TFT, yr
10/25	532.00	151.11	2.68	−1034421	−5217	13.807	87.70	437726	75.18	1.836	726.22	617.45	3.445
10/27	524.00	148.67	2.49	−894402	−7335	14.059	86.06	340222	81.16	3.054	673.75	617.45	3.279
10/29	516.00	146.22	2.32	−796024	−8069	14.317	84.46	276584	85.56	3.954	639.29	617.46	3.163
10/31	510.00	143.92	2.19	−739524	−8231	14.502	83.36	241801	88.20	4.498	619.98	617.46	3.094
11/2	506.00	141.77	2.09	−710782	−8231	14.607	82.75	224597	89.58	4.786	610.22	617.47	3.056
11/4	504.00	139.77	2.00	−704686	−8215	14.630	82.62	220988	89.87	4.848	608.15	617.47	3.045
11/6	504.00	137.91	1.93	−720348	−8242	14.570	82.96	230282	89.12	4.691	613.44	617.46	3.059
11/8	506.00	136.21	1.87	−760482	−8326	14.427	83.79	254552	87.21	4.296	627.05	617.46	3.102
11/10	512.00	134.81	1.82	−863444	−8447	14.128	85.60	319773	82.52	3.337	662.61	617.46	3.216
11/12	522.00	133.70	1.79	−1144673	−7652	13.686	88.52	520570	70.62	0.898	772.13	617.45	3.543

nomena from about 5 AU all the way down to solar impact. The flight times are quite within reason. The vehicle begins its fall into the Sun with velocities near 7 or 8 km/sec. The associated figures provide useful information regarding radio communication. For example, in 1968, the Sun is almost directly between the Earth and probe during its last few days of flight.

Refer to Fig. 30 through 51 for a graphic presentation relative to the above discussion.

Table 28. Earth–Jupiter–Sun, 1968 (launch HEV = 11.0 km/sec)

Launch date, 1968	T_{12}, days	θ_{12}, deg	ϕ_{12}, deg	$B \cdot \hat{T}$, km	$B \cdot \hat{R}$, km	V_1, km/sec	TISI, days	DOCA, km	DA, deg	V_2, km/sec	T_{23}, days	VAP, km/sec	TFT, yr
11/20	544.00	154.84	2.83	−1223341	10188	13.365	88.47	584811	67.17	0.537	788.87	617.45	3.649
11/22	532.00	152.06	2.58	−895963	2149	13.759	85.79	342197	80.89	3.380	659.40	617.46	3.263
11/24	522.00	149.44	2.39	−771497	404	14.094	83.76	262032	86.51	4.531	617.74	617.46	3.120
11/26	514.00	146.96	2.23	−696691	−272	14.359	82.22	216864	90.10	5.275	593.35	617.47	3.032
11/28	508.00	144.63	2.11	−651414	−535	14.550	81.17	190627	92.36	5.753	578.64	617.47	2.975
11/30	504.00	142.46	2.01	−627818	−606	14.659	80.57	177281	93.57	6.011	570.96	617.48	2.943
12/2	500.00	140.28	1.91	−605710	−643	14.768	79.99	164996	94.73	6.261	563.71	617.48	2.912
12/4	498.00	138.25	1.84	−601109	−602	14.791	79.86	162468	94.97	6.315	562.17	617.48	2.903
12/6	498.00	136.37	1.77	−613521	−509	14.727	80.19	169328	94.31	6.174	566.20	617.48	2.914
12/8	502.00	134.80	1.72	−663296	−312	14.495	81.45	197448	91.75	5.627	582.39	617.47	2.969
12/10	508.00	133.37	1.67	−742765	−25	14.186	83.19	244450	87.86	4.814	608.17	617.47	3.056
12/12	518.00	132.25	1.63	−906620	625	13.730	85.92	349423	80.41	3.290	662.75	617.46	3.233

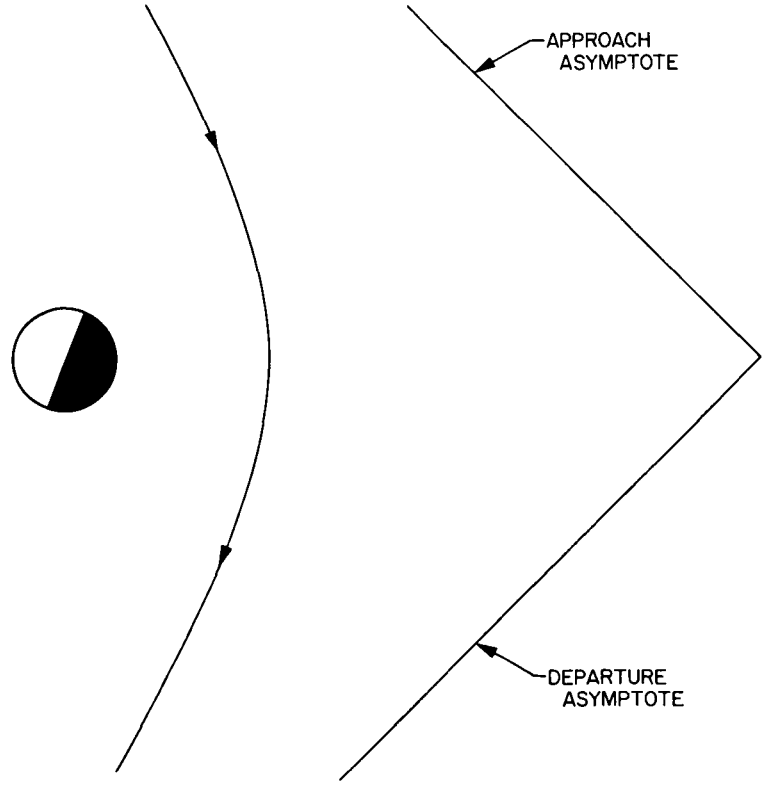

Fig. 31. November 4, 1967, Earth–Jupiter–Sun trajectory during its closest approach to Jupiter

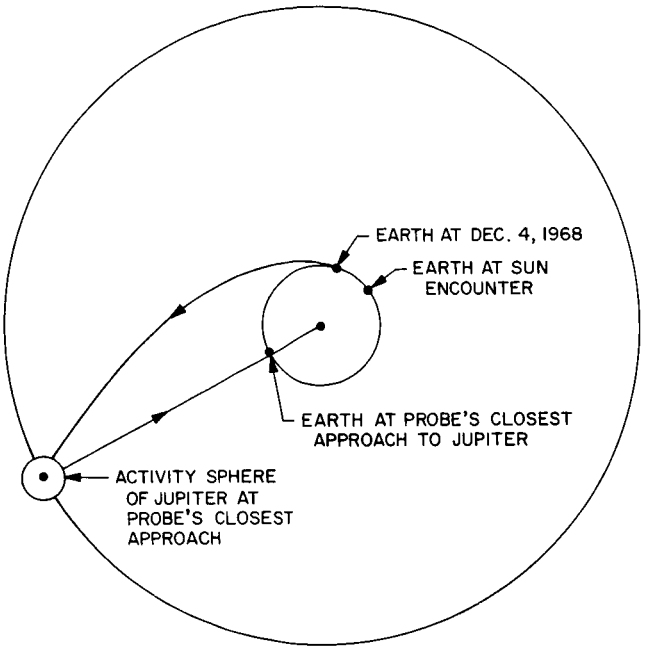

Fig. 32. Planetary configuration for Earth–Jupiter–Sun, 1968 (Dec. 4 trajectory)

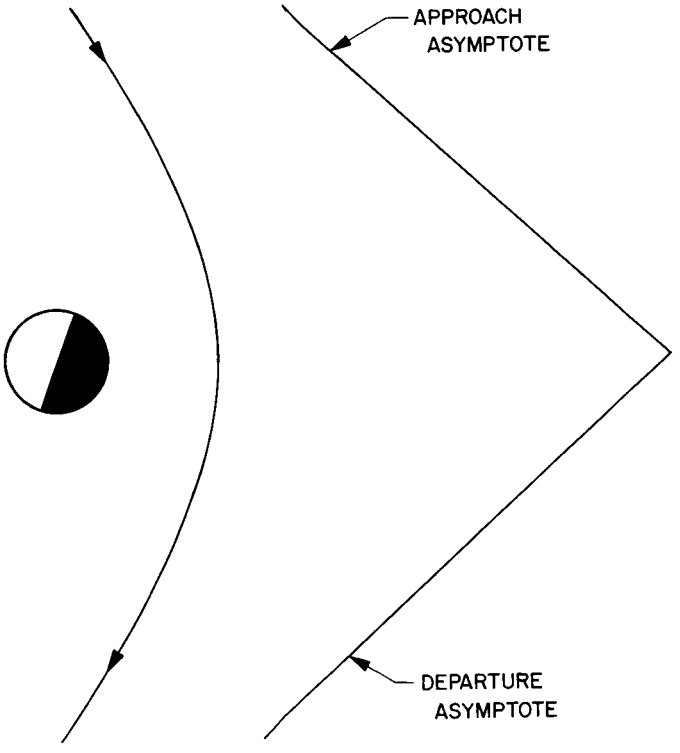

Fig. 33. December 4, 1968, Earth–Jupiter–Sun trajectory during its closest approach to Jupiter

Table 29. Earth–Jupiter–Sun, 1969–70 (launch HEV = 11.0 km/sec)

Launch date, 1969–70	T_{12}, days	θ_{12}, deg	ϕ_{12}, deg	$B \cdot \hat{T}$, km	$B \cdot \hat{R}$, km	V_1, km/sec	TISI, days	DOCA, km	DA, deg	V_2, km/sec	T_{23}, days	VAP, km/sec	TFT, yr
12/18	538.0	156.48	1.98	−1130395.	15563.	13.338	85.78	519614.	69.60	1.369	730.73	617.44	3.474
12/20	528.0	153.82	1.82	−890011.	10627.	13.667	83.66	343766.	79.98	3.536	640.49	617.45	3.199
12/22	518.0	151.16	1.69	−761202.	8563.	14.009	81.66	259897.	85.93	4.770	598.06	617.46	3.056
12/24	508.0	148.50	1.58	−664843.	7274.	14.362	79.70	201677.	90.69	5.774	567.27	617.47	2.944
12/26	502.0	146.15	1.49	−620987.	6770.	14.560	78.66	176452.	92.98	6.264	553.33	617.48	2.889
12/28	496.0	143.80	1.41	−581548.	6361.	14.761	77.64	154473.	95.11	6.728	540.71	617.48	2.838
12/30	490.0	141.46	1.35	−545740.	6012.	14.963	76.62	135103.	97.11	7.173	529.11	617.49	2.790
1/1	486.0	139.26	1.29	−526922.	5863.	15.079	76.05	125149.	98.19	7.417	522.95	617.49	2.762
1/3	484.0	137.22	1.24	−522948.	5875.	15.105	75.93	123070.	98.42	7.470	521.63	617.49	2.753
1/5	484.0	135.34	1.20	−533441.	6037.	15.038	76.25	128591.	97.81	7.332	525.04	617.49	2.763
1/7	486.0	133.62	1.15	−559667.	6350.	14.881	77.01	142599.	96.31	6.999	533.53	617.48	2.791
1/9	490.0	132.05	1.11	−604977.	6828.	14.637	78.23	167502.	93.82	6.452	548.03	617.48	2.843
1/11	498.0	130.79	1.07	−697467.	7705.	14.230	80.38	221036.	89.02	5.426	577.40	617.47	2.944

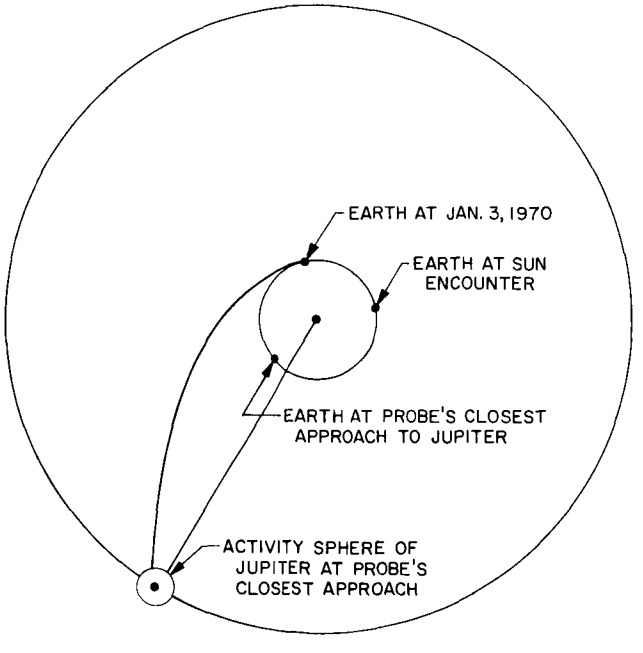

Fig. 34. Planetary configuration for Earth–Jupiter–Sun, 1969–70 (Jan. 3 trajectory)

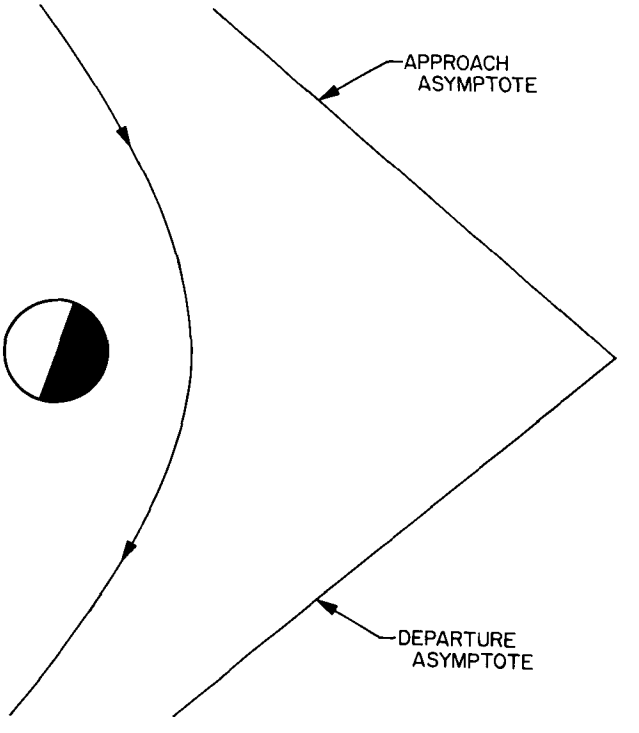

Fig. 35. January 3, 1970, Earth–Jupiter–Sun trajectory during its closest approach to Jupiter

Table 30. Earth–Jupiter–Sun, 1971 (launch HEV = 11.0 km/sec)

Launch date, 1971	T_{12}, days	θ_{12}, deg	ϕ_{12}, deg	$B \cdot \hat{T}$, km	$B \cdot \hat{R}$, km	V_1, km/sec	TISI, days	DOCA, km	DA, deg	V_2, km/sec	T_{23}, days	VAP, km/sec	TFT, yr
4/29	516.0	154.13	0.38	−925746.	15899.	13.720	80.84	377866.	76.47	3.012	639.10	617.44	3.162
5/1	506.0	151.44	0.38	−772353.	14264.	14.072	78.84	273829.	83.69	4.542	586.60	617.45	2.991
5/3	496.0	148.75	0.38	−666722.	12925.	14.438	76.90	208197.	89.02	5.685	552.47	617.46	2.870
5/5	490.0	146.39	0.37	−619864.	12294.	14.644	75.87	180627.	91.52	6.228	537.55	617.47	2.813
5/7	482.0	143.86	0.36	−561584.	11447.	14.942	74.42	147707.	94.77	6.951	518.87	617.48	2.740
5/9	478.0	141.67	0.35	−540649.	11142.	15.064	73.85	136241.	95.99	7.224	512.14	617.48	2.711
5/11	474.0	139.48	0.34	−520968.	10850.	15.186	73.28	125651.	97.15	7.489	505.74	617.48	2.682
5/13	470.0	137.28	0.33	−502440.	10570.	15.307	72.73	115852.	98.27	7.747	499.66	617.49	2.655
5/15	468.0	135.25	0.32	−498583.	10524.	15.334	72.60	113837.	98.50	7.802	498.37	617.49	2.646
5/17	468.0	133.39	0.30	−509019.	10706.	15.264	72.92	119330.	97.86	7.654	501.77	617.48	2.655
5/19	470.0	131.69	0.29	−535029.	11125.	15.099	73.67	133232.	96.30	7.298	510.21	617.48	2.684
5/21	474.0	130.15	0.26	−580138.	11803.	14.843	74.87	158071.	93.70	6.713	524.70	617.47	2.734
5/23	482.0	128.95	0.24	−672886.	13041.	14.418	76.98	211972.	88.67	5.612	554.27	617.46	2.837
5/25	494.0	128.07	0.20	−863492.	15027.	13.844	80.08	334548.	79.30	3.616	616.94	617.45	3.042

Table 31. Earth–Jupiter–Sun, 1972 (launch HEV = 11.0 km/sec)

Launch date, 1972	T_{12}, days	θ_{12}, deg	ϕ_{12}, deg	$B \cdot \hat{T}$, km	$B \cdot \hat{R}$, km	V_1, km/sec	TISI, days	DOCA, km	DA, deg	V_2, km/sec	T_{23}, days	VAP, km/sec	TFT, yr
2/23	492.0	150.51	1.09	−863697.	15459.	14.174	76.69	344199.	77.24	3.180	610.10	617.44	3.017
2/25	484.0	147.98	0.99	−746793.	15185.	14.464	75.16	264955.	83.04	4.443	568.90	617.45	2.883
2/27	476.0	145.46	0.91	−661269.	14536.	14.761	73.67	210994.	87.53	5.428	540.26	617.45	2.782
2/29	470.0	143.10	0.85	−611678.	13994.	14.976	72.65	181235.	90.26	6.035	523.95	617.46	2.721
3/2	464.0	140.75	0.79	−568098.	13423.	15.194	71.64	156028.	92.76	6.599	509.63	617.47	2.666
3/4	460.0	138.58	0.75	−545561.	13088.	15.320	71.07	143335.	94.09	6.902	502.22	617.47	2.634
3/6	456.0	136.40	0.72	−524578.	12751.	15.446	70.51	131742.	95.36	7.194	495.28	617.47	2.604
3/8	454.0	134.40	0.69	−520167.	12665.	15.474	70.39	129333.	95.63	7.256	493.81	617.47	2.595
3/10	454.0	132.58	0.68	−531816.	12836.	15.403	70.69	135724.	94.92	7.091	497.66	617.47	2.605
3/12	456.0	130.92	0.67	−561367.	13276.	15.235	71.45	152226.	93.15	6.684	507.41	617.47	2.638
3/14	458.0	129.27	0.66	−593856.	13738.	15.066	72.22	170856.	91.26	6.257	518.05	617.46	2.672
3/16	464.0	127.97	0.67	−674781.	14787.	14.715	73.89	219360.	86.78	5.260	544.70	617.45	2.762
3/18	474.0	127.02	0.69	−854568.	16458.	14.202	76.54	337923.	77.65	3.264	606.84	617.44	2.959

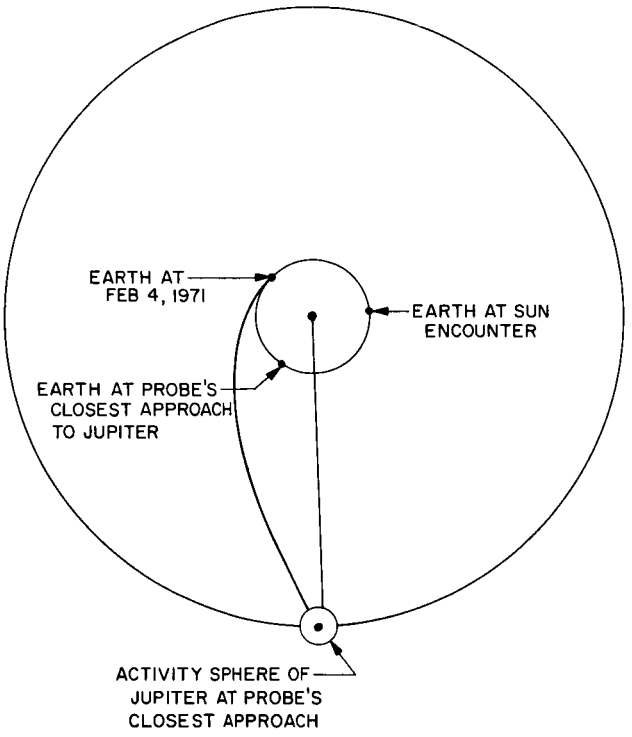

Fig. 36. Planetary configuration for Earth–Jupiter–Sun, 1971 (Feb. 4 trajectory)

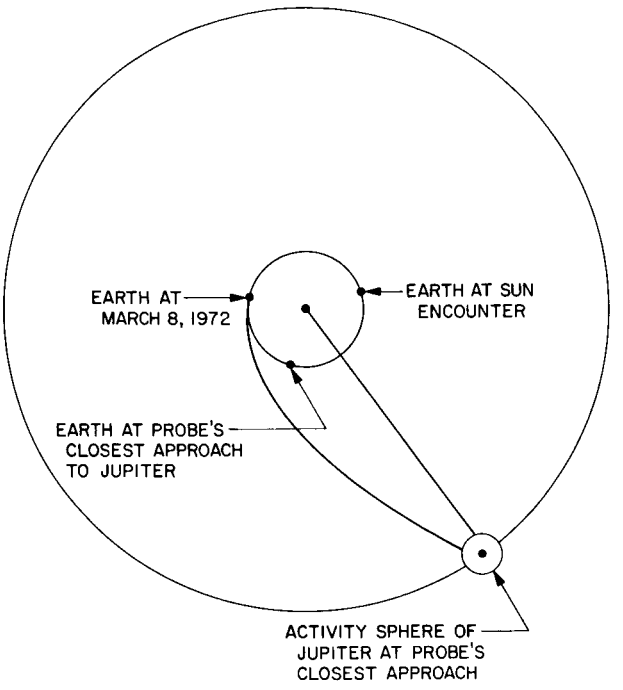

Fig. 38. Planetary configuration for Earth–Jupiter–Sun, 1972 (March 8 trajectory)

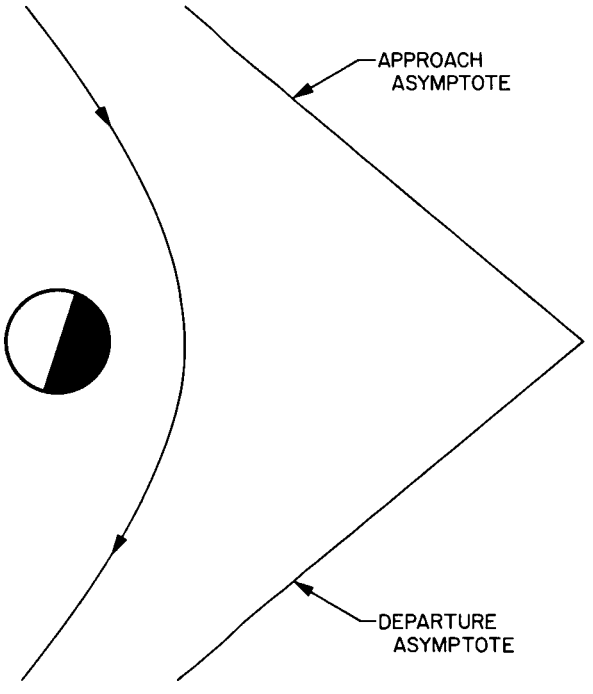

Fig. 37. Feb. 4, 1971, Earth–Jupiter–Sun trajectory during its closest approach to Jupiter

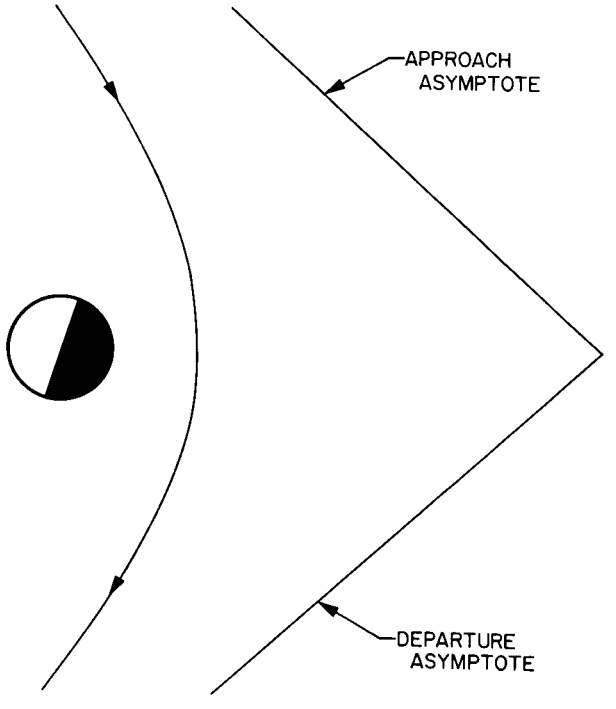

Fig. 39. March 8, 1972, Earth–Jupiter–Sun trajectory during its closest approach to Jupiter

Table 32. Earth–Jupiter–Sun, 1973 (launch HEV = 11.0 km/sec)

Launch date, 1973	T_{12}, days	θ_{12}, deg	ϕ_{12}, deg	$B \cdot \hat{T}$, km	$B \cdot \hat{R}$, km	V_1, km/sec	TISI, days	DOCA, km	DA, deg	V_2, km/sec	T_{23}, days	VAP, km/sec	TFT, yr
4/2	470.0	145.60	1.96	−863100.	10962.	14.666	73.93	351819.	75.53	2.558	613.60	617.43	2.967
4/4	464.0	143.27	1.85	−766549.	11552.	14.879	72.85	284287.	80.45	3.655	576.39	617.43	2.848
4/6	458.0	140.94	1.74	−695598.	11596.	15.095	71.79	237610.	84.21	4.493	550.70	617.44	2.762
4/8	454.0	138.79	1.67	−661492.	11510.	15.221	71.20	216032.	86.08	4.911	538.70	617.44	2.718
4/10	450.0	136.65	1.59	−630778.	11358.	15.346	70.62	197086.	87.79	5.299	527.98	617.45	2.678
4/12	448.0	134.69	1.54	−624367.	11322.	15.375	70.49	193186.	88.16	5.380	525.78	617.45	2.666
4/14	446.0	132.73	1.49	−618384.	11283.	15.401	70.36	189575.	88.50	5.457	523.69	617.45	2.655
4/16	446.0	130.96	1.45	−635093.	11420.	15.330	70.69	199737.	87.55	5.241	529.49	617.45	2.671
4/18	450.0	129.54	1.43	−705462.	11918.	15.068	71.94	243970.	83.67	4.367	554.32	617.44	2.749
4/20	454.0	128.13	1.41	−797341.	12410.	14.810	73.22	305366.	78.85	3.291	588.10	617.43	2.853

Table 33. Earth–Jupiter–Sun, 1974 (launch HEV = 11.5 km/sec)

Launch date, 1974	T_{12}, days	θ_{12}, deg	ϕ_{12}, deg	$B \cdot \hat{T}$, km	$B \cdot \hat{R}$, km	V_1, km/sec	TISI, days	DOCA, km	DA, deg	V_2, km/sec	T_{23}, days	VAP, km/sec	TFT, yr
5/9	448.0	144.33	2.24	−685441.	4073.	15.564	70.61	233224.	84.16	4.113	555.17	617.43	2.746
5/11	440.0	141.85	2.11	−603896.	4440.	15.896	69.08	182584.	88.77	5.164	525.08	617.44	2.642
5/13	434.0	139.56	2.01	−556462.	4482.	16.137	68.03	154618.	91.59	5.817	507.88	617.45	2.579
5/15	430.0	137.44	1.93	−531977.	4437.	16.278	67.43	140605.	93.10	6.168	499.05	617.45	2.544
5/17	426.0	135.33	1.86	−509277.	4360.	16.420	66.84	127888.	94.53	6.506	490.83	617.46	2.510
5/19	422.0	133.23	1.79	−488150.	4263.	16.561	66.26	116291.	95.89	6.832	483.14	617.46	2.478
5/21	420.0	131.30	1.74	−483440.	4199.	16.595	66.13	113733.	96.20	6.905	481.44	617.46	2.468
5/23	418.0	129.38	1.69	−479012.	4137.	16.626	66.00	111347.	96.48	6.976	479.81	617.46	2.458
5/25	420.0	127.83	1.65	−506357.	4188.	16.441	66.77	126267.	94.72	6.547	489.84	617.46	2.491
5/27	422.0	126.27	1.62	−536397.	4254.	16.257	67.54	143102.	92.83	6.099	500.77	617.45	2.526
5/29	426.0	124.90	1.59	−589952.	4391.	15.970	68.79	174225.	89.59	5.344	520.22	617.44	2.591
5/31	432.0	123.72	1.57	−680243.	4588.	15.589	70.53	229888.	84.45	4.170	553.45	617.43	2.698
6/2	442.0	122.90	1.55	−925792.	4639.	15.034	73.31	402051.	71.67	1.276	655.08	617.42	3.004

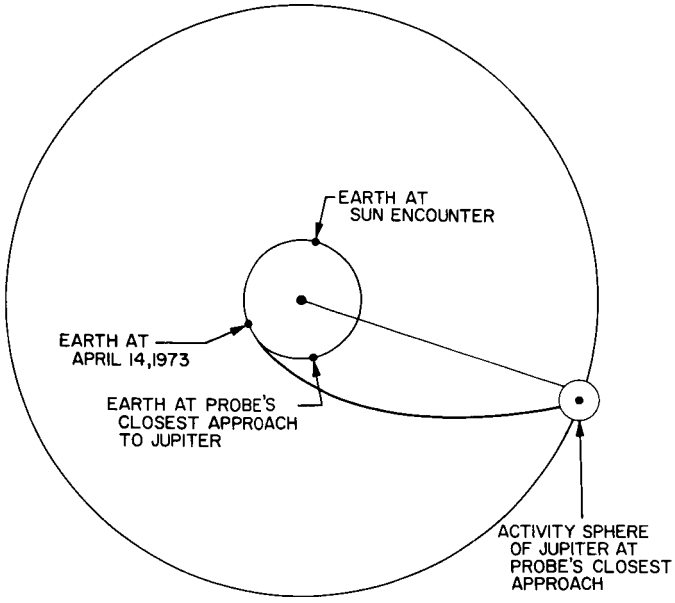

Fig. 40. Planetary configuration for Earth–Jupiter–Sun, 1973 (April 14 trajectory)

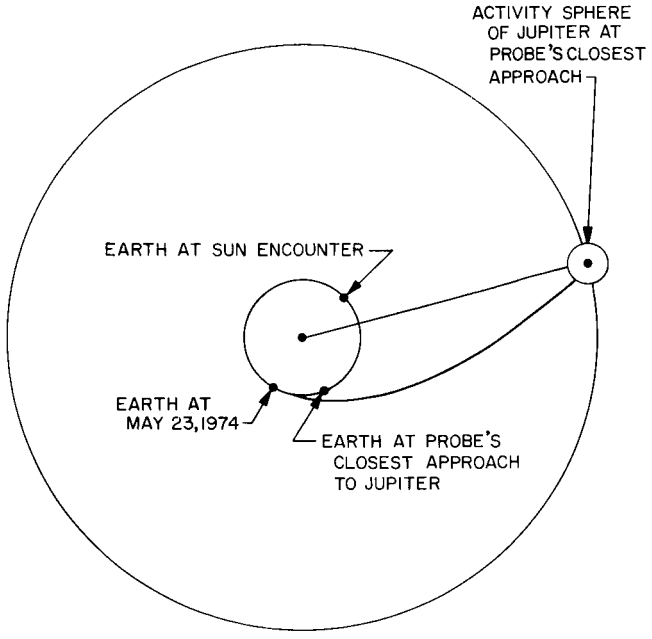

Fig. 42. Planetary configuration for Earth–Jupiter–Sun, 1974 (May 23 trajectory)

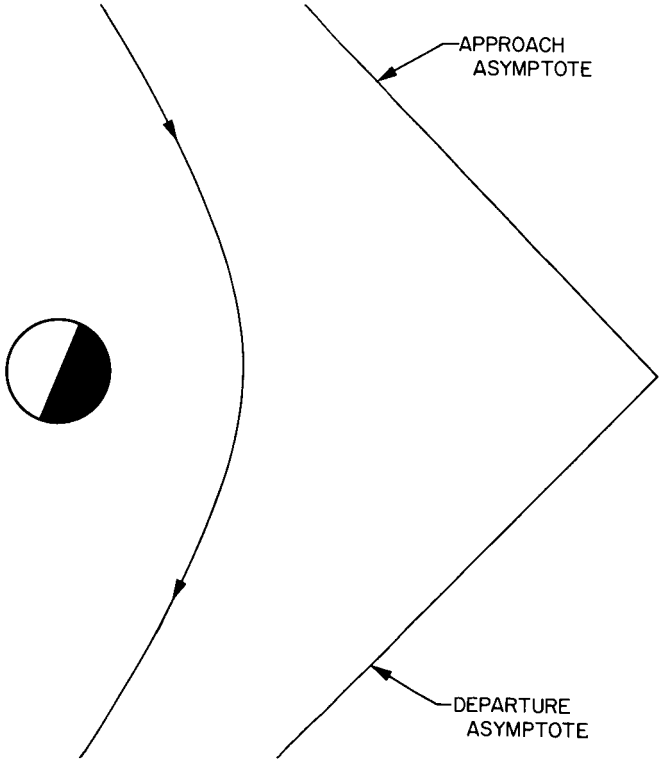

Fig. 41. April 14, 1973, Earth–Jupiter–Sun trajectory during its closest approach to Jupiter

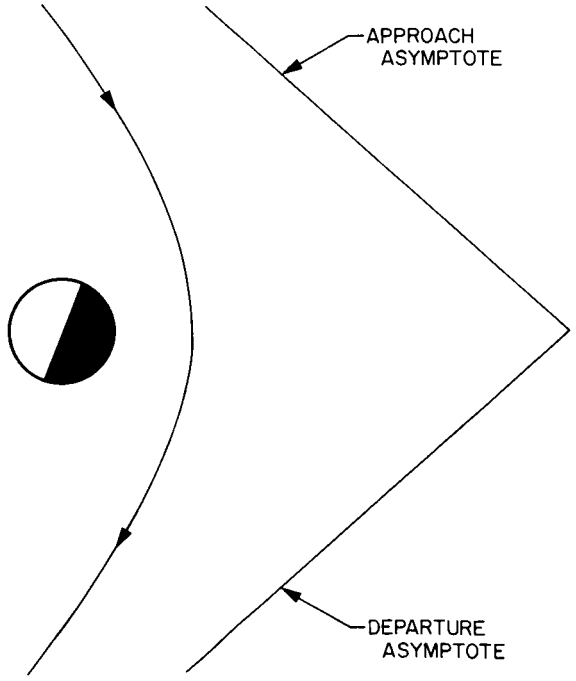

Fig. 43. May 23, 1974, Earth–Jupiter–Sun trajectory during its closest approach to Jupiter

Table 34. Earth–Jupiter–Sun, 1975 (launch HEV = 11.5 km/sec)

Launch date, 1975	T_{12}, days	θ_{12}, deg	ϕ_{12}, deg	$B \cdot \hat{T}$, km	$B \cdot \hat{R}$, km	V_1, km/sec	TISI, days	DOCA, km	DA, deg	V_2, km/sec	T_{23}, days	VAP, km/sec	TFT, yr
6/15	458.0	146.58	1.81	−870068.	−7357.	15.352	74.10	356223.	75.32	1.665	647.81	617.43	3.027
6/17	450.0	144.13	1.72	−734772.	−5483.	15.669	72.46	262518.	82.25	3.217	590.70	617.43	2.849
6/19	444.0	141.87	1.64	−668018.	−4733.	15.899	71.35	219629.	85.85	4.022	564.60	617.44	2.761
6/21	438.0	139.60	1.57	−612631.	−4202.	16.132	70.25	185687.	88.95	4.726	543.45	617.44	2.687
6/23	434.0	137.51	1.51	−584495.	−3973.	16.270	69.63	169001.	90.58	5.098	532.86	617.44	2.647
6/25	430.0	135.42	1.46	−558681.	−3784.	16.407	69.02	154037.	92.11	5.452	523.15	617.45	2.609
6/27	428.0	133.52	1.41	−552726.	−3766.	16.441	68.88	150621.	92.47	5.534	520.94	617.45	2.598
6/29	426.0	131.61	1.37	−547137.	−3751.	16.472	68.74	147441.	92.81	5.614	518.85	617.45	2.586
7/1	426.0	129.88	1.33	−560233.	−3871.	16.399	69.07	154911.	92.02	5.430	523.81	617.45	2.600
7/3	428.0	128.34	1.29	−594379.	−4118.	16.222	69.87	174785.	90.02	4.964	536.73	617.44	2.641
7/5	430.0	126.79	1.26	−632611.	−4365.	16.044	70.69	197719.	87.83	4.466	551.22	617.44	2.686
7/7	436.0	125.60	1.23	−733627.	−4931.	15.674	72.48	261682.	82.33	3.229	590.51	617.43	2.810
7/9	444.0	124.60	1.20	−977926.	−6051.	15.222	74.87	437783.	69.99	0.451	700.38	617.42	3.133

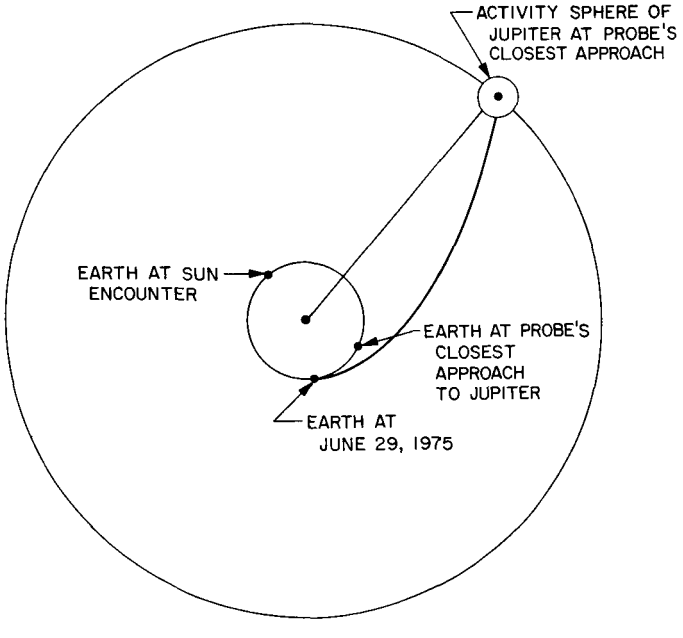

Fig. 44. Planetary configuration for Earth–Jupiter–Sun, 1975 (June 29 trajectory)

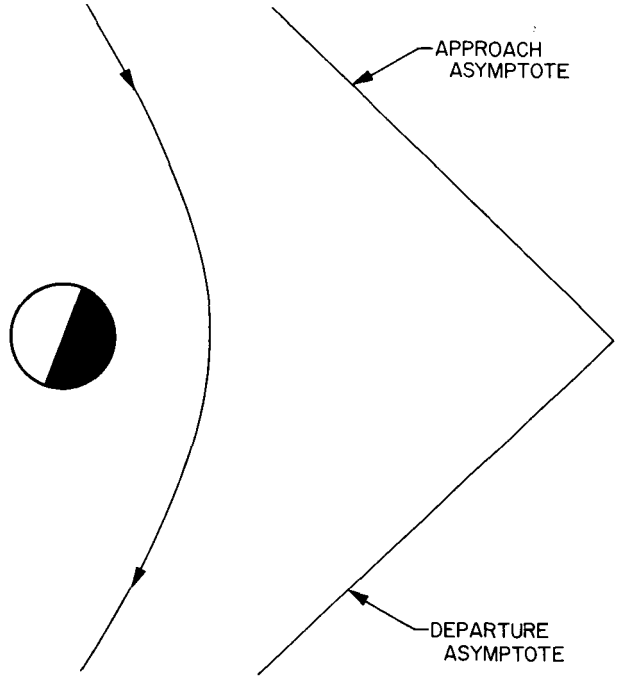

Fig. 45. June 29, 1975, Earth–Jupiter–Sun trajectory during its closest approach to Jupiter

Table 35. Earth–Jupiter–Sun, 1976 (launch HEV = 11.5 km/sec)

Launch date, 1976	T_{12}, days	θ_{12}, deg	ϕ_{12}, deg	$B \cdot \hat{T}$, km	$B \cdot \hat{R}$, km	V_1, km/sec	TISI, days	DOCA, km	DA, deg	V_2, km/sec	T_{23}, days	VAP, km/sec	TFT, yr
7/21	472.0	148.15	0.57	−907198.	−14725.	15.200	77.62	373223.	75.58	1.445	680.01	617.43	3.154
7/23	464.0	145.73	0.55	−771384.	−13296.	15.504	75.94	279372.	82.21	2.891	622.48	617.44	2.975
7/25	458.0	143.47	0.53	−703247.	−12493.	15.724	74.80	235570.	85.69	3.653	595.64	617.44	2.885
7/27	452.0	141.22	0.52	−646571.	−11797.	15.947	73.67	200773.	88.71	4.319	573.84	617.45	2.809
7/29	448.0	139.13	0.50	−617641.	−11430.	16.078	73.04	183567.	90.30	4.673	562.86	617.45	2.768
7/31	444.0	137.05	0.49	−591049.	−11086.	16.208	72.41	168101.	91.79	5.009	552.77	617.45	2.729
8/2	442.0	135.14	0.47	−584845.	−11016.	16.241	72.26	164529.	92.15	5.089	550.46	617.45	2.717
8/4	440.0	133.22	0.46	−579042.	−10949.	16.271	72.12	161214.	92.48	5.165	548.26	617.45	2.706
8/6	440.0	131.48	0.44	−592423.	−11139.	16.200	72.46	168872.	91.72	4.993	553.36	617.45	2.719
8/8	442.0	129.91	0.42	−627258.	−11584.	16.031	73.28	189202.	89.78	4.556	566.61	617.45	2.761
8/10	446.0	128.50	0.40	−690575.	−12329.	15.767	74.59	227586.	86.38	3.802	590.89	617.44	2.839
8/12	452.0	127.27	0.37	−801913.	−13426.	15.416	76.44	299563.	80.72	2.565	635.03	617.44	2.976

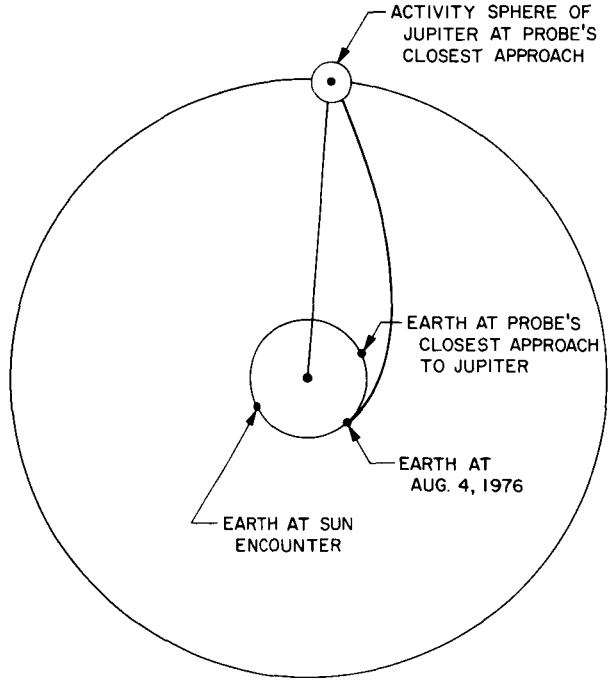

Fig. 46. Planetary configuration for Earth–Jupiter–Sun, 1976 (Aug. 4 trajectory)

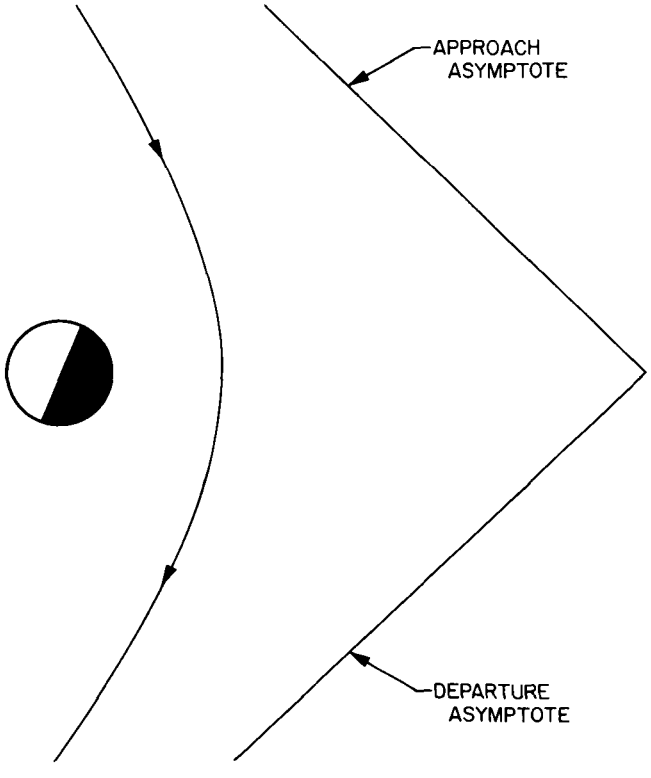

Fig. 47. August 4, 1976, Earth–Jupiter–Sun trajectory during its closest approach to Jupiter

Table 36. Earth–Jupiter–Sun, 1977 (launch HEV = 11.5 km/sec)

Launch date, 1977	T_{12}, days	θ_{12}, deg	ϕ_{12}, deg	$B \cdot \hat{T}$, km	$B \cdot \hat{R}$, km	V_1, km/sec	TISI, days	DOCA, km	DA, deg	V_2, km/sec	T_{23}, days	VAP, km/sec	TFT, yr
8/23	498.0	152.07	1.05	−1019777.	−16297.	14.668	82.61	443147.	72.92	0.866	736.55	617.44	3.380
8/25	488.0	149.49	0.94	−821756.	−16337.	15.033	80.40	303506.	81.93	2.777	652.92	617.44	3.124
8/27	480.0	147.07	0.86	−726237.	−15707.	15.326	78.76	242431.	86.54	3.757	616.46	617.45	3.002
8/29	474.0	144.82	0.80	−671291.	−15158.	15.538	77.62	209073.	89.33	4.354	596.03	617.45	2.929
8/31	468.0	142.56	0.74	−623260.	−14565.	15.752	76.50	180988.	91.85	4.904	578.27	617.46	2.864
9/2	462.0	140.30	0.70	−580590.	−13955.	15.970	75.40	156889.	94.17	5.420	562.45	617.46	2.805
9/4	458.0	138.20	0.66	−558164.	−13598.	16.096	74.78	144539.	95.43	5.703	554.13	617.46	2.771
9/6	456.0	136.26	0.64	−552915.	−13500.	16.127	74.63	141670.	95.73	5.771	552.20	617.46	2.760
9/8	454.0	134.32	0.62	−548008.	−13406.	16.155	74.49	139010.	96.01	5.836	550.36	617.47	2.750
9/10	454.0	132.54	0.61	−559491.	−13577.	16.086	74.83	145246.	95.36	5.689	554.65	617.46	2.761
9/12	458.0	131.08	0.61	−607035.	−14295.	15.828	76.12	171689.	92.73	5.100	572.34	617.46	2.821
9/14	462.0	129.62	0.61	−661454.	−15053.	15.573	77.44	203183.	89.85	4.470	592.44	617.45	2.887
9/16	470.0	128.48	0.62	−778766.	−16438.	15.146	79.76	275417.	84.00	3.219	636.39	617.45	3.029
9/18	482.0	127.66	0.64	−1147760.	−18189.	14.571	83.29	543529.	67.29	0.354	801.48	617.44	3.514

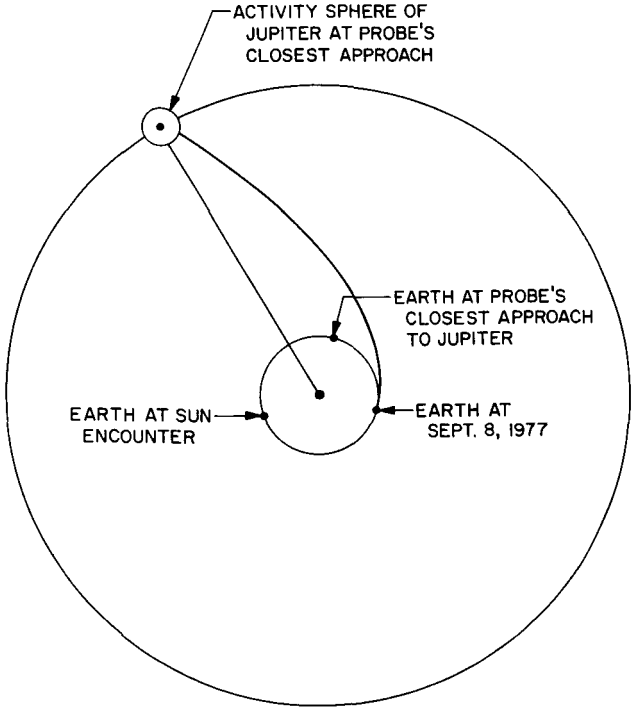

Fig. 48. Planetary configuration for Earth–Jupiter–Sun, 1977 (Sept. 8 trajectory)

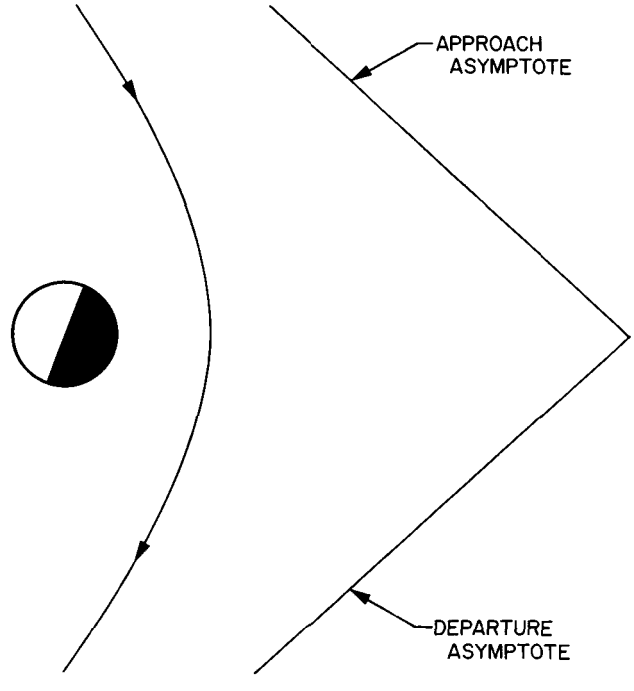

Fig. 49. September 8, 1977, Earth–Jupiter–Sun trajectory during its closest approach to Jupiter

Table 37. Earth–Jupiter–Sun, 1978 (launch HEV = 11.5 km/sec)

Launch date, 1978	T_{12}, days	θ_{12}, deg	ϕ_{12}, deg	$B \cdot \hat{T}$, km	$B \cdot \hat{R}$, km	V_1, km/sec	TISI, days	DOCA, km	DA, deg	V_2, km/sec	T_{23}, days	VAP, km/sec	TFT, yr
9/25	512.0	152.77	2.33	−862697.	−13206.	14.482	84.11	322963.	81.75	2.923	668.96	617.45	3.233
9/27	502.0	150.20	2.12	−741871.	−13506.	14.839	82.00	246105.	87.34	4.082	625.20	617.46	3.086
9/29	492.0	147.61	1.96	−649281.	−13080.	15.208	79.93	191277.	91.92	5.051	592.44	617.46	2.969
10/1	486.0	145.34	1.83	−606471.	−12692.	15.416	78.83	167099.	94.15	5.533	577.34	617.47	2.911
10/3	480.0	143.06	1.73	−567813.	−12241.	15.626	77.74	145940.	96.25	5.992	563.58	617.47	2.857
10/5	474.0	140.79	1.64	−532627.	−11757.	15.839	76.67	127244.	98.22	6.434	550.89	617.48	2.806
10/7	470.0	138.66	1.56	−513924.	−11446.	15.962	76.06	117518.	99.29	6.679	544.09	617.48	2.776
10/9	468.0	136.68	1.51	−509630.	−11322.	15.991	75.92	115300.	99.55	6.737	542.53	617.48	2.767
10/11	466.0	134.71	1.45	−505622.	−11204.	16.017	75.79	113247.	99.78	6.792	541.04	617.48	2.757
10/13	468.0	133.04	1.42	−529622.	−11480.	15.856	76.58	125651.	98.39	6.475	549.82	617.48	2.787
10/15	470.0	131.37	1.39	−555506.	−11777.	15.693	77.39	139323.	96.93	6.148	559.15	617.47	2.818
10/17	476.0	130.00	1.37	−617682.	−12509.	15.352	79.15	173324.	93.57	5.410	581.29	617.47	2.895
10/19	486.0	128.95	1.37	−736031.	−13717.	14.851	81.91	242486.	87.64	4.149	623.07	617.46	3.036
10/21	500.0	128.20	1.37	−992019.	−15178.	14.213	85.78	411913.	76.11	1.771	718.74	617.45	3.337

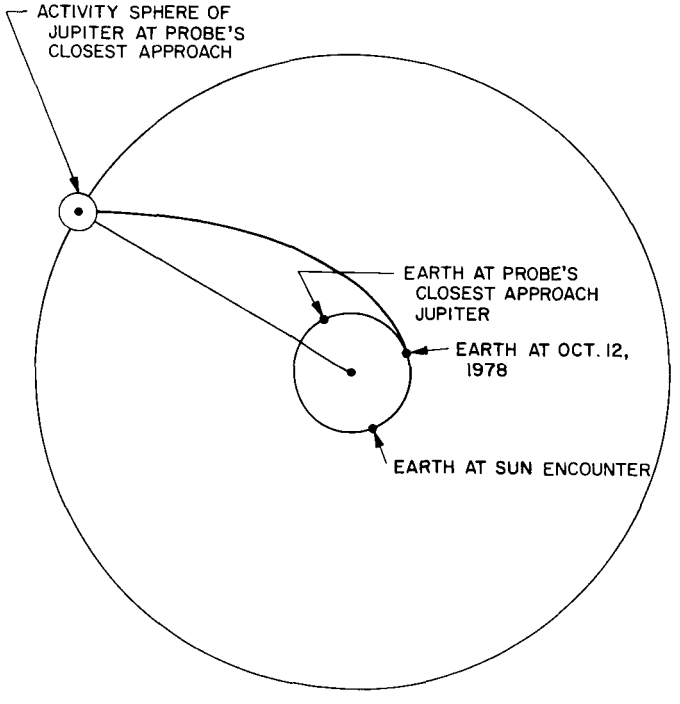

Fig. 50. Planetary configuration for Earth–Jupiter–Sun, 1978 (October 11 trajectory)

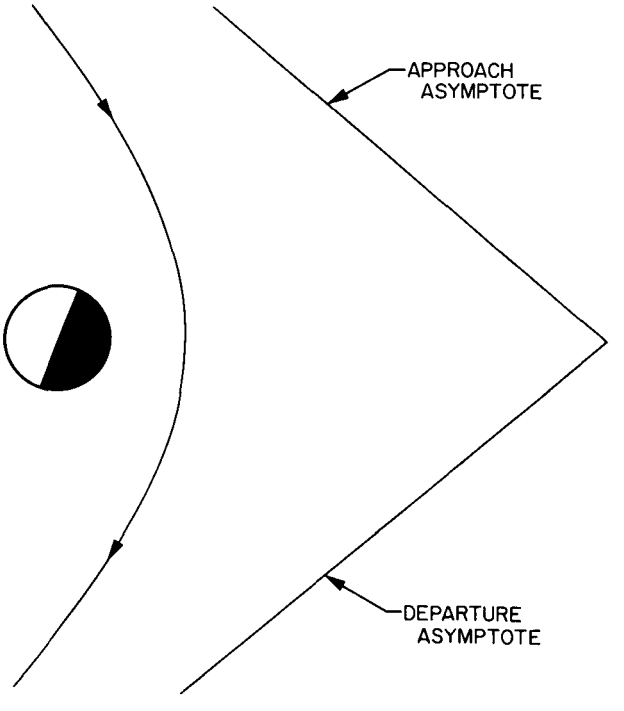

Fig. 51. October 11, 1978, Earth–Jupiter–Sun trajectory during its closest approach to Jupiter

B. The Determination of Solar Probe Post-encounter Trajectories Corresponding to the Initial Conditions ($P_1, T_1; P_2, T_2; d$)

Some solar probe missions may require approaches of only 0.2 to 0.3 AU from the Sun. In this case, Venus would certainly provide a means for reducing launch energies. Let q denote the perihelion distance of a post-encounter trajectory. We proceed by solving the following system:

$$\frac{\partial q}{\partial x} - \lambda_1 \frac{\partial G_1}{\partial x} - \lambda_2 \frac{\partial G_2}{\partial x} = 0$$

$$\frac{\partial q}{\partial y} - \lambda_1 \frac{\partial G}{\partial y} - \lambda_2 \frac{\partial G}{\partial y} = 0$$

$$\frac{\partial q}{\partial z} - \lambda_1 \frac{\partial G}{\partial z} - \lambda_2 \frac{\partial G}{\partial z} = 0$$

$$G_1 = 0$$

$$G_2 = 0$$

The first three equations become

$$\frac{\partial a}{\partial x}(1-e) - a\frac{\partial e}{\partial x} - 2\lambda_1(x-u_1) - \lambda_2 v_1 = 0$$

$$\frac{\partial a}{\partial y}(1-e) - a\frac{\partial e}{\partial y} - 2\lambda_1(y-u_2) - \lambda_2 v_2 = 0$$

$$\frac{\partial a}{\partial z}(1-e) - a\frac{\partial e}{\partial z} - 2\lambda_1(z-u_3) - \lambda_2 v_3 = 0$$

By denoting

$$\lambda^* = \pm \frac{\mathbf{R}_p - \mathbf{V}_2}{\mu e \lambda_2} \qquad \lambda = -\frac{2\lambda_1 + \lambda_2}{\lambda_2}$$

these equations can be written as

$$(\lambda^* \mathbf{R}_p + \lambda \mathbf{V}_p + \mathbf{V}_1)\mathbf{V}_2 = 0 \tag{31}$$

The positive or negative sign in the formula for λ^* is chosen according to whether one wishes to minimize perihelion or maximize aphelion. In either case Eq. (31) shows that V_2 must have the form

$$\mathbf{V}_2 = \alpha(\lambda^* \mathbf{R}_p + \lambda \mathbf{V}_p + \mathbf{V}_1) \tag{32}$$

where α is some undetermined scalar. Consequently when we give the distance of closest approach a specified value the desired postencounter trajectory will not in general be coplanar with P_2's orbit.

Now the scalars λ^*, λ, and α are all unknown thus Eq. (32) just shows that $\mathbf{V}_2$ is not necessarily confined to a certain plane. The solution is best obtained by using

Table 38. Earth–Venus minimum solar approach (launch date Aug. 30, 1970)

T_{12}, days	HEV, km/sec	θ_{12}, deg	ϕ_{12}, deg	a_1, AU	e_1	$\mathbf{B} \cdot \hat{\mathbf{T}}$, km	$\mathbf{B} \cdot \hat{\mathbf{R}}$, km	V_1, km/sec	TISI, days	DOCA, km	DA deg	V_2, km/sec	q_m, AU
67.0	8.641	56.75	3.23	0.6775	0.4957	7078.	394.	33.744	0.82	0.	17.16	28.563	0.229
67.0	8.641	56.75	3.23	0.6775	0.4957	7582.	434.	33.744	0.82	500.	16.03	28.904	0.236
67.0	8.641	56.75	3.23	0.6775	0.4957	8099.	−93.	33.744	0.82	1000.	15.04	29.190	0.242
67.0	8.641	56.75	3.23	0.6775	0.4957	8562.	837.	33.744	0.82	1500.	14.17	29.484	0.247
71	7.635	63.13	2.75	0.7003	0.4469	7273.	412.	34.396	0.90	0.	20.23	28.861	0.256
71	7.635	63.13	2.75	0.7003	0.4469	7775.	513.	34.396	0.90	500.	18.94	29.217	0.263
71	7.635	63.13	2.75	0.7003	0.4469	8276.	−605.	34.396	0.90	1000.	17.80	29.516	0.270
71	7.635	63.13	2.75	0.7003	0.4469	8793.	438.	34.396	0.90	1500.	16.80	29.796	0.275
75	6.757	69.51	2.33	0.7220	0.4032	7497.	−573.	34.971	0.99	0.	23.78	29.077	0.281
75	6.757	69.51	2.33	0.7220	0.4032	8005.	−612.	34.971	0.99	500.	22.31	29.438	0.289
75	6.757	69.51	2.33	0.7220	0.4032	8531.	334.	34.971	0.99	1000.	21.01	29.761	0.295
75	6.757	69.51	2.33	0.7220	0.4032	9038.	367.	34.971	0.99	1500.	19.86	30.047	0.301
79	5.993	75.91	1.93	0.7424	0.3642	7773.	−622.	35.476	1.09	0.	27.86	29.248	0.302
79	5.993	75.91	1.93	0.7424	0.3642	8286.	−663.	35.476	1.09	500.	26.20	29.611	0.311
79	5.993	75.91	1.93	0.7424	0.3642	8821.	265.	35.476	1.09	1000.	24.72	29.940	0.317
79	5.993	75.91	1.93	0.7424	0.3642	9331.	296.	35.476	1.09	1500.	23.41	30.231	0.324
83	5.329	82.32	1.56	0.7612	0.3300	8074.	−969.	35.917	1.20	0.	32.50	29.398	0.323

the constraining equations to express two of the three variables x, y, z in terms of a third, say x, and then solving

$$\frac{d}{dx}\left[a\left(1-e\right)\right]=0$$

The algebraic solution involves very complicated expressions. Numerical solutions, however, are easily obtained by computer.

Table 38 contains a good representation of Earth–Venus–solar probe trajectories. Comparing this table with Fig. 29, we find that for the same launch energies, these postencounter trajectories enable the probe to come about 0.25 AU (37,400,000 km) closer than those launched on direct trajectories. The necessary guidance can be carried out by Earth-based orbit determinations and midcourse maneuvers similar to those of the *Mariner* vehicles.

V. OUT-OF-ECLIPTIC POSTENCOUNTER TRAJECTORIES

A. Introduction

In the previous section we saw that if $V' > V_p$, it is possible to give $\mathbf{V}_2$ any desired direction. In particular, we can give it a direction parallel to the vector $\hat{\mathbf{R}}$ shown in Fig. 52. This figure is drawn in the plane determined by $\mathbf{R}_p$ and $\hat{\mathbf{k}}$. Thus, the resulting trajectory will have an inclination of 90 deg; that is to say, its orbit will be perpendicular to the ecliptic plane. This vector is seen to be calculated by

$$\mathbf{R}=\frac{\mathbf{R}_p\times(\hat{\mathbf{k}}\times\mathbf{R}_p)}{|\mathbf{R}_p\times(\hat{\mathbf{k}}\times\mathbf{R}_p)|}$$

The velocity vector $\mathbf{V}_2$ is then

$$\mathbf{V}_2=\{\mathbf{V}_p\cdot\hat{\mathbf{R}}\pm[(\mathbf{V}_p\cdot\hat{\mathbf{R}})^2+V'^2-V_p^2]^{1/2}\}\hat{\mathbf{R}}$$

The sign is chosen the same as the sign of $\mathbf{V}_p\cdot\hat{\mathbf{R}}$ so that the magnitude of $\mathbf{V}_2$ has greatest value.

B. Earth-Jupiter Out-of-Ecliptic, 1967-1978

Tables 39 through 49 give truly wonderful out-of-ecliptic trajectories. These trajectories would ordinarily require launch hyperbolic excess velocities of about 45 km/sec if they were obtained from direct Earth launches. The periods are not too long, so that information obtained when the probe is near maximum distance from ecliptic plane can be stored and transmitted at a later time when the probe comes near the Earth. The figures describe the configuration of these trajectories. The out-of-ecliptic trajectories are drawn with a solid line. They are perpendicular to the ecliptic plane. The edge-wise view of this plane is shown by the dotted straight line. The Earth's orbit is drawn by the curved dotted line. A projection of the Earth's orbit in the plane of the postencounter trajectory is shown as the short straight line. The numbers correspond to the locations of the probe and Earth at various points along the trajectories. The columns labeled H_1 and H_2 refer to the maximum distances out of the ecliptic plane. The minus numbers refer to distances below this plane.

Figures 53 through 64 relate to the above discussion.

The preceding trajectories take a vehicle a maximum distance of about 2 AU from the ecliptic plane. These were designed so that their periods would not be too long. If, however, the primary goal of an out-of-ecliptic mission is to reach great distances from the plane of the ecliptic, other postencounter trajectories should be constructed. It should be borne in mind, however, that since escape trajectories are possible, there is really no limit as to how far from the plane one can get.

The planets Mars and Venus can be used to obtain inclinations of about 10 to 15 deg. The launch hyperbolic excess velocities are in the neighborhood of 3.5 km/sec. The maximum distances out of the ecliptic plane are about 23 million miles (0.233 AU).

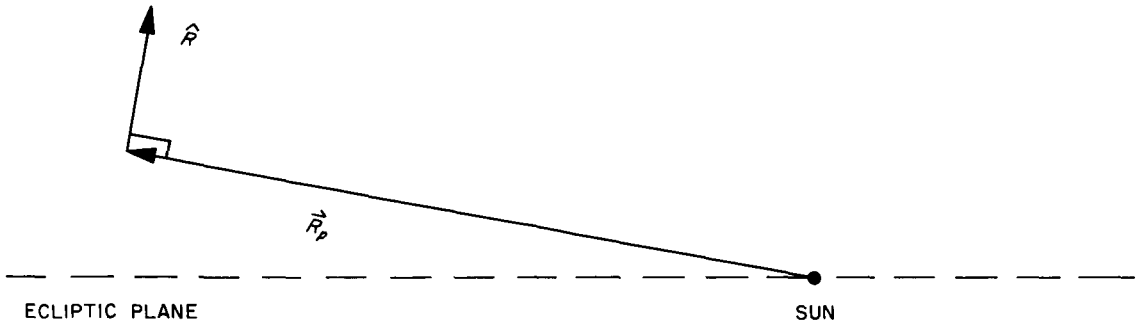

Fig. 52. Description of vectors R and R_p in relation to ecliptic plane of the Sun

Table 39. Earth–Jupiter out-of-ecliptic, 1967 (i = 90 deg, launch HEV = 11.0 km/sec)

Launch date, 1967	T_{12}, days	θ_{12}, deg	ϕ_{12}, deg	B • $\hat{T}$, km	B • $\hat{R}$, km	V_1, km/sec	TISI, days	DOCA, km	DA, deg	V_2, km/sec	a_3, AU	e_3	H_1, AU	H_2, AU	Perihelion, AU	Period, days
10/25	532.0	151.11	2.68	−1177224.	203334.	13.807	87.83	568013.	67.38	1.992	2.758	0.9756	0.6690	−0.5474	0.0673	4.580
10/27	524.0	148.67	2.49	−1083542.	299795.	14.059	86.25	523012.	68.54	3.218	2.814	0.9364	1.0485	−0.9296	0.1790	4.719
10/29	516.0	146.22	2.32	−999743.	352360.	14.317	84.68	482829.	69.59	4.125	2.874	0.8955	1.3384	−1.2224	0.3003	4.872
10/31	510.0	143.92	2.19	−946094.	376283.	14.502	83.59	457067.	70.28	4.675	2.920	0.8658	1.5189	−1.4050	0.3918	4.989
11/2	506.0	141.77	2.09	−917617.	386583.	14.607	82.98	443407.	70.65	4.965	2.947	0.8487	1.6159	−1.5033	0.4459	5.058
11/4	504.0	139.77	2.00	−911909.	388525.	14.630	82.85	440757.	70.70	5.027	2.953	0.8448	1.6370	−1.5246	0.4583	5.074
11/6	504.0	137.91	1.93	−928558.	383005.	14.570	83.19	448937.	70.46	4.867	2.937	0.8545	1.5832	−1.4701	0.4273	5.034
11/8	506.0	136.21	1.87	−969037.	367246.	14.427	84.01	468624.	69.91	4.468	2.902	0.8774	1.4506	−1.3358	0.3555	4.943
11/10	512.0	134.81	1.82	−1062579.	315787.	14.128	85.80	513724.	68.70	3.498	2.831	0.9248	1.1373	−1.0191	0.2129	4.762
11/12	522.0	133.70	1.79	−1228386.	105182.	13.686	88.59	593410.	66.66	1.042	2.734	0.9933	0.3826	−0.2597	0.0183	4.520

Table 40. Earth–Jupiter out-of-ecliptic, 1968 (i = 90 deg, launch HEV = 11.0 km/sec)

Launch date, 1968	T_{12}, days	θ_{12}, deg	ϕ_{12}, deg	B • $\hat{T}$, km	B • $\hat{R}$, km	V_1, km/sec	TISI, days	DOCA, km	DA, deg	V_2, km/sec	a_3, AU	e_3	H_1, AU	H_2, AU	Perihelion, AU	Period, days
11/20	544.0	154.84	2.83	−1282687.	−31901.	13.365	88.52	634904.	64.68	0.387	2.720	0.9991	−0.0727	0.1868	0.0024	4.487
11/22	532.0	152.06	2.58	−1126721.	−317191.	13.759	86.02	562535.	66.25	3.282	2.812	0.9340	−0.9511	1.0620	0.1856	4.717
11/24	522.0	149.44	2.39	−1013103.	−387699.	14.094	84.01	507948.	67.58	4.438	2.895	0.8792	−1.3262	1.4341	0.3497	4.926
11/26	514.0	146.96	2.23	−934036.	−417910.	14.359	82.49	469349.	68.59	5.185	2.965	0.8351	−1.5791	1.6844	0.4889	5.1051
11/28	508.0	144.63	2.11	−882714.	−431384.	14.550	81.43	443995.	69.28	5.665	3.018	0.8032	−1.7467	1.8500	0.5939	5.242
11/30	504.0	142.46	2.01	−854858.	−436905.	14.659	80.84	430089.	69.68	5.924	3.049	0.7847	−1.8395	1.9415	0.6564	5.324
12/2	500.0	140.28	1.91	−828287.	−441190.	14.768	80.25	416825.	70.06	6.175	3.081	0.7661	−1.9306	2.0314	0.7206	5.409
12/4	498.0	138.25	1.84	−822310.	−442017.	14.791	80.12	413776.	70.16	6.229	3.088	0.7620	−1.9502	2.0507	0.7349	5.427
12/6	498.0	136.37	1.77	−836550.	−440000.	14.727	80.46	420796.	69.98	6.087	3.069	0.7728	−1.8983	1.9995	0.6973	5.378
12/8	502.0	134.80	1.72	−893563.	−428860.	14.495	81.71	448924.	69.21	5.537	3.003	0.8120	−1.7017	1.8054	0.5646	5.203
12/10	508.0	133.37	1.67	−979256.	−402219.	14.186	83.44	490876.	68.11	4.720	2.919	0.8634	−1.4206	1.5274	0.3987	4.988
12/12	518.0	132.25	1.63	−1130091.	−315057.	13.730	86.14	563619.	66.30	3.189	2.807	0.9377	−0.9218	1.0325	0.1749	4.702

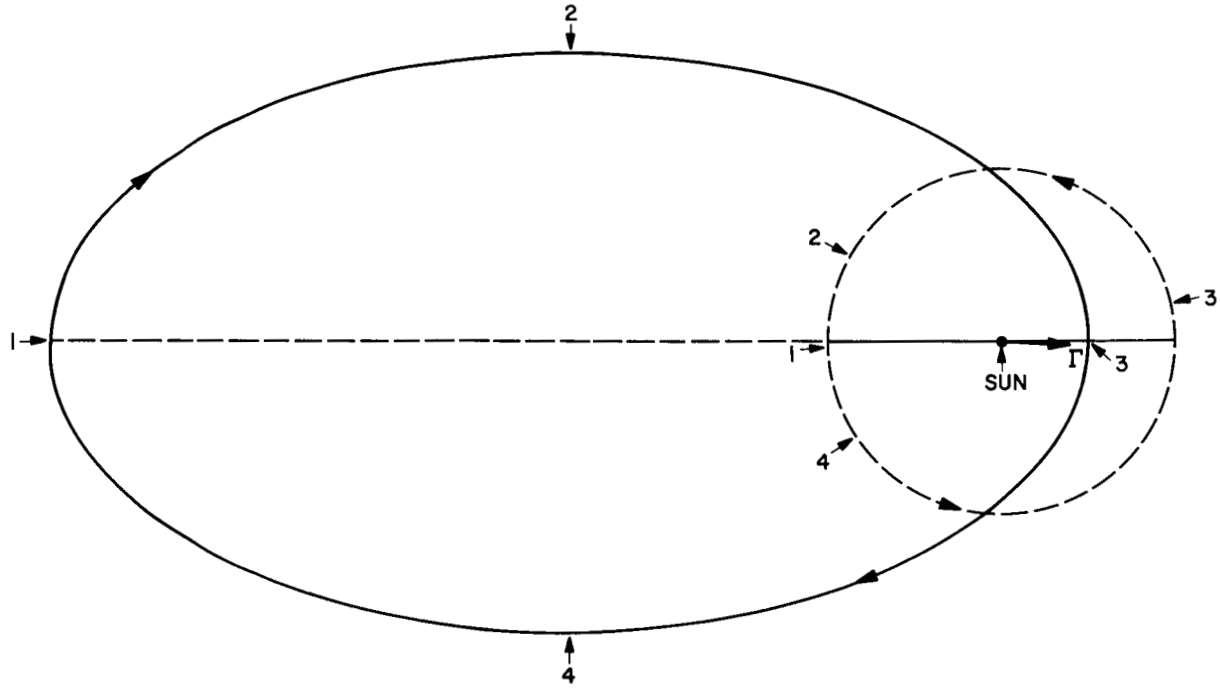

Fig. 53. Planetary configuration for Earth–Jupiter out-of-ecliptic, 1967 (November 4 trajectory)

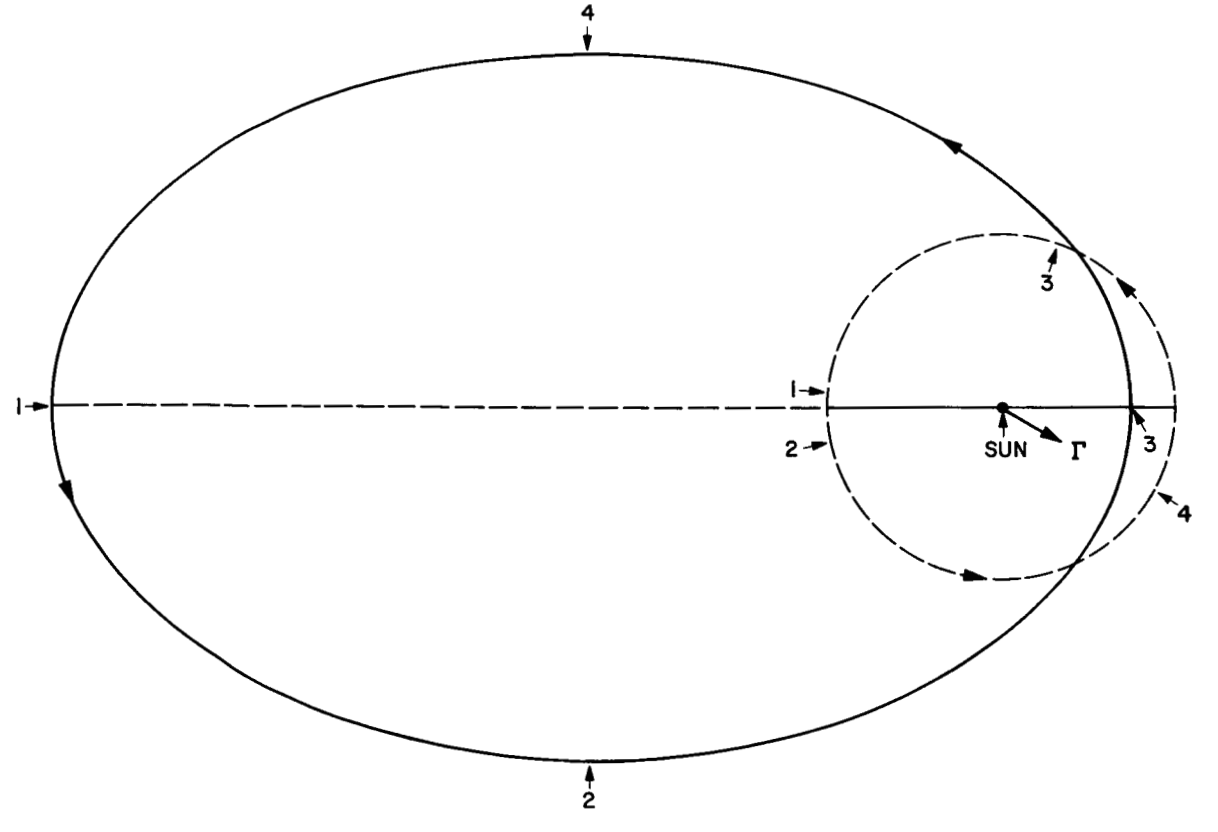

Fig. 54. Earth–Jupiter out-of-ecliptic trajectory, December 4, 1968

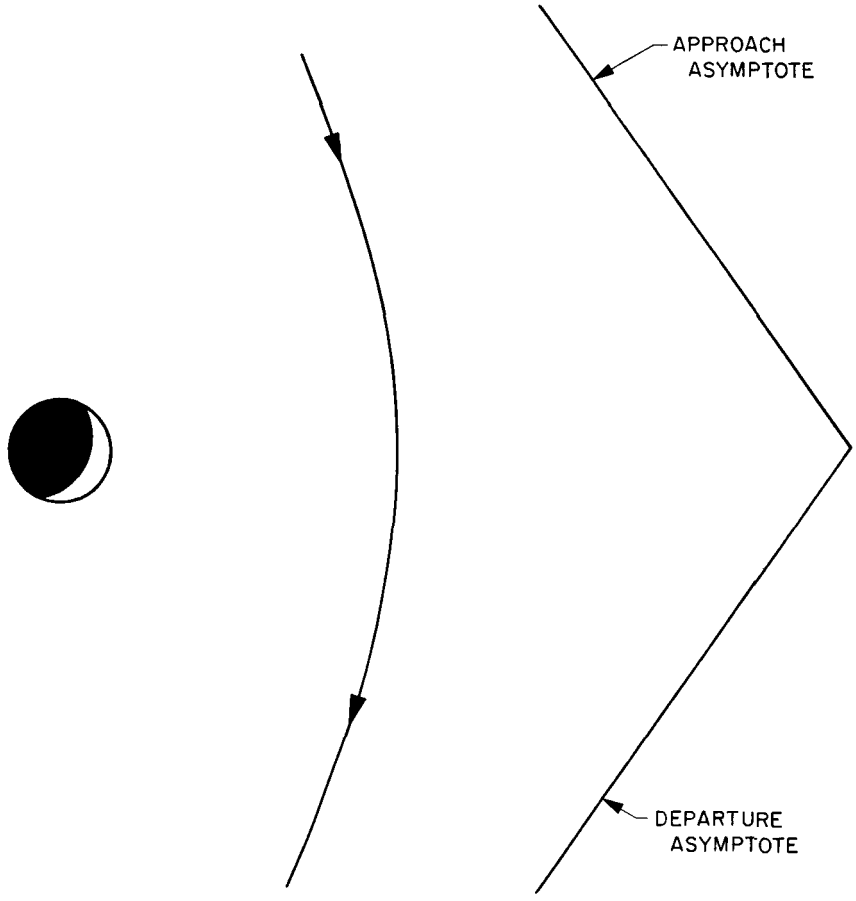

Fig. 55. December 4, 1968, Earth–Jupiter out-of-ecliptic trajectory during its closest approach to Jupiter

Table 41. Earth–Jupiter out-of-ecliptic, 1969–70 (i = 90 deg, launch HEV = 11.0 km/sec)

Launch date, 1969–70	T_{12}, days	θ_{12}, deg	ϕ_{12}, deg	B • $\hat{T}$, km	B • $\hat{R}$, km	V_1, km/sec	TISI, days	DOCA, km	DA, deg	V_2, km/sec	a_3, AU	e_3	H_1, AU	H_2, AU	Perihelion, AU	Period, days
12/19	532.0	155.08	1.89	−1180897.	−258152.	13.538	84.66	595770.	64.42	2.647	2.739	0.9577	−0.7527	0.8257	0.1159	4.532
12/21	522.0	152.42	1.75	−1055230.	−361479.	13.875	82.67	534728.	65.92	4.069	2.823	0.8999	−1.1957	1.2674	0.2826	4.743
12/23	514.0	149.91	1.63	−968831.	−402524.	14.144	81.16	492085.	67.04	4.917	2.894	0.8538	−1.4717	1.5422	0.4231	4.9233
12/25	506.0	147.41	1.53	−890707.	−426654.	14.420	79.67	453134.	68.11	5.664	2.972	0.8059	−1.7250	1.7940	0.5769	5.1226
12/27	498.0	144.90	1.45	−819821.	−440002.	14.703	78.19	417468.	69.13	6.349	3.057	0.7561	−1.9674	2.0347	0.7456	5.3449
12/29	492.0	142.55	1.38	−774035.	−444731.	14.905	77.17	394193.	69.83	6.802	3.122	0.7200	−2.1338	2.1996	0.8742	5.516
12/31	488.0	140.36	1.32	−749332.	−446069.	15.021	76.60	381523.	70.22	7.050	3.160	0.6992	−2.2273	2.2922	0.9505	5.618
1/2	486.0	138.32	1.27	−743706.	−446195.	15.048	76.47	378556.	70.32	7.104	3.169	0.6945	−2.2478	2.3125	0.9681	5.641
1/4	484.0	136.28	1.22	−738458.	−446357.	15.072	76.34	375836.	70.41	7.156	3.177	0.6901	−2.2675	2.3319	0.9846	5.663
1/6	486.0	134.56	1.17	−770498.	−444764.	14.916	77.11	392091.	69.93	6.823	3.125	0.7183	−2.1415	2.2070	0.8803	5.523
1/8	488.0	132.83	1.13	−804563.	−441715.	14.759	77.88	409373.	69.42	6.479	3.074	0.7460	−2.0142	2.0808	0.7808	5.390
1/10	494.0	131.42	1.09	−883988.	−428143.	14.432	79.56	449354.	68.28	5.700	2.975	0.8035	−1.7373	1.8057	0.5846	5.132
1/12	504.0	130.32	1.05	−1024457.	−378081.	13.951	82.18	519103.	66.39	4.334	2.843	0.8865	−1.2807	1.3513	0.3227	4.792

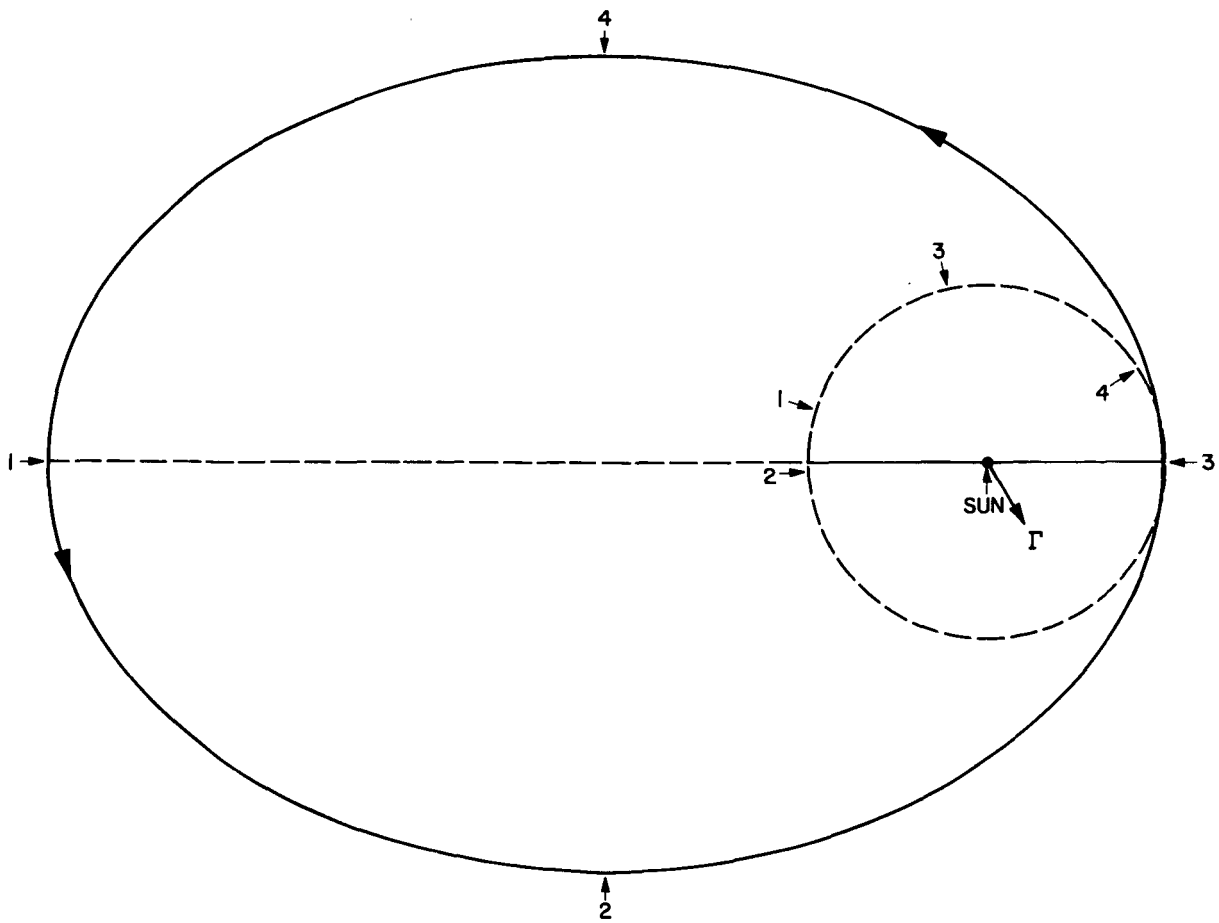

Fig. 56. Planetary configuration for Earth–Jupiter-escape, 1969–70 (January 4 trajectory)

Table 42. Earth–Jupiter out-of-ecliptic, 1971 (i = 90 deg, launch HEV = 11.0 km/sec)

Launch date, 1971	T_{12}, days	θ_{12}, deg	ϕ_{12}, deg	B • $\hat{T}$, km	B • $\hat{R}$, km	V_1, km/sec	TISI, days	DOCA, km	DA, deg	V_2, km/sec	a_3, AU	e_3	H_1, AU	H_2, AU	Perihelion, AU	Period, days
1/19	516.0	154.13	0.38	−1142994.	−242192.	13.720	81.03	576538.	63.96	2.625	2.674	0.9593	−0.7475	0.7623	0.1088	4.372
1/21	506.0	151.44	0.38	−1014727.	−348577.	14.072	79.08	513485.	65.62	4.180	2.763	0.8968	−1.2150	1.2306	0.2851	4.594
1/23	496.0	148.75	0.38	−904222.	−397309.	14.438	77.15	458511.	67.14	5.333	2.863	0.8319	−1.5807	1.5969	0.4813	4.8440
1/25	490.0	146.39	0.37	−850486.	−411859.	14.644	76.12	431391.	67.94	5.880	2.922	0.7956	−1.7618	1.7782	0.5973	4.9936
1/27	482.0	143.86	0.36	−780424.	−424121.	14.942	74.67	395913.	69.01	6.606	3.013	0.7418	−2.0121	2.0287	0.7780	5.230
1/29	478.0	141.67	0.35	−754392.	−426652.	15.064	74.09	382542.	69.43	6.880	3.052	0.7199	−2.1095	2.1262	0.8549	5.331
1/31	474.0	139.48	0.34	−729578.	−428271.	15.186	73.53	369799.	69.83	7.146	3.092	0.6978	−2.2062	2.2228	0.9344	5.436
2/2	470.0	137.28	0.33	−705919.	−429111.	15.307	72.97	357647.	70.22	7.405	3.134	0.6755	−2.3023	2.3189	1.0170	5.547
2/4	468.0	135.25	0.32	−700896.	−429163.	15.334	72.84	355044.	70.31	7.460	3.143	0.6707	−2.3228	2.3393	1.0350	5.571
2/6	468.0	133.39	0.30	−714155.	−428827.	15.264	73.16	361842.	70.09	7.312	3.118	0.6836	−2.2673	2.2837	0.9865	5.505
2/8	470.0	131.69	0.29	−746940.	−427060.	15.099	73.91	378638.	69.56	6.954	3.062	0.7139	−2.1359	2.1522	0.8760	5.358
2/10	474.0	130.15	0.26	−802432.	−420699.	14.843	75.12	406916.	68.68	6.366	2.980	0.7603	−1.9276	1.9436	0.7143	5.144
2/12	482.0	128.95	0.24	−910074.	−394709.	14.418	77.23	461177.	67.08	5.258	2.854	0.8366	−1.556	1.5712	0.4663	4.822
2/14	494.0	128.07	0.20	−1094936.	−290331.	13.844	80.29	552834.	64.57	3.241	2.702	0.9380	−0.9298	0.9438	0.1675	4.443

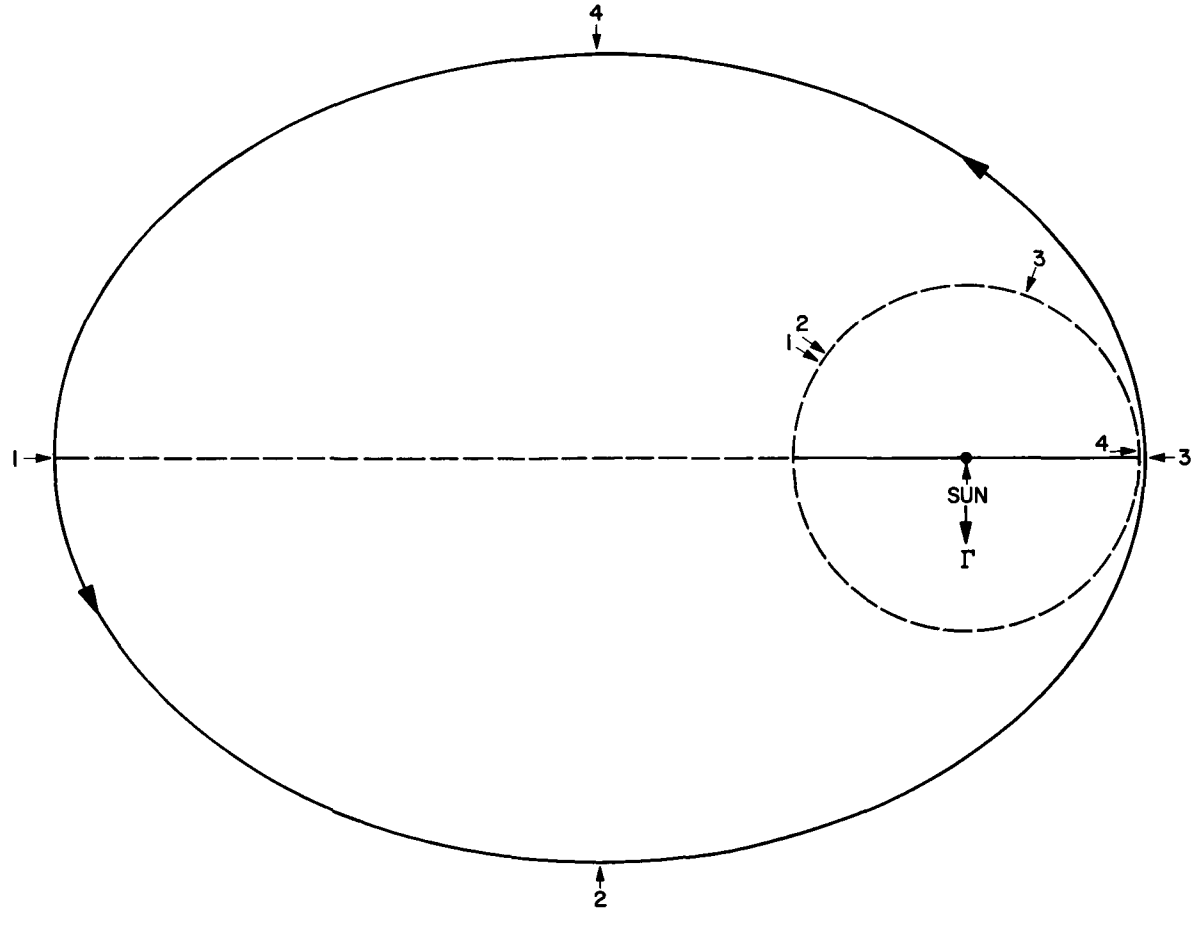

Fig. 57. Planetary configuration for Earth–Jupiter out-of-ecliptic, 1971 (February 4 trajectory)

Table 43. Earth–Jupiter out-of-ecliptic, 1972 (i = 90 deg, launch HEV = 11.0 km/sec)

Launch date, 1972	T_{12}, days	θ_{12}, deg	ϕ_{12}, deg	$B \cdot \hat{T}$, km	$B \cdot \hat{R}$, km	V_1, km/sec	TISI, days	DOCA, km	DA, deg	V_2, km/sec	a_3, AU	e_3	H_1, AU	H_2, AU	Perihelion, AU	Period, yr
2/23	492.0	150.51	1.09	−1065851.	−238225.	14.174	76.86	530469.	64.57	2.815	2.612	0.9544	−0.8034	0.7566	0.1191	4.221
2/25	484.0	147.98	0.99	−969033.	−317506.	14.464	75.37	482719.	65.93	4.094	2.683	0.9035	−1.1721	1.1274	0.2589	4.394
2/27	476.0	145.46	0.91	−883634.	−359806.	14.761	73.90	440376.	67.17	5.086	2.760	0.8511	−1.4703	1.4279	0.4109	4.585
2/29	470.0	143.10	0.85	−829462.	−377768.	14.358	72.87	413297.	67.99	5.695	2.818	0.8132	−1.6606	1.6199	0.5264	4.731
3/2	464.0	140.75	0.79	−779378.	−389594.	15.194	71.86	388158.	68.77	6.260	2.881	0.7742	−1.8430	1.8039	0.6505	4.890
3/4	460.0	138.58	0.75	−752725.	−394095.	15.320	71.30	374693.	69.20	6.564	2.918	0.7517	−1.9437	1.9056	0.7245	4.985
3/6	456.0	136.40	0.72	−727411.	−397399.	15.446	70.74	361893.	69.61	6.857	2.957	0.7290	−2.0427	2.0055	0.8013	5.085
3/8	454.0	134.40	0.69	−722154.	−397913.	15.474	70.61	359233.	69.70	6.920	2.965	0.7241	−2.0639	2.0269	0.8180	5.107
3/10	454.0	132.58	0.68	−736561.	−396178.	15.403	70.92	366543.	69.45	6.754	2.943	0.7372	−2.0073	1.9695	0.7734	5.048
3/12	456.0	130.92	0.67	−772217.	−390552.	15.235	71.68	384554.	68.87	6.346	2.891	0.7680	−1.8710	1.8318	0.6707	4.914
3/14	458.0	129.27	0.66	−810318.	−382372.	14.445	72.45	403779.	68.25	5.918	2.841	0.7983	−1.7316	1.6910	0.5730	4.789
3/16	464.0	127.97	0.67	−899392.	−352550.	14.715	74.12	448279.	66.89	4.918	2.744	0.8608	−1.4185	1.3750	0.3819	4.546
3/18	474.0	127.02	0.69	−1060640.	−241646.	14.202	76.72	527843.	64.61	2.902	2.614	0.9516	−0.8280	0.7803	0.1265	4.227

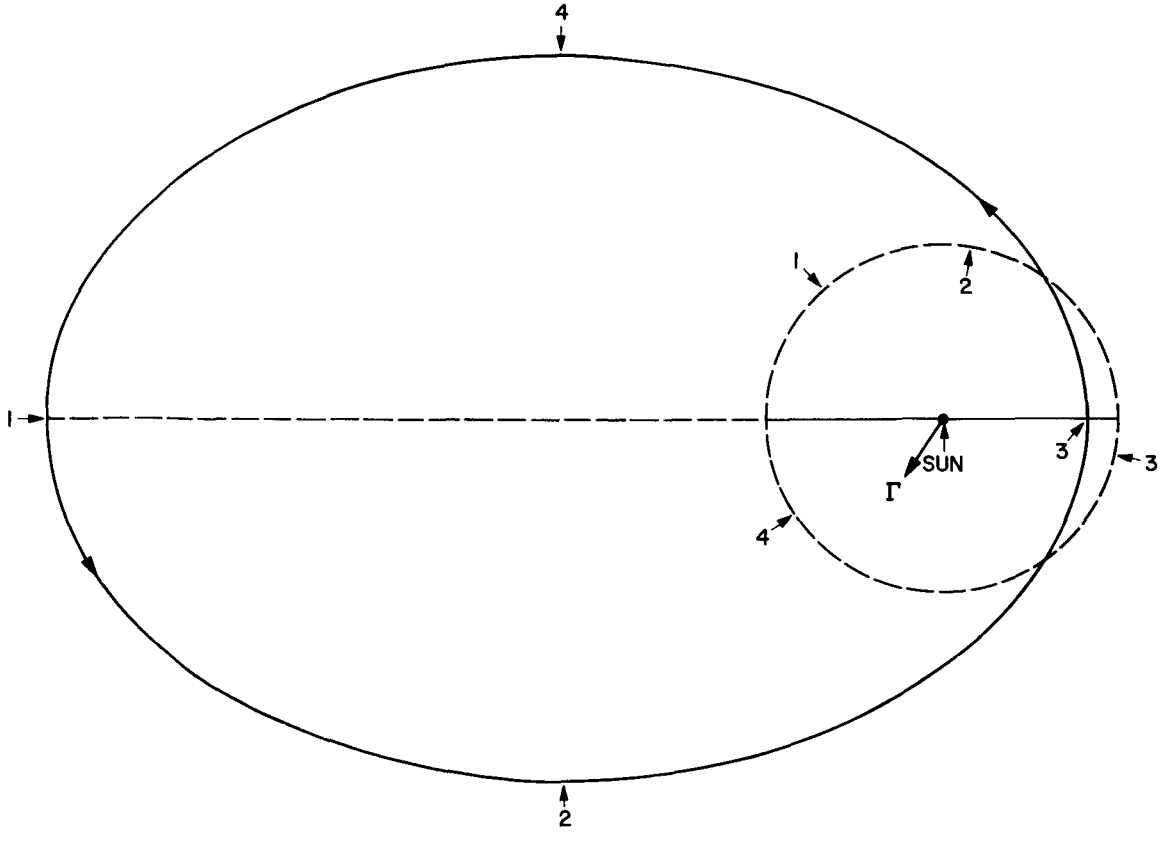

Fig. 58. Planetary configuration for Earth–Jupiter out-of-ecliptic, 1972 (March 8 trajectory)

Table 44. Earth–Jupiter out-of-ecliptic, 1973 (i = 90 deg, launch HEV = 11.0 km/sec)

Launch date, 1973	T_{12}, days	θ_{12}, deg	ϕ_{12}, deg	$B \cdot \hat{T}$, km	$B \cdot \hat{R}$, km	V_1, km/sec	TISI, days	DOCA, km	DA, deg	V_2, km/sec	a_3, AU	e_3	H_1, AU	H_2, AU	Perihelion, AU	Period, yr
4/2	470.0	145.60	1.96	−1023620.	−185725.	14.666	74.07	496641.	65.46	2.331	2.537	0.9694	−0.6721	0.5770	0.0776	4.040
4/4	464.0	143.27	1.85	−956184.	−256970.	14.879	73.02	463747.	66.44	3.434	2.584	0.9336	−0.9736	0.8807	0.1716	4.154
4/6	458.0	140.94	1.74	−895074.	−299362.	15.095	71.98	433960.	67.34	4.274	2.634	0.8971	−1.2102	1.1195	0.2708	4.2754
4/8	454.0	138.79	1.67	−862799.	−316347.	15.221	71.39	418167.	67.82	4.692	2.664	0.8760	−1.3305	1.2412	0.3303	4.348
4/10	450.0	136.65	1.59	−832224.	−329917.	15.346	70.81	403218.	68.28	5.080	2.695	0.8546	−1.4442	1.3562	0.3919	4.4243
4/12	448.0	134.69	1.54	−825898.	−332334.	15.375	70.69	400121.	68.37	5.161	2.702	0.8499	−1.4682	1.3805	0.4056	4.441
4/14	446.0	132.73	1.49	−819961.	−334631.	15.401	70.56	397267.	68.45	5.239	2.709	0.8454	−1.4913	1.4038	0.4185	4.458
4/16	446.0	130.96	1.45	−837531.	−327575.	15.330	70.89	405936.	68.17	5.023	2.690	0.8579	−1.4273	1.3390	0.3822	4.412
4/18	450.0	129.54	1.43	−905836.	−292210.	15.068	72.12	439301.	67.14	4.149	2.626	0.9030	−1.1744	1.0831	0.2547	4.254
4/20	454.0	128.13	1.41	−981700.	−232681.	14.810	73.38	476230.	66.03	3.071	2.566	0.9469	−0.8733	0.7792	0.1363	4.110

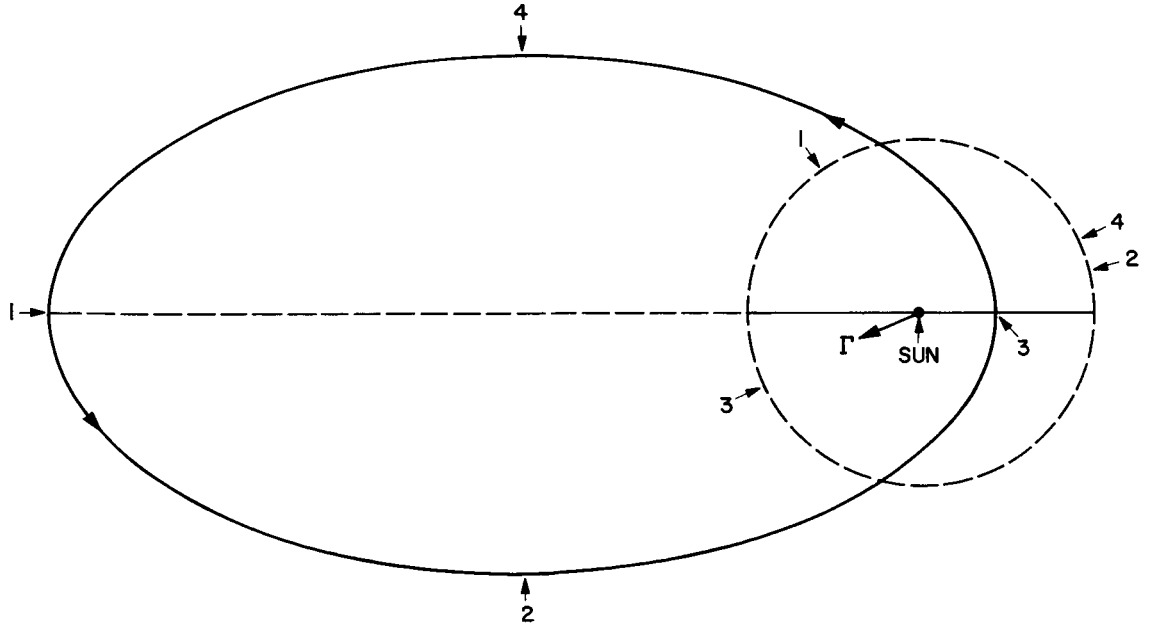

Fig. 59. Earth–Jupiter out-of-ecliptic, April 14, 1973 trajectory

Table 45. Earth–Jupiter out-of-ecliptic, 1974 (i = 90 deg, launch HEV = 11.5 km/sec)

Launch date, 1974	T_{12}, days	θ_{12}, deg	ϕ_{12}, deg	$B \cdot \hat{T}$, km	$B \cdot \hat{R}$, km	V_1, km/sec	TISI, days	DOCA, km	DA, deg	V_2, km/sec	a_3, AU	e_3	H_1, AU	H_2, AU	Perihelion, AU	Period, yr
5/7	456.0	146.81	2.38	−947209.	−207158.	15.242	72.31	446875.	67.50	2.753	2.530	0.9577	−0.7854	0.6751	0.1070	4.024
5/9	448.0	144.33	2.24	−861302.	−276835.	15.564	70.78	405837.	68.76	4.087	2.597	0.9068	−1.1501	1.0429	0.2420	4.186
5/11	440.0	141.85	2.11	−784763.	−314622.	15.896	69.26	369158.	69.91	5.134	2.673	0.8528	−1.4488	1.3449	0.3935	4.370
5/13	436.0	139.74	2.02	−756309.	−324523.	16.037	68.66	355386.	70.36	5.513	2.706	0.8303	−1.5600	1.4576	0.4592	4.451
5/15	430.0	137.44	1.93	−709564.	−337437.	16.278	67.62	332822.	71.11	6.135	2.767	0.7898	−1.7477	1.6481	0.5812	4.603
5/17	426.0	135.33	1.86	−684543.	−342551.	16.420	67.03	320689.	71.52	6.472	2.804	0.7661	−1.8519	1.7540	0.6559	4.696
5/19	422.0	133.23	1.79	−660695.	−346447.	16.561	66.45	309120.	71.91	6.798	2.843	0.7420	−1.9546	1.8585	0.7335	4.7940
5/21	420.0	131.30	1.74	−655536.	−347136.	16.595	66.32	306639.	71.99	6.871	2.852	0.7364	−1.9781	1.8823	0.7518	4.817
5/23	420.0	129.56	1.69	−668677.	−345186.	16.520	66.63	313079.	71.75	6.696	2.831	0.7497	−1.9222	1.8255	0.7086	4.762
5/25	420.0	127.83	1.65	−682423.	−342908.	16.441	66.95	319843.	71.51	6.515	2.809	0.7631	−1.8651	1.7675	0.6655	4.708
5/27	422.0	126.27	1.62	−716254.	−335780.	16.257	67.73	336338.	70.93	6.068	2.760	0.7944	−1.7270	1.6271	0.5675	4.585
5/29	426.0	124.90	1.59	−773465.	−318550.	15.970	68.97	364044.	70.01	5.317	2.689	0.8422	−1.5020	1.3989	0.4243	4.408
5/31	432.0	123.72	1.57	−860101.	−277126.	15.589	70.69	405651.	68.68	4.147	2.601	0.9040	−1.1668	1.0598	0.2497	4.195
6/2	442.0	122.90	1.55	−1015045.	−97393.	15.034	73.38	479421.	66.50	1.259	2.487	0.9912	−0.3908	0.2787	0.0219	3.923

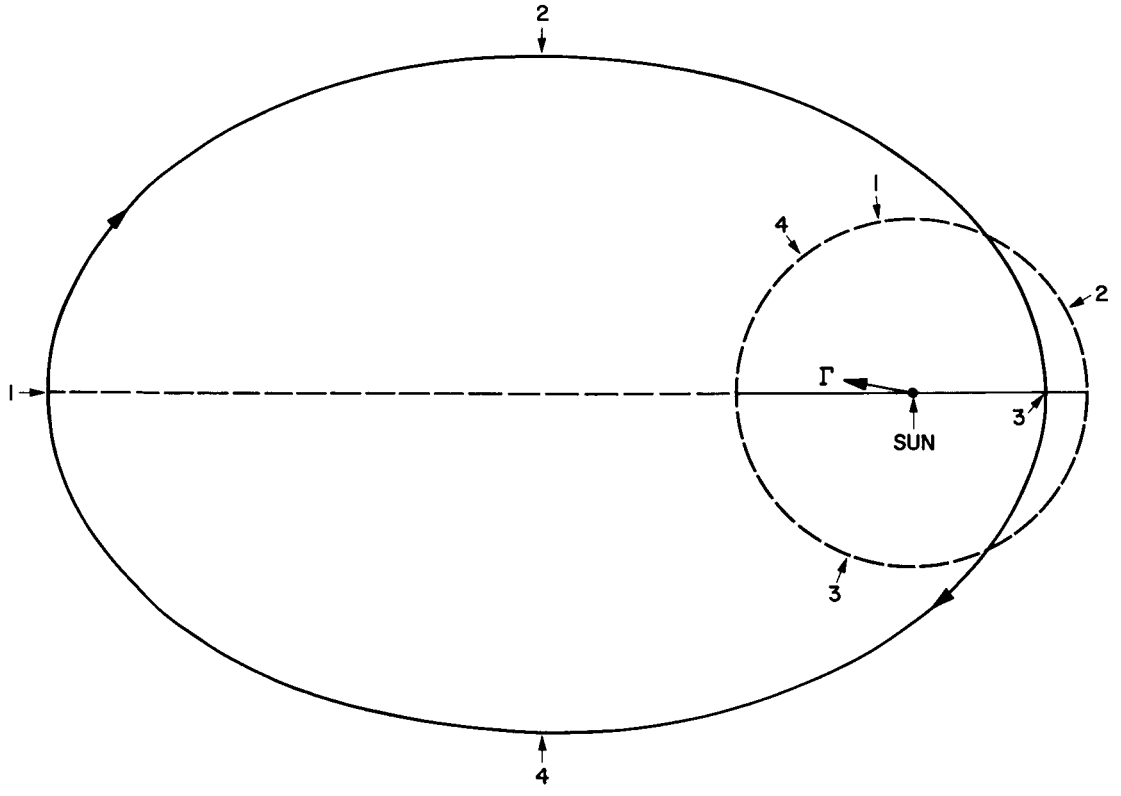

Fig. 60. Earth–Jupiter out-of-ecliptic, May 21, 1974 trajectory

Table 46. Earth–Jupiter out-of-ecliptic, 1975 (i = 90 deg, launch HEV = 11.5 km/sec)

Launch date, 1975	T_{12}, days	θ_{12}, deg	ϕ_{12}, deg	B • $\hat{T}$, km	B • $\hat{R}$, km	V_{∞_1}, km/sec	TISI, days	DOCA, km	DA, deg	V_{∞_2}, km/sec	a_3, AU	e_3	H_{∞_1}, AU	H_{∞_2}, AU	Perihelion, AU	Period, yr
6/15	458.0	146.58	1.81	−971288.	161200.	15.352	74.19	448904.	68.59	2.213	2.534	0.9724	0.5495	−0.6354	0.0699	4.033
6/17	452.0	144.31	1.72	−909104.	234638.	15.576	73.08	420412.	69.42	3.379	2.581	0.9357	0.8693	−0.9539	0.1659	4.147
6/19	444.0	141.87	1.64	−828846.	291207.	15.899	71.51	383347.	70.54	4.571	2.654	0.8823	1.2082	−1.2909	0.3124	4.323
6/21	440.0	139.78	1.57	−798373.	306092.	16.035	70.88	369003.	71.00	4.983	2.685	0.8602	1.3290	−1.4108	0.3754	4.400
6/23	434.0	137.51	1.51	−748941.	325298.	16.270	69.81	345819.	71.74	5.643	2.743	0.8207	1.5274	−1.6075	0.4918	4.542
6/25	432.0	135.60	1.46	−741861.	327382.	16.306	69.66	342344.	71.88	5.732	2.751	0.8151	1.5546	−1.6344	0.5087	4.564
6/27	428.0	133.52	1.41	−715654.	334873.	16.441	69.05	329957.	72.29	6.078	2.786	0.7921	1.6619	−1.7406	0.5792	4.651
6/29	426.0	131.61	1.37	−709503.	336413.	16.472	68.92	327000.	72.40	6.157	2.795	0.7866	1.6868	−1.7652	0.5965	4.672
7/1	426.0	129.88	1.33	−722964.	332923.	16.399	69.24	333306.	72.20	5.975	2.776	0.7991	1.6300	−1.7089	0.5577	4.625
7/3	428.0	128.34	1.29	−757437.	322251.	16.222	70.04	349479.	71.68	5.513	2.731	0.8289	1.4883	−1.5685	0.4673	4.513
7/5	432.0	126.97	1.26	−816301.	297436.	15.946	71.32	376973.	70.82	4.716	2.665	0.8748	1.2510	−1.3329	0.3337	4.350
7/7	436.0	125.60	1.23	−881067.	257752.	15.674	72.62	407057.	69.89	3.787	2.604	0.9192	0.9844	−1.0678	0.2104	4.202

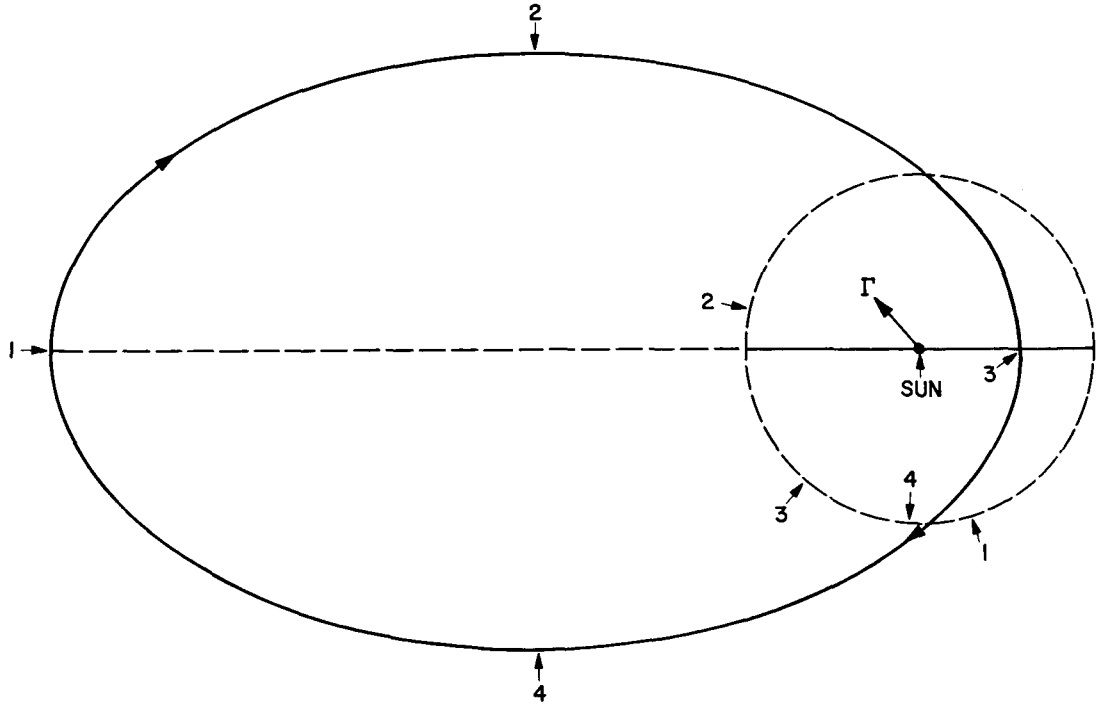

Fig. 61. Earth–Jupiter out-of-ecliptic, June 29, 1975 trajectory

Table 47. Earth–Jupiter out-of-ecliptic, 1976 (i = 90 deg, launch HEV = 11.5 km/sec)

Launch date, 1976	T_{12}, days	θ_{12}, deg	ϕ_{12}, deg	$B \cdot \hat{T}$, km	$B \cdot \hat{R}$, km	V_1, km/sec	TISI, days	DOCA, km	DA, deg	V_2, km/sec	a_3, AU	e_3	H_1, AU	H_2, AU	Perihelion, AU	Period, yr
7/21	472.0	148.15	0.57	−994426.	166538.	15.200	77.70	454564.	69.81	2.270	2.598	0.9703	0.6158	−0.6421	0.0772	4.187
7/23	464.0	145.73	0.55	−907687.	258330.	15.504	76.08	414697.	71.00	3.743	2.666	0.9192	1.0366	−1.0632	0.2154	4.353
7/25	458.0	143.47	0.53	−852189.	293963.	15.724	74.95	389002.	71.79	4.511	2.717	0.8827	1.2635	−1.2901	0.3187	4.478
7/27	452.0	141.22	0.52	−800835.	318063.	15.947	73.84	365134.	72.54	5.180	2.771	0.8453	1.4671	−1.4937	0.4287	4.613
7/29	448.0	139.13	0.50	−772915.	328269.	16.078	73.21	352057.	72.96	5.535	2.804	0.8234	1.5777	−1.6043	0.4952	4.695
7/31	444.0	137.05	0.49	−746346.	336455.	16.208	72.58	339613.	73.37	5.872	2.838	0.8013	1.6847	−1.7112	0.5639	4.781
8/2	442.0	135.14	0.47	−739951.	338178.	16.241	72.44	336573.	73.48	5.952	2.847	0.7958	1.7105	−1.7369	0.5814	4.803
8/4	440.0	133.22	0.46	−733935.	339811.	16.271	72.30	333757.	73.57	6.029	2.855	0.7906	1.7353	−1.7616	0.5978	4.824
8/6	440.0	131.48	0.44	−747471.	336231.	16.200	72.63	340097.	73.37	5.856	2.837	0.8023	1.6801	−1.7063	0.5609	4.778
8/8	442.0	129.91	0.42	−781861.	325375.	16.031	73.45	356175.	72.85	5.419	2.794	0.8307	1.5421	−1.5682	0.4730	4.669
8/10	446.0	128.50	0.40	−840467.	300445.	15.767	74.75	383453.	71.99	4.663	2.729	0.8746	1.3102	−1.3361	0.3422	4.509
8/12	452.0	127.27	0.37	−929517.	241314.	15.416	76.56	424662.	70.73	3.416	2.649	0.9327	0.9429	−0.9684	0.1783	4.311

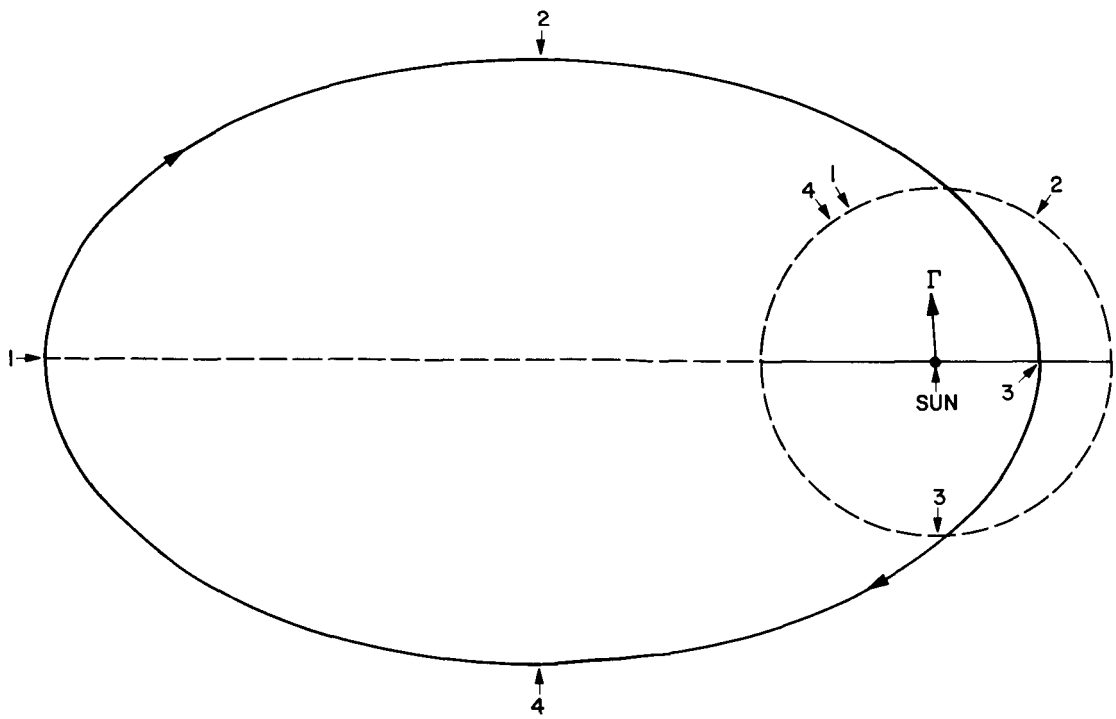

Fig. 62. Earth–Jupiter out-of-ecliptic, August 4 ,1976 trajectory

Table 48. Earth–Jupiter out-of-ecliptic, 1977 (i = 90 deg, launch HEV = 11.5 km/sec)

Launch date, 1977	T_{12}, days	θ_{12}, deg	ϕ_{12}, deg	$B \cdot \hat{T}$, km	$B \cdot \hat{R}$, km	V_1, km/sec	TISI, days	DOCA, km	DA, deg	V_2, km/sec	a_3, AU	e_3	H_1, AU	H_2, AU	Perihelion, AU	Period, yr
8/23	478.0	152.07	1.05	−1079469.	130883.	14.668	82.67	498017.	69.45	1.635	2.656	0.9841	0.4942	−0.4495	0.0422	4.328
8/25	488.0	149.49	0.94	−962042.	271248.	15.033	80.54	443172.	71.05	3.607	2.739	0.9228	1.0768	−1.0347	0.2115	4.533
8/27	480.0	147.07	0.86	−882974.	319025.	15.326	78.93	406269.	72.14	4.599	2.809	0.8745	1.3823	−1.3423	0.3525	4.707
8/29	474.0	144.82	0.80	−832091.	340286.	15.538	77.80	382404.	72.87	5.201	2.861	0.8395	1.5739	−1.5354	0.4592	4.840
8/31	468.0	142.56	0.74	−784733.	355116.	15.752	76.69	360154.	73.56	5.755	2.918	0.8035	1.755	−1.7182	0.5734	4.983
9/2	462.0	140.30	0.70	−740568.	365228.	15.970	75.59	339354.	74.21	6.275	2.978	0.7665	1.9304	−1.8949	0.6954	5.139
9/4	458.0	138.20	0.66	−716682.	369310.	16.096	74.97	328071.	74.58	6.560	3.014	0.7448	2.0288	−1.9942	0.7692	5.233
9/6	456.0	136.26	0.64	−711131.	370145.	16.127	74.82	325456.	74.66	6.628	3.024	0.7395	2.053	−2.0181	0.7878	5.258
9/8	454.0	134.32	0.62	−705916.	370960.	16.155	74.68	323041.	74.73	6.693	3.033	0.7344	2.0756	−2.0412	0.8056	5.281
9/10	454.0	132.54	0.61	−718544.	369274.	16.086	75.02	329094.	74.53	6.545	3.013	0.7460	2.0239	−1.9890	0.7653	5.230
9/12	458.0	131.08	0.61	−769048.	359538.	15.828	76.31	353019.	73.76	5.952	2.940	0.7899	1.8218	−1.7848	0.6177	5.042
9/14	462.0	129.62	0.61	−823962.	343931.	15.573	77.62	378979.	72.94	5.316	2.873	0.8323	1.6124	−1.5735	0.4818	4.870
9/16	470.0	128.48	0.62	−930085.	294339.	15.146	79.92	428746.	71.43	4.052	2.769	0.9025	1.2137	−1.1715	0.2700	4.608

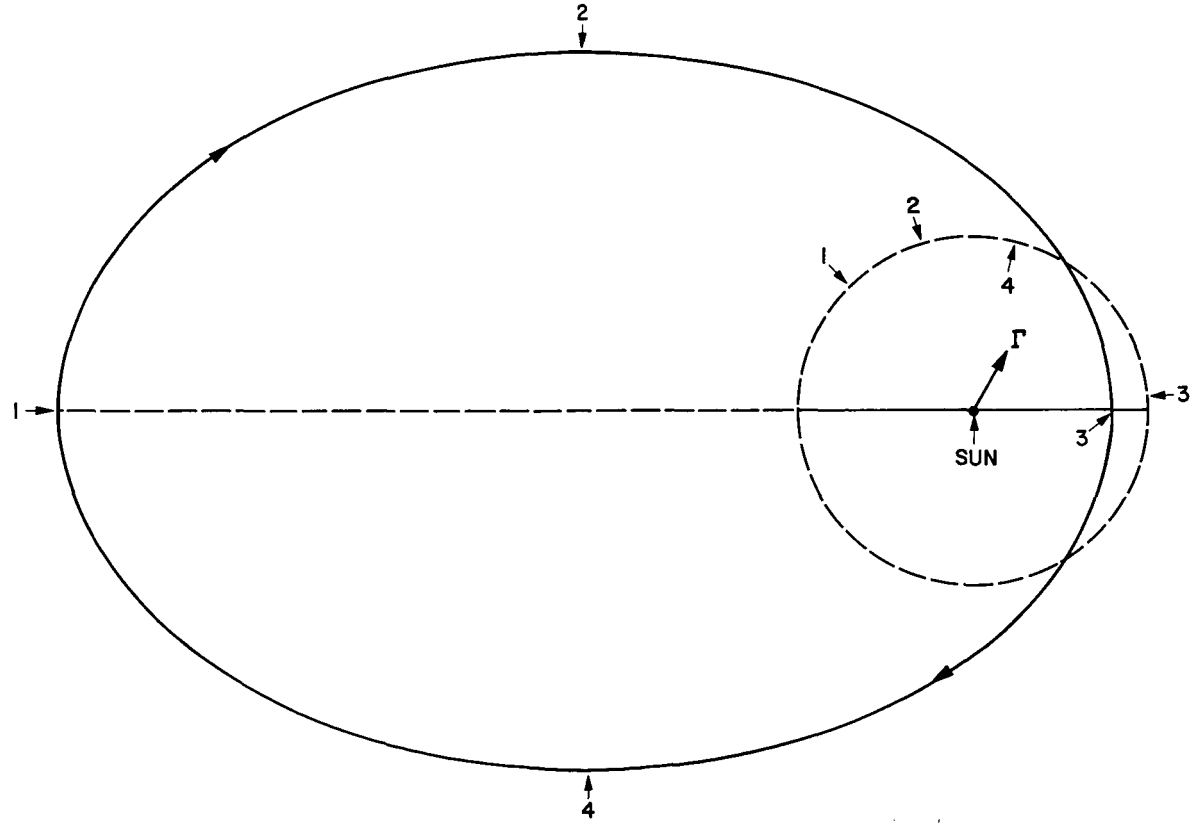

Fig. 63. Earth–Jupiter out-of-ecliptic, September 8, 1977 trajectory

Table 49. Earth–Jupiter out-of-ecliptic, 1978 (i = 90 deg, launch HEV = 11.5 km/sec)

Launch date, 1978	T_{12}, days	θ_{12}, deg	ϕ_{12}, deg	B • $\hat{T}$, km	B • $\hat{R}$, km	V_1, km/sec	TISI, days	DOCA, km	DA, deg	V_2, km/sec	a_3, AU	e_3	H_1, AU	H_2, AU	Perihelion, AU	Period, yr
9/23	522.0	155.35	2.57	−1145171.	159999.	14.138	86.39	540474.	68.46	1.712	2.721	0.9822	0.5638	−0.4637	0.0484	4.487
9/25	512.0	152.77	2.33	−1024108.	292966.	14.482	84.28	482759.	70.06	3.469	2.798	0.9269	1.0994	−1.0030	0.2045	4.679
9/27	502.0	150.20	2.12	−920056.	351153.	14.839	82.20	433366.	71.45	4.640	2.883	0.8692	1.4723	−1.3799	0.3771	4.895
9/29	492.0	147.61	1.96	−828480.	381492.	15.208	80.14	389738.	72.72	5.619	2.979	0.8083	1.7988	−1.7107	0.5711	5.142
10/1	486.0	145.34	1.83	−783361.	390924.	15.416	79.04	368112.	73.37	6.105	3.037	0.7737	1.9672	−1.8816	0.6873	5.292
10/3	480.0	143.06	1.73	−741126.	396991.	15.626	77.96	347834.	73.99	6.569	3.098	0.7381	2.1325	−2.0495	0.8114	5.454
10/5	474.0	140.79	1.64	−701518.	400415.	15.839	76.88	328773.	74.59	7.015	3.165	0.7013	2.297	−2.2163	0.9454	5.630
10/7	470.0	138.66	1.56	−680192.	401388.	15.962	76.27	318503.	74.91	7.263	3.205	0.6799	2.3898	−2.3112	1.0259	5.737
10/9	468.0	136.68	1.51	−675518.	401567.	15.991	76.13	316308.	74.97	7.320	3.215	0.6748	2.4118	−2.3336	1.0455	5.764
10/11	466.0	134.71	1.45	−671133.	401776.	16.017	76.00	314290.	75.02	7.376	3.224	0.6699	2.433	−2.355	1.0642	5.789
10/13	468.0	133.04	1.42	−699453.	400875.	15.856	76.80	328138.	74.56	7.055	3.171	0.6979	2.3116	−2.2315	0.9580	5.648
10/15	470.0	131.37	1.39	−729447.	398829.	15.693	77.61	342805.	74.07	6.724	3.121	0.7256	2.1894	−2.1071	0.8564	5.514
10/17	476.0	130.00	1.37	−798717.	388953.	15.352	79.37	376333.	73.02	5.977	3.022	0.7830	1.9232	−1.8364	0.6558	5.252
10/19	486.0	128.95	1.37	−919609.	352671.	14.851	82.12	434273.	71.30	4.702	2.889	0.8657	1.4934	−1.4007	0.3880	4.911
10/21	500.0	128.20	1.37	−1117846.	204561.	14.213	85.90	528391.	68.70	2.292	2.741	0.9681	0.7391	−0.6392	0.0874	4.538

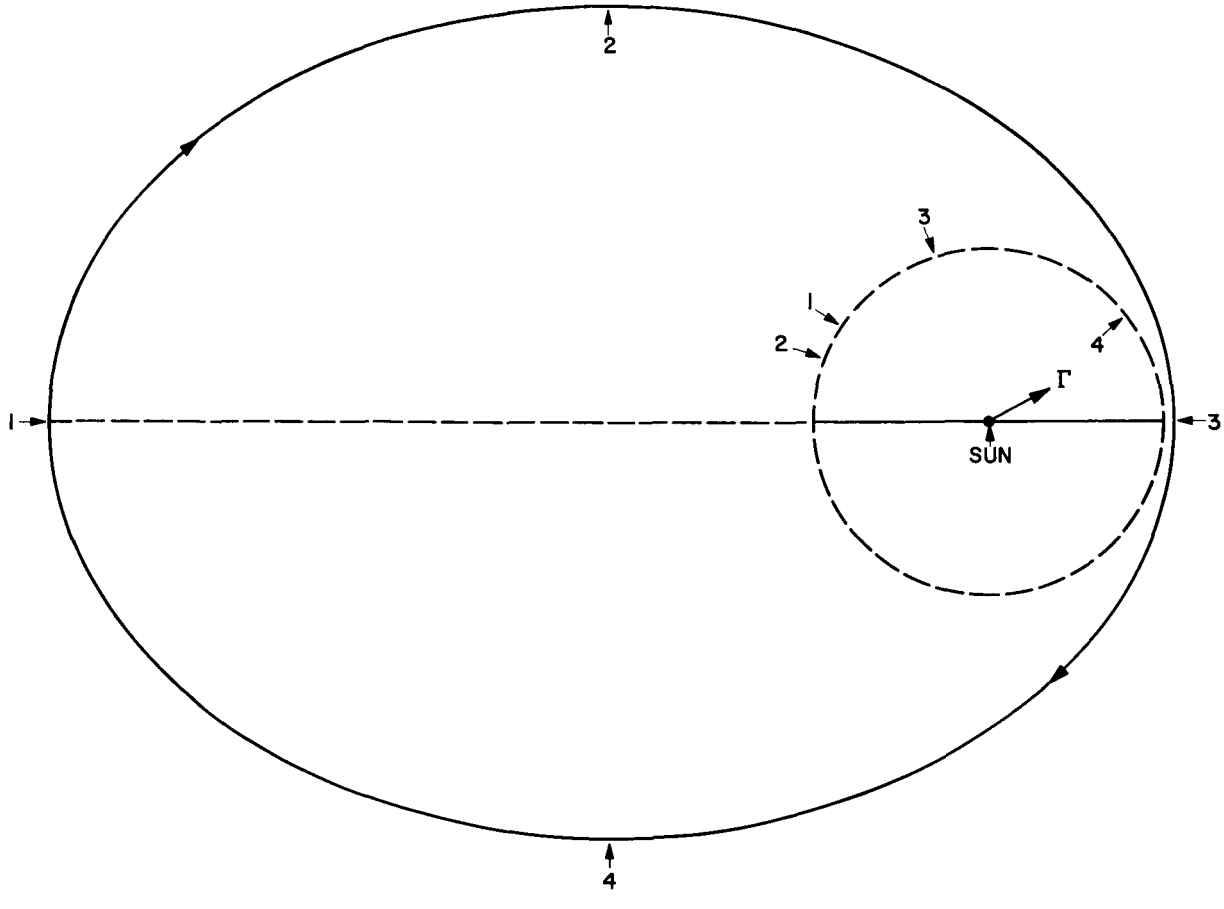

Fig. 64. Earth–Jupiter out-of-ecliptic, October 11, 1978 trajectory

VI. CONCLUDING COMMENTS

The underlying concept which forms the basis of Ref. 1 and this report is very simple. Any space vehicle approaching a member of the solar system will experience a perturbation of its orbit. If the mission is not terminated at that particular planet or moon, it may be possible to utilize its gravitational influence to place the vehicle on a new trajectory having specified characteristics. For example, it may be desired to change the trajectory so that it will rendezvous with another planet. Consequently many missions which would ordinarily require very high launch energies can be carried out by this technique. Without the aid of these planetary perturbations, many interplanetary missions both manned and unmanned must wait until very powerful boosters and rocket engines become available. Recent studies at the Jet Propulsion Laboratory show that the required planetary approach guidance is within present capabilities. The very high energy missions such as those considered in this report should be prime candidates for this technique. Manned or unmanned missions to Mercury, Venus, or Mars are other examples where this approach can yield significant savings in launch energies and in some cases even flight times. In 1976 or 1977 high energy missions to Saturn, Uranus, Neptune, and Pluto could be carried out by means of a Jupiter flyby. Utilizing planetary perturbations to augment a vehicle's onboard rocket engine is another attractive possibility.

It should be borne in mind, however, that the key to real interplanetary mission capability rests upon the rocket engine. Trajectory design and profile changes do cause great differences in terms of energy requirements, but as in aviation it ultimately depends upon the available powerplants. Until these nuclear powerplants with very high exhaust velocities become available, perhaps a nice compact planetary approach guidance system will provide a means for carrying out these missions.

REFERENCES

1. Minovitch, M. A., *The Determination and Characteristics of Ballistic Interplanetary Trajectories Under the Influence of Multiple Planetary Attractions*, Technical Report No. 32-464, Jet Propulsion Laboratory, Pasadena, California, October 31, 1963.

2. Hunter, M. W. II, *Future Unmanned Exploration of the Solar System*, National Aeronautics and Space Council, Washington, D. C., September 1963.

3. *Asteroid Belt and Jupiter Fly-By Mission Study*, M-49-64-2, National Aeronautics and Space Administration, Washington, D. C., September 15, 1964.

ACKNOWLEDGMENT

The author would like to take this opportunity to thank Mr. Maxwell Hunter of the National Aeronautics and Space Council for directing the author's attention to very large planetary perturbations such as those obtained from a Jupiter flyby.

Reports which include large quantities of computations usually require hard work from many people. The author wishes to express his sincere appreciation to the computing facilities of both the University of California at Los Angeles and the Jet Propulsion Laboratory for their kind and helpful assistance. The author especially wants to thank Professor Charles B. Tompkins and Dr. Michael A. Melkanoff of UCLA and Mr. Carl Theis of JPL for providing access to computers, which is usually so hard and difficult to obtain.

Finally, the author owes a great deal of thanks to Mr. Elliott Cutting of the Systems Analysis Section at JPL for all his help in putting this report in its final form.